AN EXPERIMENTAL STUDY OF THE ROTATIONAL DISTRIBUTION OF N_2^+B (v) STATES EXCITED BY ELECTRON BEAM IMPINGEMENT UPON HELIUM AND NITROGEN GAS MIXTURES

by

John Cameron Hoppe

Dissertation submitted to the Graduate Faculty of the Virginia Polytechnic Institute and State University in partial fulfillment of the requirements for the degree of

DOCTOR OF PHILOSOPHY

in

Physics

APPROVED:

T. E. Leinhardt, Chairman

V. L. Teplitz

R. L. Bowden

S. P. Bowen

C. D. Williams

May, 1977

Blacksburg, Virginia

ACKNOWLEDGEMENTS

The author would like to thank most kindly Dr. T. E. Leinhardt for his enduring patience and especially for his continued interest and encouragement. Appreciation is also expressed to Dr. C. D. Williams and to the other committee members for their interest and assistance.

The research was conducted at the Langley Research Center, Hampton, Virginia. A sincere thank you is given to Dr. W. W. Hunter, Jr. of Langley's staff for his continuing support and encouragement.

To two people, my wife,
heartfelt appreciation is extended for their long hours of typing this paper.

TABLE OF CONTENTS

LIST OF TABLES

LIST OF FIGURES

1. INTRODUCTION

This work describes how nitrogen, as an impurity in helium, may be efficiently excited and ionized from its ground $N_2X\ ^1\Sigma_g^+$ state to the $N_2^+B\ ^2\Sigma_u^+$ excited state. A moderately energetic electron beam supplies the excitation source, which distinguishes this particular study from most previous work. Numerous reports have been published about studies of helium in discharges and flowing afterglow. Some have included the effects of impurities.

The underlying basis for this investigation will be examined completely. For the moment, however, some of the concepts which are involved can be introduced. Electrons of one hundred electron volts or more excite and ionize gas atoms or molecules to higher energy states upon impact. Often, fluorescence results as the excited particles decay radiatively to lower states, and ultimately to the ground state.[1] Some diatomic molecules exhibit spectra which, when dispersed with sufficient resolving power, may be related to the thermodynamic properties of the gas. Figure 1.1 illustrates that point. E. P. Muntz[2] and a number of researchers[3-9] following his lead have provided descriptions of how to exploit the fluorescence characteristics to obtain gas property measurements. They have experimentally verified the basic concepts. But, at the same time their work has raised a number of specific questions about how faith-

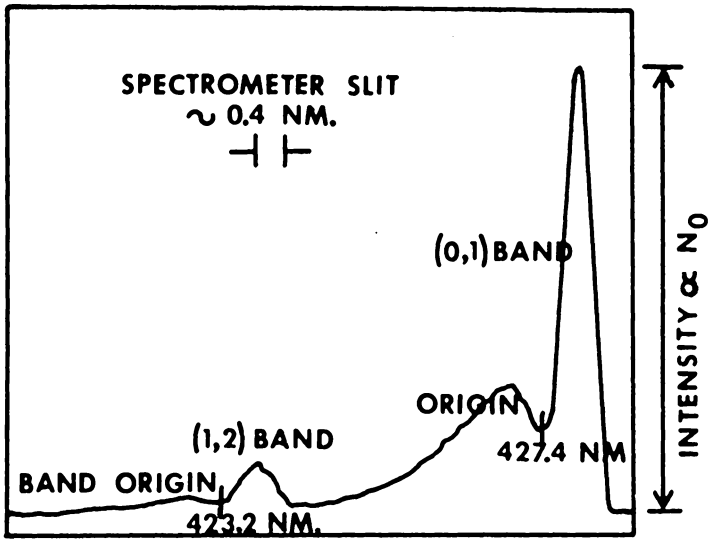

SPECTROMETER TRACE, COARSE RESOLUTION

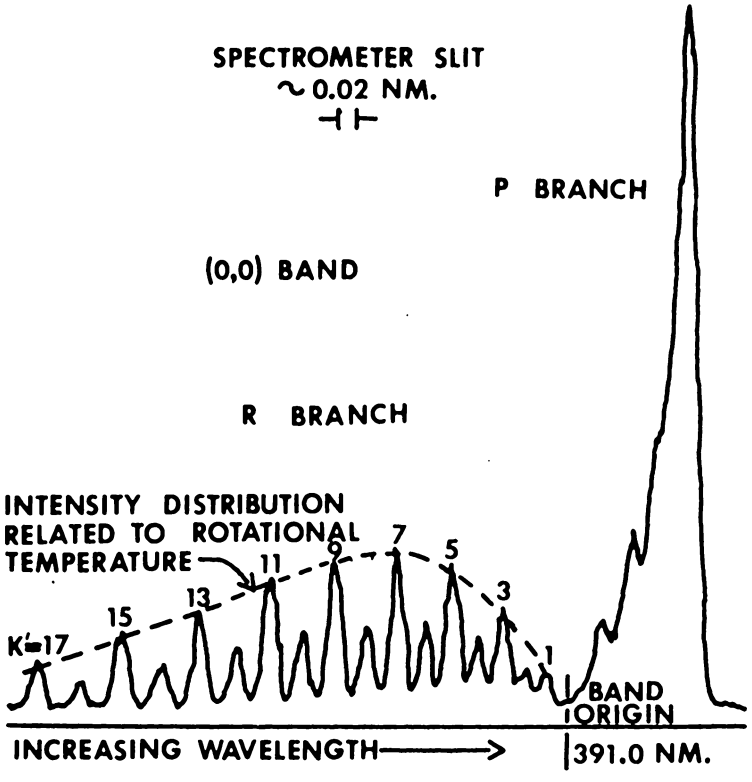

SPECTROMETER TRACE, FINE RESOLUTION

FIGURE 1.1. VIBRATIONAL BANDS OF $N_2^+(B^2\Sigma_u^+(v'K'-X^2\Sigma_g^+(v''K''))$ PRODUCED BY ELECTRON IMPACT IN N_2 AT 300° K. THE INTENSITY OF THE BAND IS RELATED TO GAS DENSITY AND THE ROTATIONAL DISTRIBUTION TO TEMPERATURE.

fully those basics are followed, particularly at low temperature ($\lesssim 100^{o}K$) and high density ($\gtrsim 10^{17} cm^{-3}$). For instance, Ashkenas[8] examined the behavior of measurement temperature values depending upon the number of rotational lines used to calculate temperature. He reported a correlation of the value of measured temperature with the number of lines used.

Within limitations, the total radiant signal emitted when electrons pass through a gas defines the density. I_s represents the total fluorescence produced and is proportional to N_o, the number density. Since the gas pressure p is a directly measured quantity and $p = N_o k_B T$, experimental results are conveniently expressed in terms of p. The translational temperature, T, must be constant.

Two steps of the process involved in measuring I_s are particularly important. Electrons impinging upon the gas excite and ionize molecules to radiative states. Muntz[3] and others[4-8] have obtained results which support the concept of treating this excitation like electric dipole radiation.

$$(\Delta N_j)_+ \text{ per unit time} = N_o Q_{oj}^{P} J_B / e \qquad (1.1)$$

Equation (1.1) describes the rate of increase in density for state j (N_j) due to electron impact excitation. J_B is the current density (amperes/m^2) and Q_{oj}^{P} the cross section for

primary (P) electron impact excitation (state o → state j). Q_{oj}^{P} is determined by invoking the electric dipole approximation to evaluate matrix elements between states o and j.

The second step to emphasize is the emission of a photon as the excited molecules decay radiatively to a lower state. Specifying helium for a moment, ionization is a rare occurrence among the direct electron processes. Excited atomic states are produced more copiously by electron impact and radiate as the excited atoms decay to lower atomic states. In either case,

$$(\Delta N_j)_{-} \text{ per unit time} = - \sum_k N_j A_{jk} \qquad (1.2)$$

represents the radiation process. A_{jk} is the spontaneous electric dipole photon emission probability (Einstein coefficient). The process represented by equation (1.2) is an approximation of well established, widely applicable validity. However, the dipole approximation applied to determine Q_{oj}^{P} of equation (1.1) is much more restricted.

Our purpose is to develop a model adequate to describe what takes place as the electron beam indirectly excites $N_2^+(B\ ^2\Sigma_u^+ - X\ ^2\Sigma_g^+)$ rotational distributions. In turn, unknown gas conditions can then be analyzed using the model and the observed spectra. While essentially experimental in content,

the work has required understanding the theory of some complex physical processes.

Those complex processes have been the subject of numerous investigations conducted in gases over the last 300 years or so, especially those related to arcs and to discharge phenomena. The results reported here represent a very modest addition to that wealth of knowledge. General treatises which serve to indicate the time span and extensive research include references 10, 11 and 12. Even with the efforts expended over the years in the physics of gases, much remains to be explained.

Attempts to quantify the processes of energy transfer took on new meaning upon the development of quantum mechanics. The great accumulation of data related to arc and glow discharge phenomena, for example, were interpreted in a much more consistent manner. Unraveling the quantum theory depended directly upon spectroscopic observations in gases, after all. Effects of the transfer of charge from ions, the transfer of energy of excitation from atoms and molecules, and the conversion of energy, from electronic to rotational for instance, produce complicated results which vary with the particular conditions. Strides are being made to solve the theoretical problems even more precisely. However, experiment still provides much of the information.

The specific situation in which nitrogen, especially the first negative band system of the ion $N_2^+(B^2\Sigma_u^+ - X^2\Sigma_g^+)$, is excited in the presence of helium has been recognized for many years. Pearse and Gaydon[13] indicate that the first negative system is the most prominent in N_2 and that these bands "occur readily in discharge tubes at very low pressure or at moderate pressure in the presence of excess helium". They list several references which date from 1925. Because these same nitrogen bands are observed in the atmosphere (auroral spectra[14], for example), charged particle impingement in known to produce them. As illustrated in the article of McCaa and Rothe[1], electrons passing through gases of many various types have produced excitation and/or ionization which in turn results in optical radiation (fluorescence).

Passing a beam of moderately energetic electrons, 5 kev or more, through pure nitrogen at low pressures, N_2^+ first negative band spectra can be readily observed. Very little interference occurs from other band systems (such as N_2 second positive, $C^3\Pi - B^3\Pi$). A number of investigators[9,15-21], prior to and since the definitive work of Muntz, have observed these bands. Energetic electrons and positive ions have produced the spectra in other experiments. Discharge and afterglow production of nitrogen spectra, described by Dunn[22] and the numerous references he cites, becomes con-

siderably more complicated than the spectra produced by electron impact of a single constituent gas.

By initiating energy transfer and charge exchange processes in a relatively well defined manner, i.e., passing a beam of electrons through the test gas, a technique is provided to study those processes. Previous work[13,23-26] has shown that small partial pressures of nitrogen present in larger amounts of helium constitutes a medium wherein significant N_2^+ first negative excitation may be observed. That particular fluorescence can be extremely useful to determine gas properties. However, even with simplifying steps as described, the spectra produced relate to the properties of the test medium in a complicated manner. Sorting out that relationship constitutes the bulk of the task undertaken here.

To accomplish that sorting process, important electron impact processes in helium must be identified. The next few paragraphs will serve to outline the nature of the effort in this regard. Direct electron impact excitation of helium by energetic electrons (26 kev) can be considered to obey selection rules for dipole radiation to a first approximation. That is, $|\Delta L| = 1$ and $|\Delta S| = 0$ apply. So, helium $He(1^1S)$ would be excited to n^1P states according to those rules. In classic papers, Lees[27] and Lees and Skinner[28] identified a number of excited helium states which are produced

as a result of electron impact. The energy of the incident electrons in this work was less than 1 kev and they observed excited helium in many other states than ^1P, violating strict obedience of the simple dipole rules (which apply to the model of electron impact processes of Muntz[15]).

Other more recent work[29-32] confirms the significant role of excited helium in other than ^1P states. St. John, Miller and Lin[29] have examined a great number of such states, giving evidence for how substantially they are populated and the particular mechanism. Cermak[30] and Holt and Krotkov[31] reported studies of n = 2 states excited by relatively lower energy electrons. vanEck and deJongh[32] observed n^1P levels. A majority of the related work with electron excitation in helium has utilized lower energy electrons, about 100 ev and less. That represents a significant difference from the effort reported here.

After the pioneering efforts to determine atomic states excited in helium by electron impact, other studies of energy transfer and collision effects have been reported. Populating the levels of types ^1D, ^1F, ^3S, ^3P, ^3D and so forth will be discussed at greater length in succeeding sections. Papers by Jobe and St. John[33] and Frish and Ionikh[34] discuss such results. The former report concerned 4F state population and the latter ^1P to ^1D energy transfer.

Drake[35] discussed how triplet states may become populated by singlet-triplet mixing. Adequately explaining the spectra observed when nitrogen electronic states are excited (and incidentally redistributed among rotational and vibrational levels) constitutes a very complicated task. This is especially true when the process is initiated by electrons but occurs mainly through transfer involving helium.

Exploratory tests in mixtures of helium and nitrogen agreed with previous work[24], indicating that a significant interaction must exist between helium atoms and nitrogen molecules when mixtures of the two are excited by electron impact. These tests were cursory observations of N_2^+ first negative band fluorescence, which included a preliminary examination of the rotational distribution within the bands. Both N_2^+, B-X, (0,0) and (0,1) bands were examined. The HeI 3^3P-2^3S (388.9 nm) line occurs within the R branch of the (0,0) band. See figure 1.2. The line renders a portion of that band virtually useless for quantitative measurements with low resolution.

These preliminary data clearly indicated that under certain conditions the nitrogen was very efficiently excited from the ground neutral $N_2 X^1\Sigma_g^+$ to the ion states N_2^+, of which $N_2^+ B^2\Sigma_u^+$ is prominent. The circumstances which produced this efficient excitation are characterized by low partial

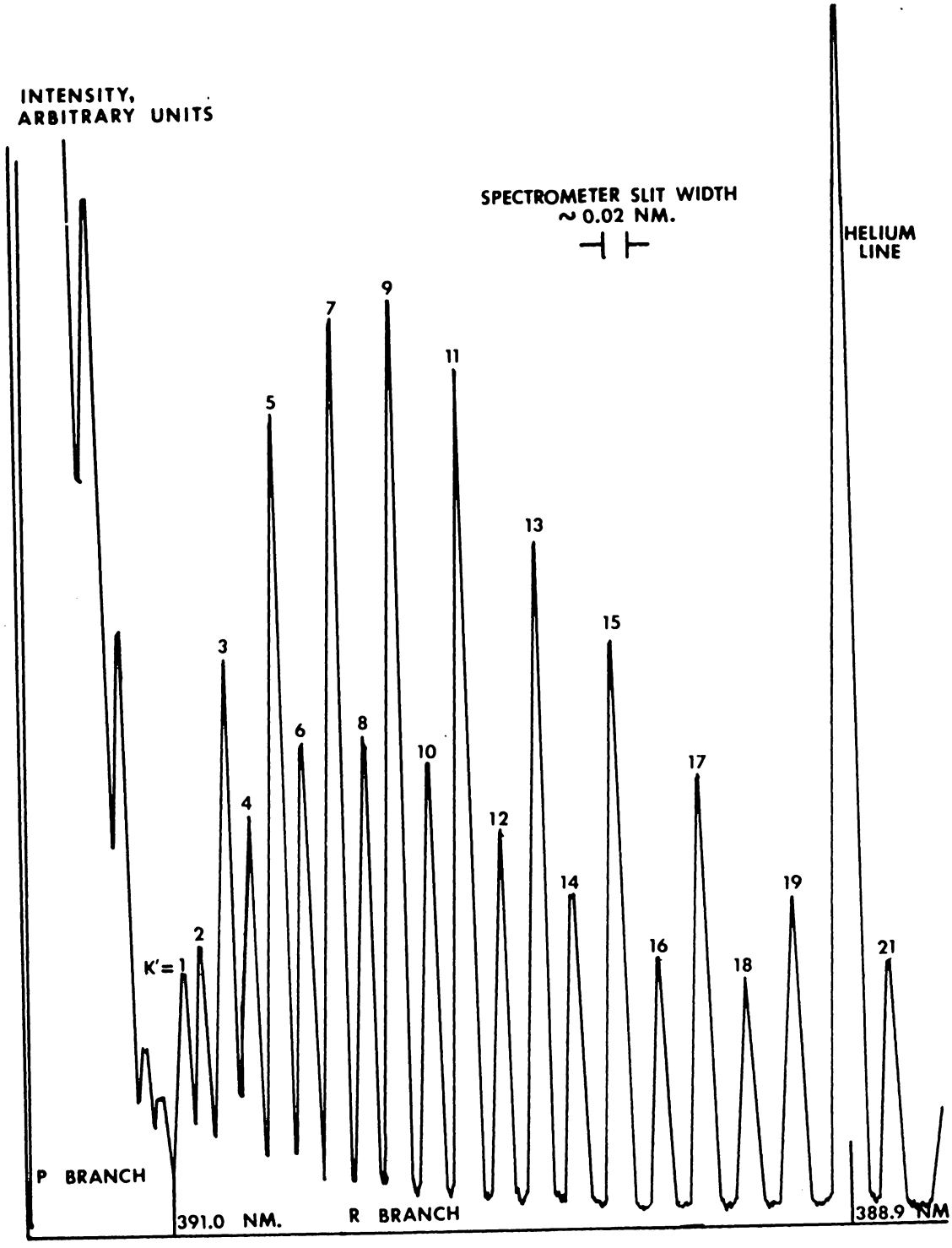

FIGURE 1.2. TRACING OF THE (0,0) BAND OF FIGURE 1.1 SHOWING THE PRESENCE OF THE HELIUM 3^3P-2^3S LINE.

pressures of nitrogen in 10 times or more as much helium. The passage of the 26 kev electron beam through the mixtures was observed to produce substantial emitted radiation. Large increases in the N_2^+,B-X fluorescence were observed as helium was added. See figure 1.3. This behavior, as will be seen later, is related to the manner in which helium excited states develop (collisional energy transfer processes).

The resolved rotational spectrum, N_2^+,B-X,(0,0) K' to K'' intensities for various K' = 0,1,2,....., showed a departure from the expected distribution according to Muntz[15] and others[36]. Results of Sebacher[24] and of Whetsel and Shofner[25] support these conclusions, that helium excitation processes give rise to an altered nitrogen spectrum. The application of electric dipole selection rules to the excitation process should be suspect. Related to that, vibrational distributions may deviate from the Franck-Condon principle of vertical transitions, which principle is illustrated in figure 1.4.

Since higher energy electrons initiate the processes in these experiments, one might expect to find some dramatic changes in the helium excited species; i.e., which ones are prominent and have the most effect. However, since the previously measured cross sections do not exhibit rapid changes away from threshold, relative populations differ slightly,

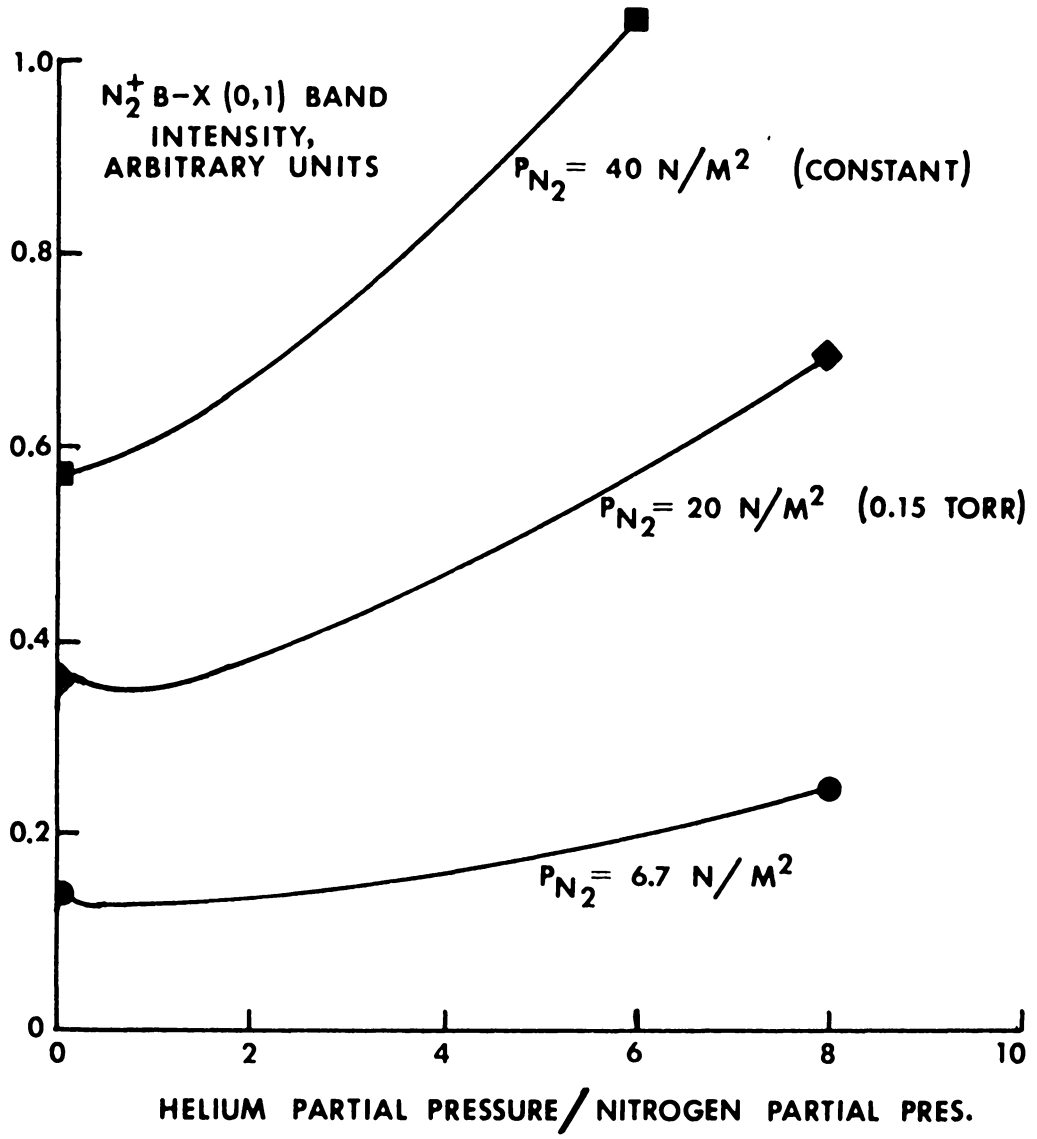

FIGURE 1.3. DEPENDENCE OF THE N_2^+ FIRST NEGATIVE BAND INTENSITY UPON THE PRESENCE OF HELIUM (EXPERIMENTAL).

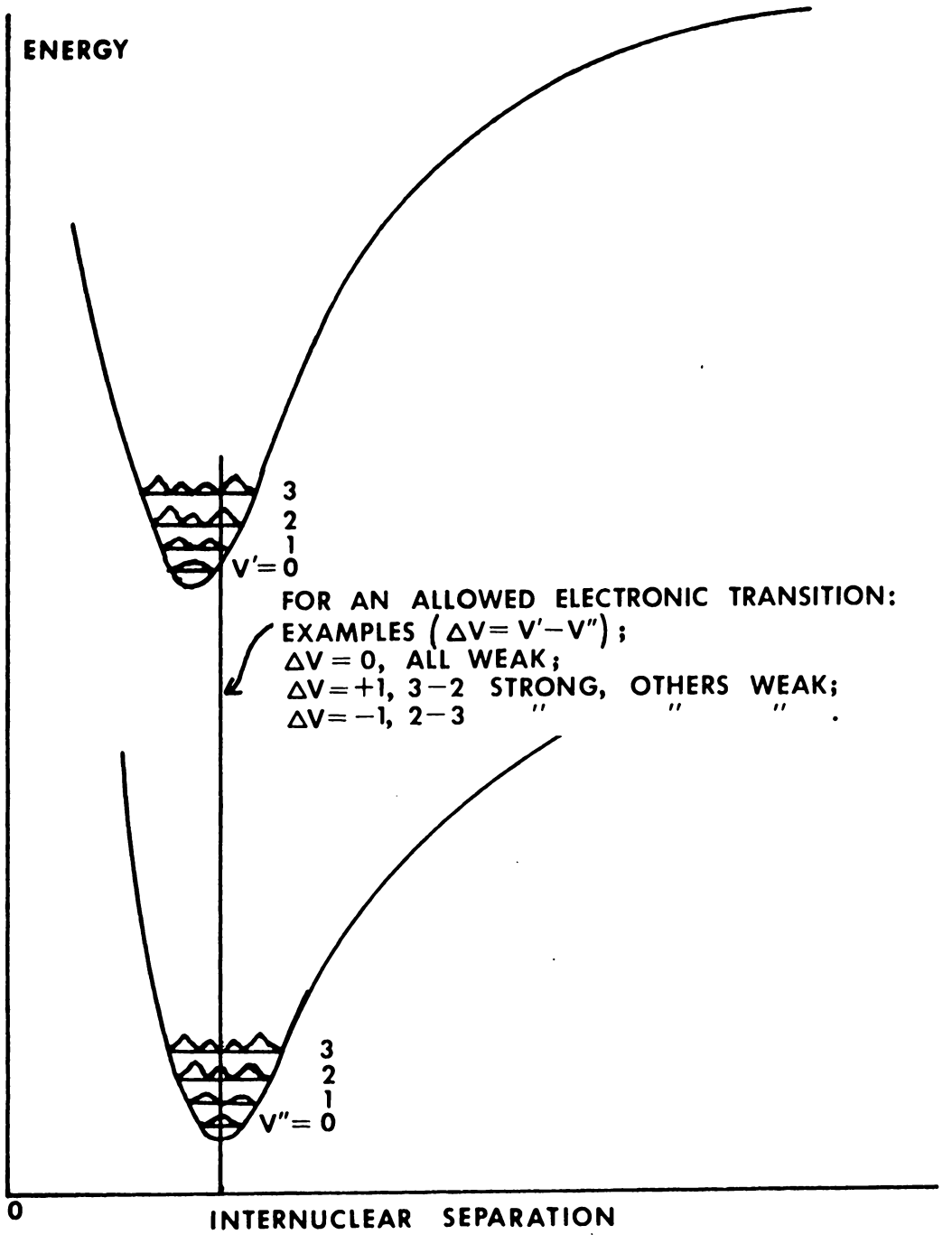

FIGURE 1.4. ILLUSTRATION OF THE FRANCK-CONDON PRINCIPLE. STRONG AND WEAK VIBRATIONAL TRANSITIONS ARE INDICATED FOR THE GIVEN INTERNUCLEAR SEPARATION .

if at all, from the lower energy excitation sources. Numerous helium excited states are generally produced, particularly helium metastable atoms, molecular helium and atomic and molecular ions. These species must efficiently excite and ionize nitrogen.

To digress a moment in concluding this chapter, abbreviations have been introduced and are continued throughout. N_2^+B for $N_2^+B^2\Sigma_u^+$ will be used, as will other single letters which designate particular molecular electronic states; N_2^+X, N_2^+C or N_2X, are examples. N_2^+, B-X is the transition from $N_2^+B^2\Sigma_u^+$ to $N_2^+X^2\Sigma_g^+$. Particular atomic electronic state designations are used for helium only as needed. He is understood to be $He(1^1S)$ in the general discussion and particular designations are not written out for He^+ or He_2^+.

2. THEORY

Helium Excitation And Energy Transfer Processes

The discussion turns now to a description of the processes initiated and sustained when a beam of electrons passes through helium, and helium containing nitrogen. Excited helium atoms, ions, and other species, such as low energy secondary electrons, are formed. Impurities other than nitrogen are present in helium but do not play a significant part, in general. This question will be addressed at greater length, however. Neon, which occurs in most bottled helium at concentrations of several parts per million, and atmospheric gases, prominently oxygen in addition to nitrogen, are the most significant impurities to be considered.

In order to develop a picture of the physical system, consider a nearly closed volume evacuable to a low pressure, approximately $1.3 \times 10^{-4} N/m^2$ (10^{-6}torr). It must be thought of as "nearly closed" because there are pumping ports, gas inlet lines and an orifice for electron entry - the last of which must be open. Helium can be contained statically within the volume defined. Its pressure can be accurately regulated from approximately one Newton per square meter to atmospheric pressure. Observations of the fluorescence produced by the interaction of the electrons with atoms and molecules in the volume are made through quartz observation

windows. Electrons pass through the test region for any arbitrary period of time, eliminating transient start up or turn off conditions from consideration. Only the longer term steady state conditions are of interest. Quite a number of research studies have reported helium excited species which are created upon electron impact[1,27-29,31,32,37,38]. The theory discussed in this chapter relates to the physical system pictured here.

Most previously reported work involved electron impingement at energies the order of 100 volts or less. Higher energies may lead to somewhat different relationships amongst the several excited species. Wine[39] provides an extensive description of these processes. Thorough reviews of the electron-atom interaction have been presented by Moiseiwitsch and Smith[40] and Massey, Burhop, and Gilbody[41]. The fundamentals of electron impact upon atomic species are widely treated in the literature and the theory is highly developed[42].

Collisional properties of gases for the range of pressures included in this work vitiate the simplified picture of helium states, excited by electron impact, decaying only by emission of radiation. Collisions occur rapidly enough that excitation transfer plays a very significant role; He*(excited helium) + He(1^1S),

excitation to states of spin 1 from the spin 0 ground state and ionization all have been observed. Ultimately, further complicating matters, nitrogen is introduced as an impurity concentration constituent. In the remainder of this chapter, the basic concepts underlying helium excitation, collisional energy transfer, and mechanisms which produce $N_2^+ B^2 \Sigma_u^+$ spectra, all developing from electron impingement upon mixtures of helium and nitrogen, are discussed.

When 26 kev electrons pass through helium without impurities present, rather extensive excitation takes place[37,40,42]. The rate of excitation can be written as

$$dN_j/dt\Big|_{\text{excitation}} = N_o Q_{oj}^P J_B/e, \qquad (2.1)$$

following the previous notation. The process itself, i.e., details of momentum exchange and selection rules based upon the interaction potential, is defined through the evaluation of Q_{oj}^P. $\frac{J}{e}_B Q_{oj}^P$ represents a probability per unit time that the ground state atom, o, will be excited to state j . If a naive analogy is made to radiation probabilities, electric dipole selection rules will provide a first approximation. Hence, applying $\Delta L = 1$ and $\Delta S = 0$ (dipole selection rules for orbital angular momentum $L\hbar$ and spin angular momentum $S\hbar$), n^1P states will be excited directly by the "allowed"

path. In reality we expect the n^1P states to exhibit relatively larger cross sections as the incident electron energy becomes large. Electron impact studies by Gabriel and Heddle[37] and many observations made in helium discharges[22] or afterglow[29,43-46] examined fluorescence for which low energy particles were responsible. The n^1P states were generally strongest.

A theoretical basis for the naive approach exists. Following Muntz[2] the total cross section for electron impact excitation in the dipole approximation can be written as

$$Q_{oj}^{D} = \frac{64\ \pi^s m_e^2 e^4}{k^2 h^4}\ |r_{oj}|^2\ \ell n\ \frac{2\ m_e v_e^2}{E_j - E_o}\ . \qquad (2.2)^{\dagger}$$

m_e is the electron mass, v_e the electron's relative velocity, e the electron charge, h Planck's constant, and k is the wave number of the incident electron. r_{oj} is the matrix element of r given by

$$r_{oj} = \int \psi_j^*\ r\ \psi_o\ d^3r \qquad (2.3)$$

which constitutes the basis for comparison with dipole radiation. These "optically allowed" transitions have an approximate energy dependence which is $E^{-1}\log E$, E being the

---

[†] See reference 42, equation (117a), p. 497.

relative kinetic energy of the incident electron.

By way of comparison, for the case where $|r_{oj}|$ vanishes, a quadrupole (next higher order) cross section can be written as

$$Q_{oj}^{Q} = \frac{128\ \pi^7 m_e^3 e^4}{k^2 h^6} |(r^2)_{oj}|^2 |E_o| . \qquad (2.4)^{**}$$

Q_{oj}^{Q} goes as E^{-1} when the orbital momentum change is zero, exhibiting a more rapid fall off with energy than Q_{oj}^{D}. Contributions of a quadrupole character are less important as the incident electron energy is increased.

Direct electron impact excitation by 26 kev electrons may be expected to develop helium excited states according to dipole rules predominantly for n^1P states, but by quadrupole and other mechanisms for singlet ^1S, ^1D, ^1F states and for triplet ^3S, ^3P, ^3D states. Put symbolically,

$$e + He(1^1S) \rightarrow e + He(n^1P) \qquad (2.5)$$

occurs via an interaction depending upon the matrix element $(f|V|i)$, $|f)$ for final state, $|i)$ for initial. $(f|V|i) \simeq (He(n^1P)|er|He(1^1S))$ for (2.5). For other states, $(f|V|i) \simeq (He(m^{2S+1}L)|e^2r^2|He(1^1S))$ written simplistically.

** See equation (117b), loc. cit.

States $m^{2S+1}L$ for L other than 1 may also be populated by other mechanisms than direct quadrupole excitation. Thus, the excitation of "optically forbidden" terms can be extensive. n^1P states may cascade by electromagnetic radiation, to $\ell^1D(n>\ell)$ for example. The rate of such transfer is represented by

$$dN_n/dt\Big|_{loss} = -\sum_{\ell} N_n A_{n\ell} = -N_n A_n, \qquad (2.6)$$

where N_n is the excited state population (n^1P), $A_{n\ell}$ the Einstein coefficient, $A_n = \sum_{\ell} A_{n\ell}$ and $\ell = 2$ to n-1.

$$dN_\ell/dt\Big|_{excitation} = \sum_{n} N_n A_{n\ell}, \quad n > \ell \qquad (2.7)$$

represents the radiative decay as a rate of excitation for the ℓ states. By consulting table I of Gabriel and Heddle[37] for values of $A_{n\ell}$, the contribution to other than ^1P states are seen to be substantial for principal quantum numbers n (of n^1P) 1 through 4. They are insignificant above 4.

Populating 3^1D, 2^1F and triplet states requires more than simple direct electron excitation. Generally, the second step, atom-atom energy transfer, proceeds at a rate described by

$$dN_j/dt\Big|_{excitation} = \sum_{x} Z_{xj} N_x, \qquad (2.8)$$

where state j is populated by collisions of atoms in state x with ground state atoms. Z_{xj}, a probability of collisional excitation, is related to the ground state density N_o by $Z_{xj} \propto N_o Q_{xj} v$; v is the relative velocity of collision. Considering the atom-atom collisions as a loss term,

$$dN_j/dt\Big|_{loss} = - \sum_x Z_{jx} N_j, \qquad (2.9)$$

where now atoms of state j are lost by energy transferred through collisions.

To this point, the description has addressed the plausibility of excitation to and from singlet states. $He(1^1S) \rightarrow He(n^1P)$ occurs directly excited by primary electrons. Other singlet states are produced by primary electrons through a weaker process, and by the secondary processes of radiative and collisional transfer. Treatment of triplet states has been only peripherally treated. These latter are of the most interest, however, because ultimately nitrogen excitation by helium depends upon the triplet metestable, 2^3S.

Electron impact excitation of states which have spin 1 is forbidden by the Wigner spin rule, $\Delta S=0$, for total spin quantum number S. Yet quite a large number of helium atoms are observed to become excited to ^3S, ^3P, ^3D states[27-29,33,47-49]. A mechanism which explains the rapid and substantial develop-

ment of triplet population was developed by Lin and Fowler[50].

Observations in early studies by Lees and Skinner[27,28], that triplet states were strongly populated during electron excitation, have been confirmed in more recent research[51,52]. Transfer represented by

$$He(1^1S) + He(n^1P) \rightarrow He(1^1S) + He(n^3D) \qquad (2.10)$$

has been observed, and Lin and Fowler explained how such a transfer process can occur based upon the higher principal quantum states ($n \geq 4$) and violation of Russell-Saunders coupling. Their concept, borne out by experiments[48,49,51,52] includes the steps

$$He(1^1S) + He(n^1P) \rightarrow He(1^1S) + He(n^{1,3}F) \qquad (2.11)$$

followed by the decay

$$He(nF) \rightarrow He(mD) + h\nu, n \geq m. \qquad (2.12)$$

The key is the mixing of singlet and triplet states for F configurations with $n \geq 4$. Thus, the ^3D states become strongly populated without violating the spin rule in the direct electron excitation.

If one considers the relative contributions to the helium electronic energy, of the electrostatic interaction term for electrons (which couples spins of the two electrons) as compared with terms coupling spin to orbital angular momentum (spin-orbit interaction and other relativistic correction terms) one observes the following. At $n \leq 3$, and

$L \leq 2$, the Russell-Saunders (L-S) coupling scheme is excellent and the electron interaction term dominates the energy correction for all interaction terms. At larger values of L and higher n, the exchange integral has become smaller than other terms. Then the L-S coupling is not strong. The wave function for nF states becomes $\psi(nF) = c_1\psi(n^1F) + c_2\psi(n^3F)$. Upon collision we will have, for an atom-atom interaction potential V_{a-a}, the expression

$$(f|V_{a-a}|i) \sim (c_1\psi(n^1F) + c_2\psi(n^3F)|V_{a-a}|\psi(n^1P)) \qquad (2.13)$$

which symbolically represents the first order matrix element. This simply illustrates the mixing of states.

Approximations which are used in the interaction potential V_{a-a} are low order, therefore, indicative of a solution and its associated behavior, but not precise. Higher order terms than the lowest dipole-dipole interaction will permit $\Delta L = \pm 1$, whereas the dipole-dipole term itself does not ($L = \pm 2, 0$). Wine[39] questions the applicability of the transfer selection $\Delta L = 0, \pm 2$. He concludes that $\Delta J = \Delta L = \pm 1$ cannot be ruled out and that $\Delta J = \Delta L = 0$ seems to provide a better interpretation of some D state transfer. There is general agreement that the populating mechanism maintains the spin rule validity.

Substantial population of the $He(2^3S)$ metastable state is virtually assured by a mechanism which populates higher

triplet levels. The reverse collisional transfer process from triplet states is reduced quite significantly[47,48]. Radiative decay is rapid[37] enough to produce many atoms in lower triplet levels. Absorption experiments in discharges and helium afterglow have shown that He(2^3S) atoms are formed in relatively large concentrations. Observations of the (3^3P-2^3S) line at 388.9 nm indicates the formation of substantial amounts of He(2^3S). Rapid collisional conversion of He(2^1S) to the 2^3S has also been observed[46,49,53,54]. In their review of the reported de-excitation of He(2^3S), Elder and Wintzer[55] observed that the dominant loss factor was diffusion to the container walls. Since diffusion is relatively slow, a large steady state population may develop. These authors also point out that impurities may be very effective in removing the 2^3S energy, among which nitrogen is prominent.

Atomic and molecular helium ions, and helium molecules are known to occur in helium discharges and afterglows. Each potentially contributes to the processes in helium containing impurity nitrogen. Consulting the relative energy scheme of figure 2.1, the molecule He_2 does not play a role in the excitation of $N_2^+B\,^2\Sigma_u^+$. Both atomic and molecular ions are energetically in the range where they may contribute to N_2^+B production. The methods and rates of He^+ and He_2^+ pro-

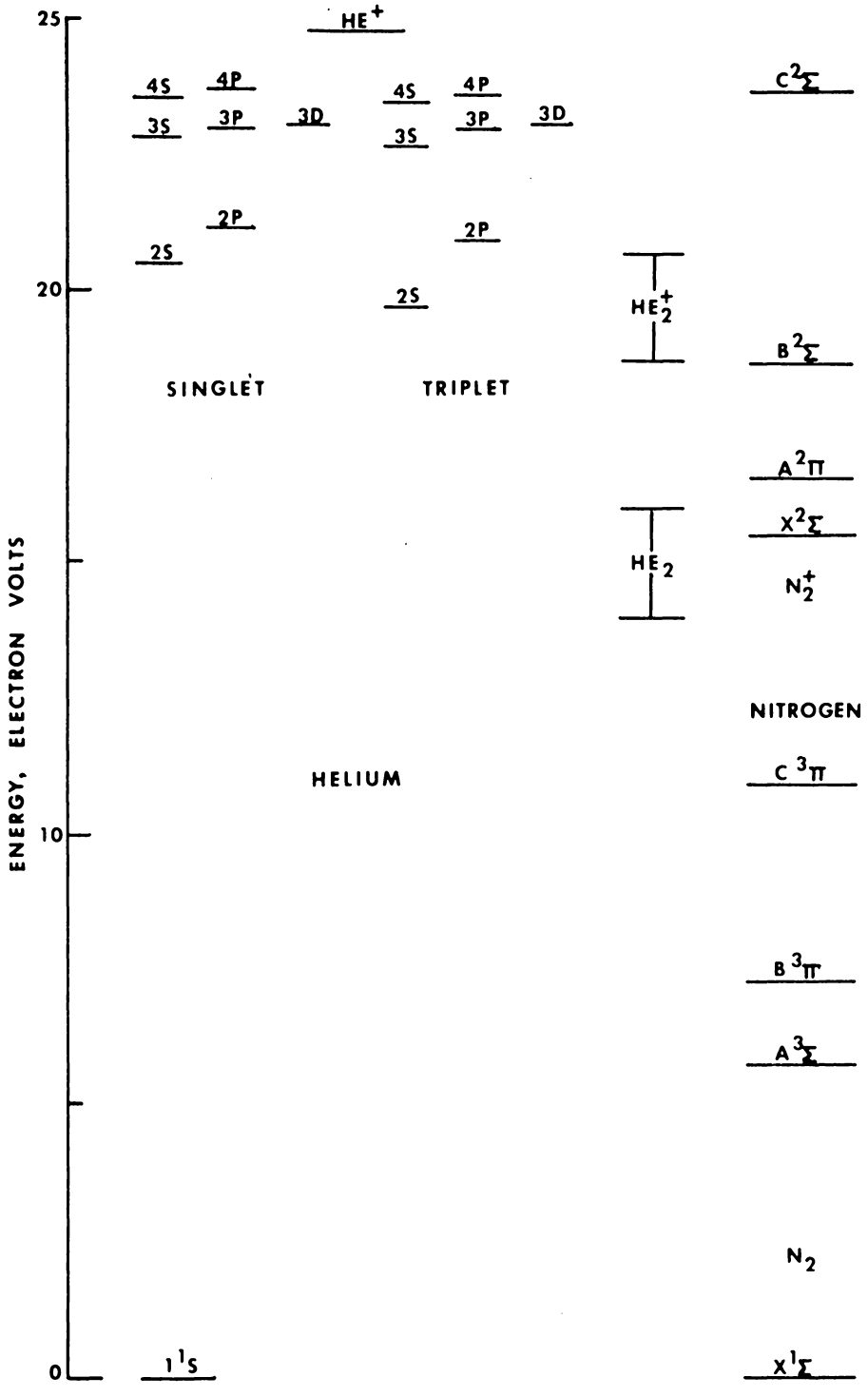

FIGURE 2.1. PARTIAL ENERGY LEVEL DIAGRAM SHOWING APPROXIMATE ENERGIES FOR HELIUM AND NITROGEN STATES. (ONLY THE LOWEST, v=0, VIBRATIONAL LEVEL IS INDICATED FOR N_2.)

duction are now considered.

He^+ can be formed by direct impact ionization of $He(1^1S)$. This source appears at first to be relatively weak, since the cross section for ionization by electron impact at 26 kv is roughly $7 \times 10^{-19} cm^2$ [56]. Other mechanisms of production include

$$e_s + He^* \rightarrow He^+ + 2e_s \ , \qquad (2.14a)$$

$$He^* + He^* \rightarrow He^+ + He + e_s . \qquad (2.14b)$$

e_s signifies secondary electron and He* the excited helium states. Because secondary electrons are generally of very low energy[2], He* in (2.14a) must be rather highly excited (within a few ev of ionization). (2.14a) may be unlikely even if the cross section is large. (2.14b) should also be a relatively unusual occurrence. Dunn[22] implies that metastable atoms give rise to the only measurable He^+ production via (2.14b). Maguire[57] concluded from indirect evidence that substantial $He(3^1P)$ population is directly attributed to secondary electron excitation. Wine[39] concluded that secondaries contribute significantly to direct excitation, but he noted that the number of them per unit path length decreased as the primary electron energy increased. Both of these reports support the occurrence of a significant ionization.

While direct primary ionization seems to be the most

likely production mechanism, it does exhibit a rather small cross section. In comparison to apparent cross sections for a number of atomic excited species which are less than $10^{-19}cm^2$, ionization may be fairly competitive. He^+ doubtless occurs as abundantly as some higher He* species do.

The ion, He_2^+, is present as the result of several production mechanisms. Previous research[49] has shown that He_2^+ dominates over He^+ in concentration at pressures above 10^2 N/m^2. He_2^+ develops by

$$He^+ + 2He \rightarrow He_2^+ + He \qquad (2.15a)$$

$$He^* + He \rightarrow He_2^+ + e \qquad (2.15b)$$

$$He^M + He^M \rightarrow He_2^+ + e \qquad (2.15c)$$

He^M here identifies $He(2^3S)$ and $He(2^1S)$. One of the fundamental references concerning the formations of ions like He^M is Hornbeck and Molnar[58]. They attributed the ion production to (2.15b), producing and identifying it by mass spectrometric means at low pressures (10^{-2} to 1 N/m^2). They further suggested that He* of (2.15b) did not include He^M due to the threshold energy required to form He_2^+.

Process (2.15b) should dominate the other two at low pressures. (2.15a) is a three body collision and (2.15c) depends upon the collision of one collision product with another. Results reported by Wellenstein and Robertson[59]

support (2.15b) as the source of He_2^+. The rate of production, 10^{14} to 10^{15} $sec^{-1}cm^{-3}$ in a discharge at 5 milliamperes current and $4x10^2$ N/m^2 pressure, is the same order or one order of magnitude less than the primary production rate of excited atoms. The rate of 3^1P production for the same conditions is about 10^{15}-$10^{16}sec^{-1}cm^{-3}$. Steady state He_2^+ population may approach and exceed particular excited atomic species. The loss rate of He_2^+ will be dominated by ambipolar diffusion at low pressure. Thus, He_2^+ may develop a relatively large steady state concentration at appropriate gas conditions.

If, in addition to (2.15b), the process (2.14a) becomes significant at higher pressures ($>10^3$ N/m^2), the amount He_2^+ may become important. Recombination serves to limit its concentration, but He_2^+ is plentiful in the helium excitation.

Having reviewed at some length the occurrence of excited species in pure helium under electron impact, consider now the addition of some nitrogen impurity. The amount of impurity dealt with in this work is typically less than one part in ten. (Experience in wind tunnel facility testing indicates that 400 parts per million represents a realistic maximal concentration.) 26 kev electrons pass through a chamber containing helium with such small

concentration of nitrogen. What processes occur? Evidence developed in past studies has been reviewed. Some of the states involved have been identified. The specific question addressed by the experiments to be reported is; Which processes affect the $N_2^+B^2\Sigma_u^+$ excitation and ionization?

Atomic excitation processes depend on resonance or near resonance conditions. Likely processes exhibit small differences of energy between the interacting species. Figure 2.1 illustrates approximately the relationship for helium and nitrogen energy states. The figure provides an idea of which exchanges are favored upon collision. The smallness of ΔE, the energy "defect" between the colliding species, is an approximate indicator, but does not absolutely exclude any particular process. Lower vibrational levels of N_2^+B have nearly the same energy as the $He(2^3S)$ and He_2^+ species of excited helium.

The ion He^+ must also be considered. Energetically, the ground state ion level lies close to vibrational levels in $N_2^+C\,^2\Sigma_u^+$ and $D^2\Pi_u$. Transfer from the He^+ to N_2^+C does occur[60] by

$$N_2(X^1\Sigma_g^+)+He^+(^2S) \rightarrow N_2^+(C^2\Sigma_u^+)+He(^1S)+0.28ev. \quad (2.16)$$

N_2^+C does not radiatively decay to N_2^+B, nor does N_2^+D, but they may transfer energy upon collision with particle A, as

$$N_2^+C,D + A \rightarrow N_2^+B + A' \qquad (2.17)$$

Inn[60] and others[61-63] suggest N_2^+ rapidly converts to N^+ through a predissociation mechanism. However, the possibility remains that He^+ may affect N_2^+B by a two-step process. Evidence supports the concept that $He(2^3S)$ and He_2^+ dominate the excitation and ionization of N_2.

Since N_2^+B states are readily excited and radiate strongly in the visible and near uv portion of the spectrum, first negative bands are very useful. They afford an accessible tool to deduce the properties of the gas. Distinct changes in the spectrum when nitrogen constitutes an impurity in helium have prompted the experiments described in the remainder of this report. In order to facilitate that discussion and to conclude the present theory chapter, the rotational intensity distribution for N_2^+,B-X in pure nitrogen is described.

Nitrogen Fluorescence

In order to define working relationships for the experimental parameters to be described, a brief outline of the dipole excitation model for the rotational and vibrational transitions is presented here. The rate of excitation to $N_2^+B^2\Sigma_u^+(v',K')$ from $N_2X^1\Sigma_g^+(v_1'',K_1'')$ can be written as

$$R_{ex} = \sum_{v_1''K_1''} \frac{J_B}{e} Q_{XB}^{P} q_{v_1''v'} N_{K_1''}^{v_1''}(N_2). \qquad (2.18)$$

e is the electronic charge, $Q_{XB}^{P}q_{v''v'}$ is Q_{oj}^{P} where $q_{v''v'}$ is the Franck-Condon factor for the vibrational levels and $N_{K_1''}^{v_1''}(N_2)$ is the number density of nitrogen molecules in the v_1'', K_1'' state. The quantum number K specifies the angular momentum of the rotational state. Spin is neglected because these are doublets which are not generally resolved. The dipole approximation for electron impact excitation yields the requirement that $K' = K_1'' \pm 1$, limiting the $\sum_{K_1''}$ to two terms. Q_{XB}^{P} includes the rotational dependence of the process. For room temperature and below, only the $v_1'' = 0$ state of $N_2 X^1\Sigma$ is populated significantly. Hence, the $\sum_{v_1''} \ldots q_{v''v'}$ becomes $\ldots q_{ov'}$.

Ideally, radiative decay constitutes the only loss mechanism. The standard intensity expression, written in general terms, is

$$I_{K'K_2''}^{v'v_2''} = N_{K'}^{v'} h\nu_{K'K_2''}^{v'v_2''} A_{K'K_2''}^{v'v_2''} \qquad (2.19)$$

I is the intensity, h Planck's constant, ν frequency, and A Einstein's spontaneous emission coefficient. The subscript

2 in v_2'' and K_2'' designates the $N_2^+X^2\Sigma$ state. $N_{K'}^{v'}$ is determined by the rate equation, $dN_{K'}^{v'}/dt = R_{ex}$ - radiative loss.

Hence, $$dN_{K'}^{v'}/dt = R_{ex} - \sum_{v_2''K_2''} N_{K'}^{v'} A_{K'K_2''}^{v'v_2''}. \qquad (2.20)$$

This expression, when $dN_{K'}^{v'}/dt = 0$ for the equilibrium case, permits $N_{K'}^{v'}$ to be written in terms of transition probabilities, the ground state rotational distribution, beam current density and so forth.

$$N_{K'}^{v'} = \frac{(J_B/e)Q_{XB}^{P} q_{ov'}(N_{K'-1}^{O} + N_{K'+1}^{O})}{A_{K'K'-1}^{v'v_2''} + A_{K'K'+1}^{v'v_2''}}. \qquad (2.21)$$

A somewhat complicated expression results when $N_{K'}^{v'}$ is substituted into equation (2.19). The result, for rotational lines of the R branch, is expressed as

$$I_{K'K'-1}^{v'v_2''} = \frac{\frac{CK'\sigma_{K'K'-1}^{4}}{2K'+1} q_{v'v_2''} \frac{N_o}{Z_v(T_v)} \frac{q_{ov'}}{Z_R(T_R)} F(K;T_R)}{A_{K'K'-1}^{v'v_2''} + A_{K'K'+1}^{v'v_2''}}. \qquad (2.22)$$

C is a constant. σ represents the transition wave number, N_o the nitrogen number density and Z_v and Z_R are the vibrational

and rotational partition functions, respectively. The function F includes two terms, one for K'+1 and one for K'-1. The desired result is a relationship between the measured intensity and the rotational temperature. Due to the nuclear symmetry requirements, since nitrogen is homonuclear, I for even K' is multiplied by a factor of ½. This accounts for the nuclear spin weighting of the rotational states.

The concluding expression can be written

$$\ell n \frac{I^{v'v''_2}_{K'K'-1}}{K' (G) \sigma^4_{K'K'-1}} = \frac{-K'(K'+1)hc}{k_B T_R} \qquad (2.23)$$

(G) is an expression which includes F from equation (2.22) and depends upon K' and T_R. Hence, the solution requires an iterative procedure. (G) values are calculated for an estimated T_R and solution is found, either graphically or by least squares analysis. Then an improved T_R value is used. The process is repeated until the convergence is completed. The linear relationship of $\ell n\ (I^{v'v''_2}_{K'K''_2})$ with T_R and K'(K'+1) is important. Throughout the text, $I^{v'v''_2}_{K'K''_2}$ will be abbreviated as $I_{K'}$, when the other parameters are fixed.

3. DEVELOPMENT OF THE EXPERIMENTS.

Preliminary Experiments

Previous work[13,22,26] supports the existence of an enhancement of nitrogen fluorescence, when observed emanating from discharges or afterglow sources rich in helium. Details, particularly of the nitrogen first negative system rotational intensity distributions in such mixtures, are sketchy. The processes which occur upon the passage of a beam of energetic electrons through helium, which contains a small amount of nitrogen, also have yet to be clearly identified. Our initial experiments, which purpose was to verify such enhancement, will be outlined in the next few paragraphs. For the sake of convenience, two different test vessels were utilized. (The experience with them contributed to the selection of a mixing chamber for the final series of observation, as discussed later.)

The initial observations of nitrogen spectra from nitrogen mixed in helium were of N_2^+ first negative (hereafter N_2^+,B-X) (0,0) and (0,1) bands and spectrometer survey scans of 350.0 - 550.0 nanometers. The respective band heads for (0,0) and (0,1) bands, usually the strongest, are 391.4 and 427.8 nanometers. Both are shaded toward the blue end of the spectrum. These scans were made in an apparatus consisting of an electron beam generating system, exiting into a small stainless steel vacuum chamber,

complete with a number of access parts and windows. The configuration is illustrated in figure 3.1. The electron gun has been described elsewhere[64,65]. Additional details will be given later in this section. For the discussion here, suffice it to say that the potential was maintained at 26 kilovolts and that beam currents up to 1 milliampere were used. Two small orifices (1 millimeter diameter, 25 millimeters in length) provided a pressure differential between the filament region of the electron gun (kept at $10^{-2}N/m^2$ or less) and the test gas region. This permitted pressures as high as $10^3N/m^2$ to be used. The beam travelled approximately 10 cm from the gun exit orifice to point of observation. Quartz windows and optics permitted unattenuated observations to wavelengths as short as 320 nm. Gas bleed-in ports and the vacuum pump attachment are indicated in the figure. The entry of gases into the chamber was controlled by means of sensitive needle valves.

Basically, two types of tests were conducted using this chamber. One was to substantiate the manner of mixing the gases. The other was to observe certain selected fluorescence, including the (0,1) band of nitrogen and the 3^1P-2^1S transition of helium using interference filters. The filters were centered at 426.6 nm and 501.6 nm, respectively. In addition, survey spectra were recorded in the wavelength

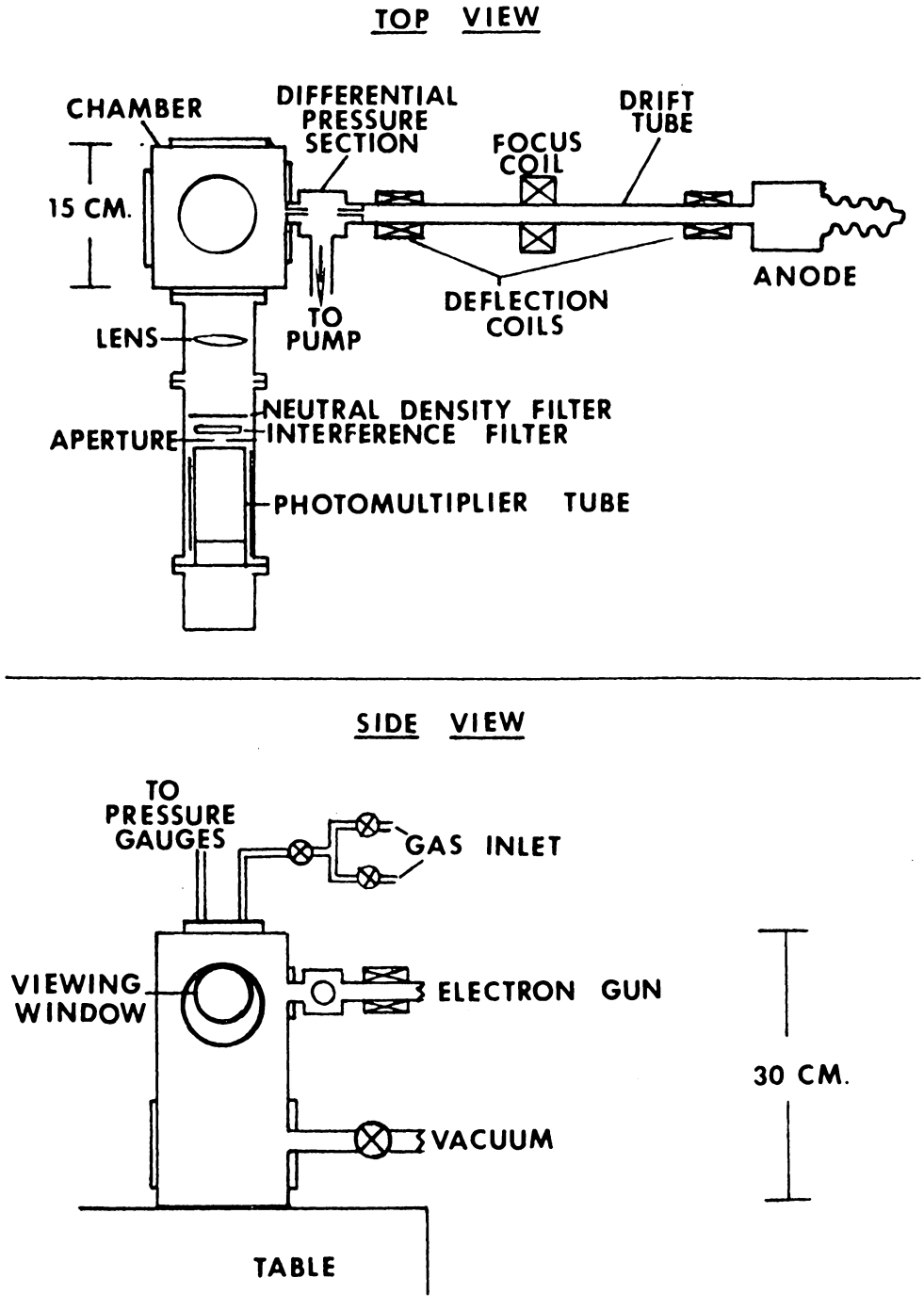

FIGURE 3.1. TOP AND SIDE VIEWS OF THE ELECTRON GUN ASSEMBLY, MOUNTED IN ONE OF THE PRELIMINARY CONFIGURATIONS.

range 350 - 550 nm using a scanning spectrometer.

The gases were mixed by first admitting one into the chamber, to a pressure determined by a mercury manometer (McLeod gauge). After dynamic equilibrium was established, the second gas was admitted until the desired total pressure and mixture were achieved. The equilibrium was considered dynamic because the chamber was not a closed system. Orifices permitted the electron entry, which caused a slight vacuum effect through the differential pressure section.

Two methods were used to confirm that this technique achieved and maintained proper mixtures. First, a stainless steel capillary tube was connected to the chamber and to a helium leak detector (a gas mass analyzer tuned to helium). The tube provided a pressure differential between the chamber and leak detector such that the requirement to maintain low pressure in the detector ($p \leq 10^{-2} N/m^2$) was met.

Partial pressures of helium were determined independently of the McLeod gauge reading by obtaining a meter deflection reading from the leak detector. A standard leak was used to calibrate the detector, allowing meter readings to be converted to flow rate.

Flow rates were converted to pressure at the test chamber by knowing the capillary conductance. A linear

relationship existed between the leak detector and the chamber for a limited pressure range, which corresponded to the molecular flow regime. When the chamber pressure became too large (>40 N/m^2), the mixture reading erred. However, in this lower pressure range the method of mixing was confirmed to $\pm 20\%$ or better.

In order to support the leak detector results at higher pressures, so-called "grab samples" were taken, then analyzed mass spectrometrically. A stainless steel sampling bottle (approximately 0.1 liter volume) was attached to the chamber through a small opening. The bottle had been previously evacuated to $10^{-4} N/m^2$ or lower pressure. Once the mixture had been developed, the sample was obtained by opening a stopcock on the bottle for several seconds to attain equilibrium. Then the stopcock was closed. The captured sample was analyzed by attachment to a mass spectrometer and reversing the process. The best samples were obtained at fairly high test chamber ($\geq 4 \times 10^2 N/m^2$) pressures. Even for very large ratios, 1000 times more helium than nitrogen, the mixtures were confirmed to be correct with $\pm 10\%$.

Either of two optical systems recorded the fluorescence produced as the electron beam passed through the mixture. As depicted in figure 3.1, the interference filter obser-

vation system consisted of a simple lens, narrow band-pass filter, neutral density filter, aperture (to limit the source volume) and photomultiplier detector. The aperture was square, 2.5 cm on a side, permitting observation of a region approximately 3.75 cm square at the electron beam position, due to the lens magnification. The light collected by the lens was focused at the aperture, just ahead of a photocathode. It passed through the filter as a converging beam, thus changing the effective filter characteristics (broadening the half width). Neither of the filters was severely affected. For the (0,1) band of N_2^+,B-X, the filter full width at half maximum transmission was 0.9 nm, centered at 426.6 nm for normal incidence. Its effective halfwidth became roughly 2.5 nm. A similar change occurred for the helium filter. The broadening did not overlap any spectral feature of the other gas.

Because the total fluorescence produced by the electron beam is proportional to the gas density, these filter detector systems were intended to monitor one particular spectral feature, which represented the partial pressure (density). When radiation is the only significant decay mode for N_j, as defined earlier, we have

$$N_o Q_{oj}^P J_B / e = \sum_k N_j A_{jk}. \qquad (3.1)$$

Therefore, $$N_j = N_o Q^P_{oj} J_B / e \sum_k A_{jk} \quad (3.2)$$

The intensity of transition j to m, to which the recorded signal is proportional, is

$$I_{jm} = N_j h\nu_{jm} A_{jm}. \quad (3.3)$$

Since $\sum_k A_{jk}$ = constant for a given specie and J_B is a measured quantity $I_{jm}/J_B \propto N_o$. A single transition may represent the gas density. In the case of nitrogen, the signal is a sum over several rotational lines within one vibrational band, weighted by the interference filter characteristics.

Results of this preliminary phase are summarized in figures 3.2 and 1.3. The signal at 501.6 nm in helium decreases as nitrogen is added, rapidly at first, then leveling out. Quite the opposite sort of behavior characterizes nitrogen's signal as helium is added. The observed fluorescence enhancement of nitrogen in mixtures led to the investigation of its rotational structure.

The one-half meter scanning spectrometer, shown in figure 3.3, was utilized to record qualitative surveys of the spectral region between 350 - 550 nm. The effective spectral resolution was 0.4 nm and the rate of scan was 5.0 nm per minute. Table 3.1 lists the prominent features

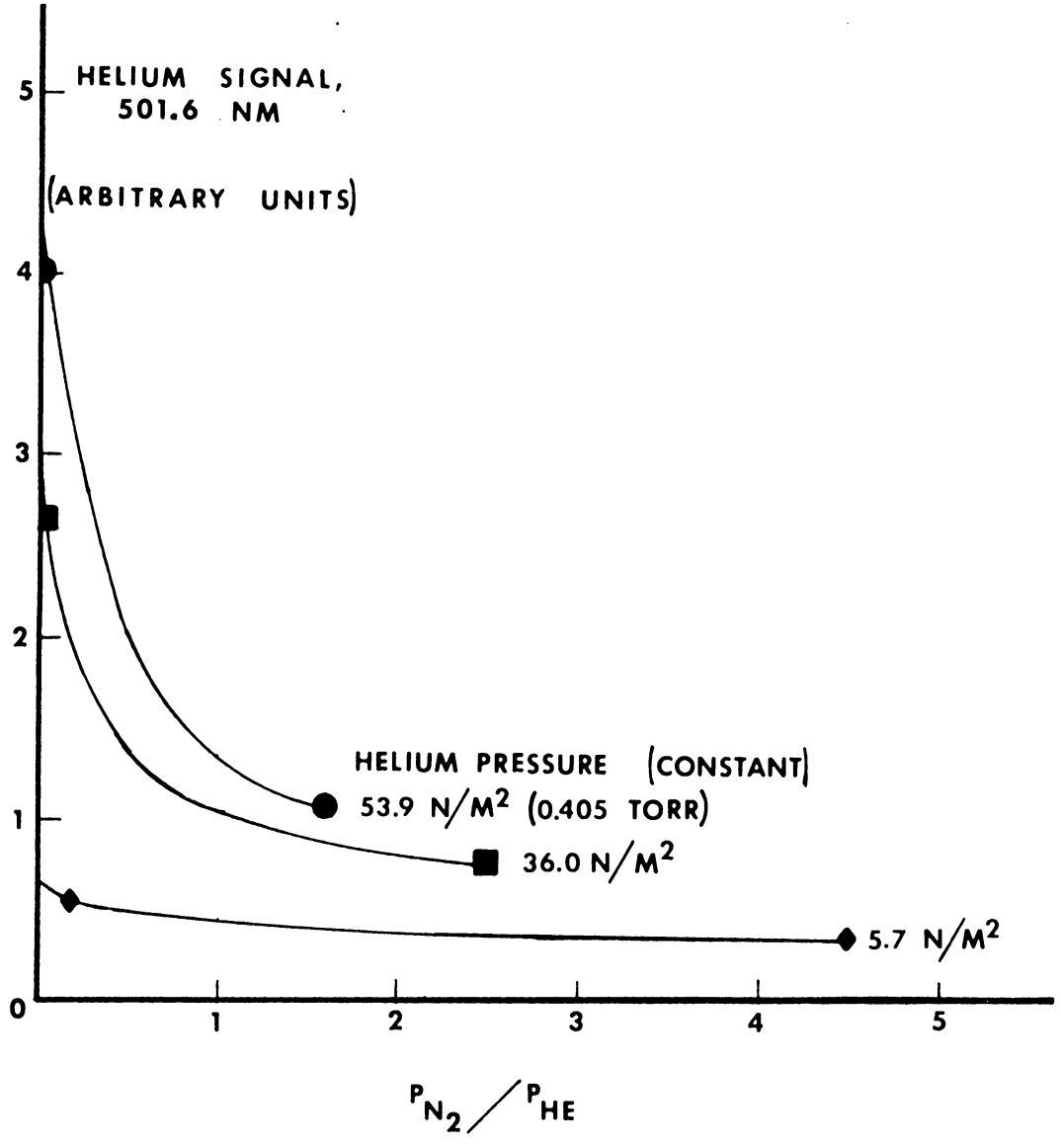

FIGURE 3.2. VARIATION OF THE HELIUM 3^1P-2^1S INTENSITY WITH MIXTURE, AS OBSERVED IN THE APPARATUS OF FIGURE 3.1.

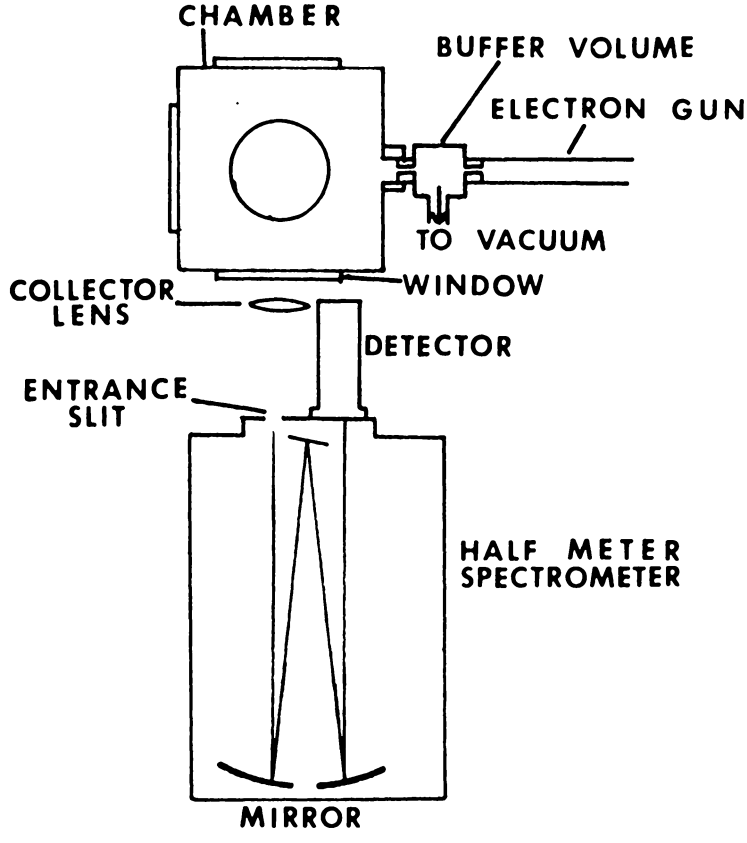

FIGURE 3.3. SPECTROMETER ARRANGEMENT USED TO OBTAIN SPECTRAL SURVEY.

Table 3.1. Spectral Features Observed In A Typical Spectral Survey.*

Spectral Feature	Assigned Wavelength
N_2^+,B-X, (5,4)	353.26 nm.
" " , (4,3)	353.83
" " , (3,2)	354.89
" " , (2,1)	356.39
" " , (1,0)	358.21
He I, 5^1P-2^1S	361.36
" , 8^3D-2^3P	362.43
" , 7^3D-2^3P	370.50
" , 6^3D-2^3P	381.96
N_2^+,B-X, (2,2)	385.79
" " , (1,1)	388.43
He I, 3^3P-2^3S	388.88
N_2^+,B-X, (0,0)	391.44
He I, 8^1D-2^1P	392.65
" , 4^1P-2^1S	396.47
" , 7^1D-2^1P	400.93
" , 7^1S-2^1P	402.40
" , 5^3D-2^3P	402.62
" , 5^3S-3^3P	412.08
N_2^+,B-X, (4,5)	414.05
He I, 6^1D-2^1P	414.38
N_2^+,B-X, (3,4)	416.68
" " , (2,3)	419.91
" " , (1,2)	423,65
" " , (0,1)	427.81
Hg (tentative)	435.8
He I, 5^1D-2^1P	438.79
" , 5^1S-2^1P	443.76
" , 4^3D-2^3P	447.15
N_2^+,B-X, (1,3)	465.18
" " , (0,2)	470.92
He I, 4^3S-2^3P	471.31
" , 4^1D-2^1P	492.19
" , 3^1P-2^1S	501.57
" , 4^1S-2^1P	504.77

*Nominal Test Conditions: 1.3 N/m^2 N_2 partial pressure; 14.1 N/m^2 He partial pressure. The spectrometer output was set to keep the most prominent helium features on scale.

observed during the course of several preliminary tests. Each survey scan was divided into 4 segments, in order to keep the duration abbreviated and the uncertainty in mixture small. A segment was accomplished in less than 15 minutes; 4-5 minutes to establish a mixture and $\sim$10 minutes to scan 50 nm. While the rate of pressure rise was not precisely determined, the 15 minute period was brief enough to assure that only small changes occurred in the observed fluorescence.

Figure 3.4 illustrates the apparatus utilized to make preliminary rotational spectra measurements of the N_2^+, B-X (0,0) and (0,1) bands in mixtures. A somewhat larger test chamber was used, with the electron gun mounted as indicated and a 1 meter focal length, Czerny-Turner scanning spectrometer positioned as shown. When properly evacuated (for several days) with no exposure to atmospheric conditions, this chamber "leaked" upward in pressure at less than $10^{-2} N/m^2$ per minute, an improvement over the previously described chamber. Spectrometer resolution was 0.04 nm and the scanning rate 1.25 nm/min. The total test time necessary to record the rotational intensity distribution of one band was less than 5 minutes assuring that pressure changes were negligible for all tests. Table 3.2 includes the parameters used in the preliminary test series, which

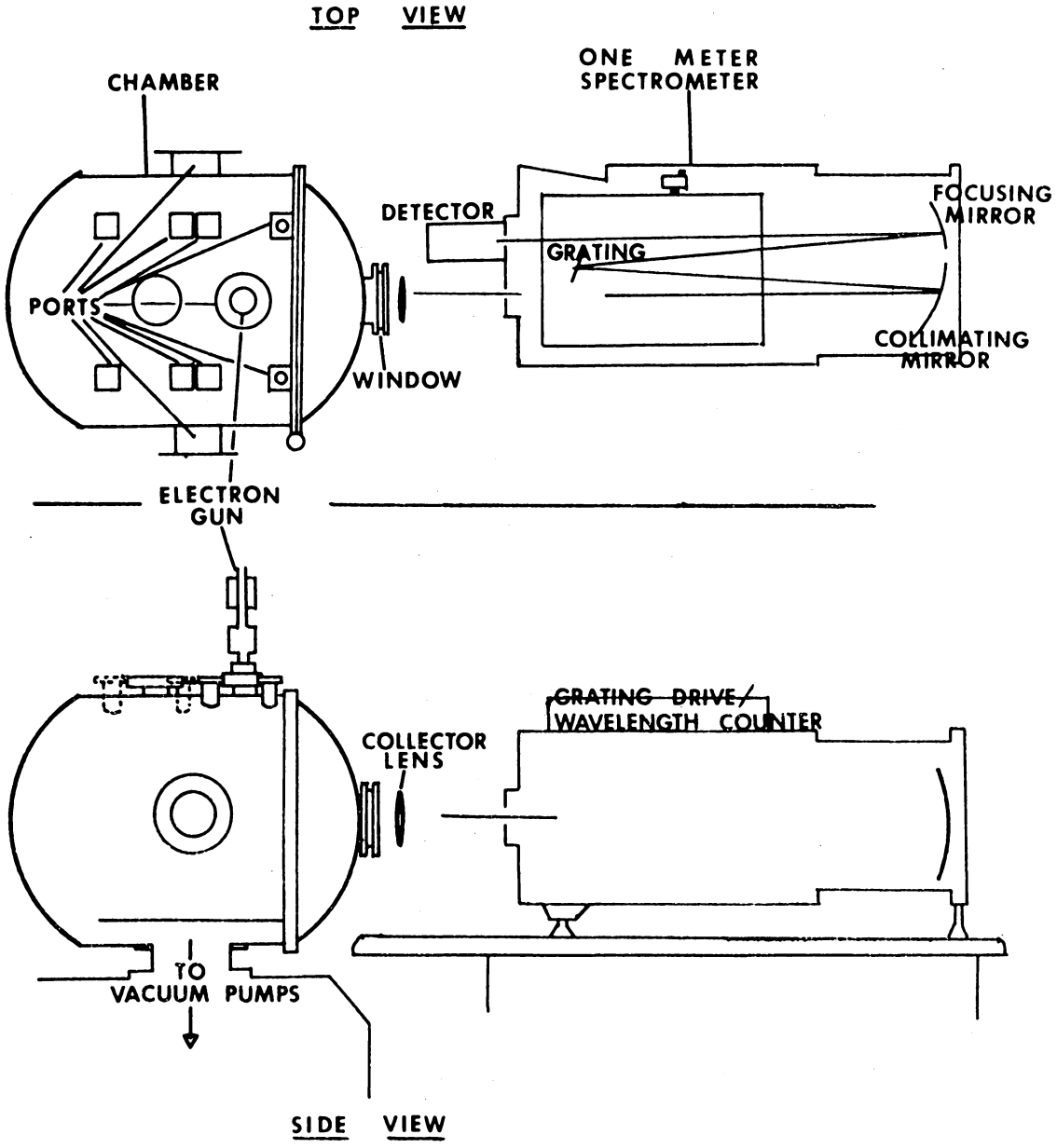

FIGURE 3.4. TOP AND SIDE VIEWS OF THE SECOND CHAMBER USED FOR PRELIMINARY TESTS.

Table 3.2. Rotational Intensity Observations.
Preliminary tests; ambient temperature.

Nominal Gas Pressures		Resultant Gas	Observed Band
Nitrogen (microns)	Helium (microns)	Mixture (He/N_2)	N_2^+, B-X (v',v'')
10	10 (R)	1	(0,0)
(1.33 N/m^2)	50	5	"
	100 (R)	10	"
	1000	100	"
	10000 (R)	1000	"
20	2000	100	(0,0)
(2.66 N/m^2)	4000	200	"
	10000	500	"
100	100 (R)	1	(0,0)
(13.30 N/m^2)	200	2	"
	300	3	"
	400	4	"
	500 (R)	5	"
	600	6	"
	700 (R)	7	"
	800	8	"
	900 (R)	9	"
	1000 (R)	10	"

(R) = repeated tests.

can be compared with the final tests later in the discussion.

These preliminary results indicated not only that there exists a substantial interaction between helium and nitrogen when an electron beam is passed through mixtures of the two, but also the range of rotational data necessary to quantify the effects. The remainder of this section is devoted to describing the laboratory apparatus and tests used to study in detail the effects of helium upon nitrogen fluorescence. As will be evident, the rotational distribution was extensively investigated.

Apparatus Used To Obtain The Rotational Data

The apparatus is discussed in four parts: electron gun, vacuum chamber, optical system, and electronic equipment. Each part provides a technical overview and summarizes the operating parameters.

Electron Gun

The electron source was essentially identical to that described in earlier work[64,65]. A small vee-shaped tungsten cathode was heated by high current at low potential to produce free electrons. These electrons were directed through the field determined by the grid cap shown in figure 3.5, through a small opening to form a beam. The exiting electrons were then accelerated between the cathode and the

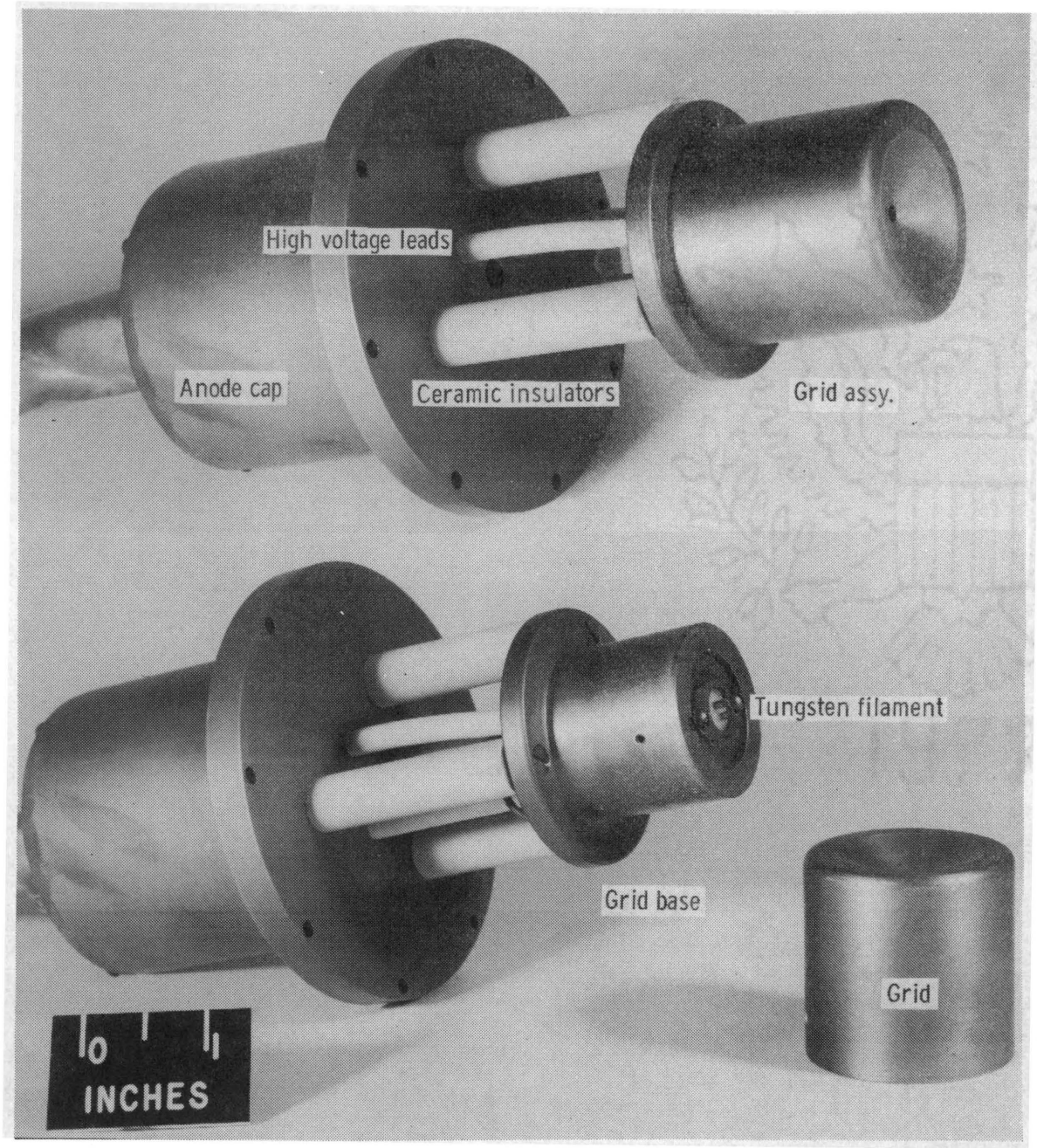

FIGURE 3.5. Electron gun - filament and grid cap assembly.

anode assembly (the latter shown in figure 3.6). Since the anode was maintained at nearly ground potential for safety reasons, the grid and cathode were approximately 26 kilovolts negative with respect to ground (grid roughly 150 volts more positive than cathode).

A substantial drift region between the grid cap and exit orifice was used in practice. Deflection and focus coils were attached along the drift region as shown in figure 3.6, permitting control of the beam size and position at an observation point external to the gun. The interior of the electron gun assembly was maintained at a relatively hard vacuum, $10^{-4}$to $10^{-2}N/m^2$, in order to permit long term filament operation and unattenuated electron passage. The necessary buffer to allow test pressures outside the exit orifice to reach several hundred N/m^2 has been described. That small evacuable volume (cylinder $\sim$ 2.5 cm. in diameter and $\sim$ 5 cm. long) was used only when necessary, to fulfill the aforementioned conditions. The nominal beam current for most experiments was 600 microamperes. The entire operating system is illustrated schematically in figure 3.7, including the current collector plate.

Both the electron gun cathode and drift regions, as well as the buffer region, were evacuated with a 5 cm. oil diffusion pump, backed with a mechanical pump. Each

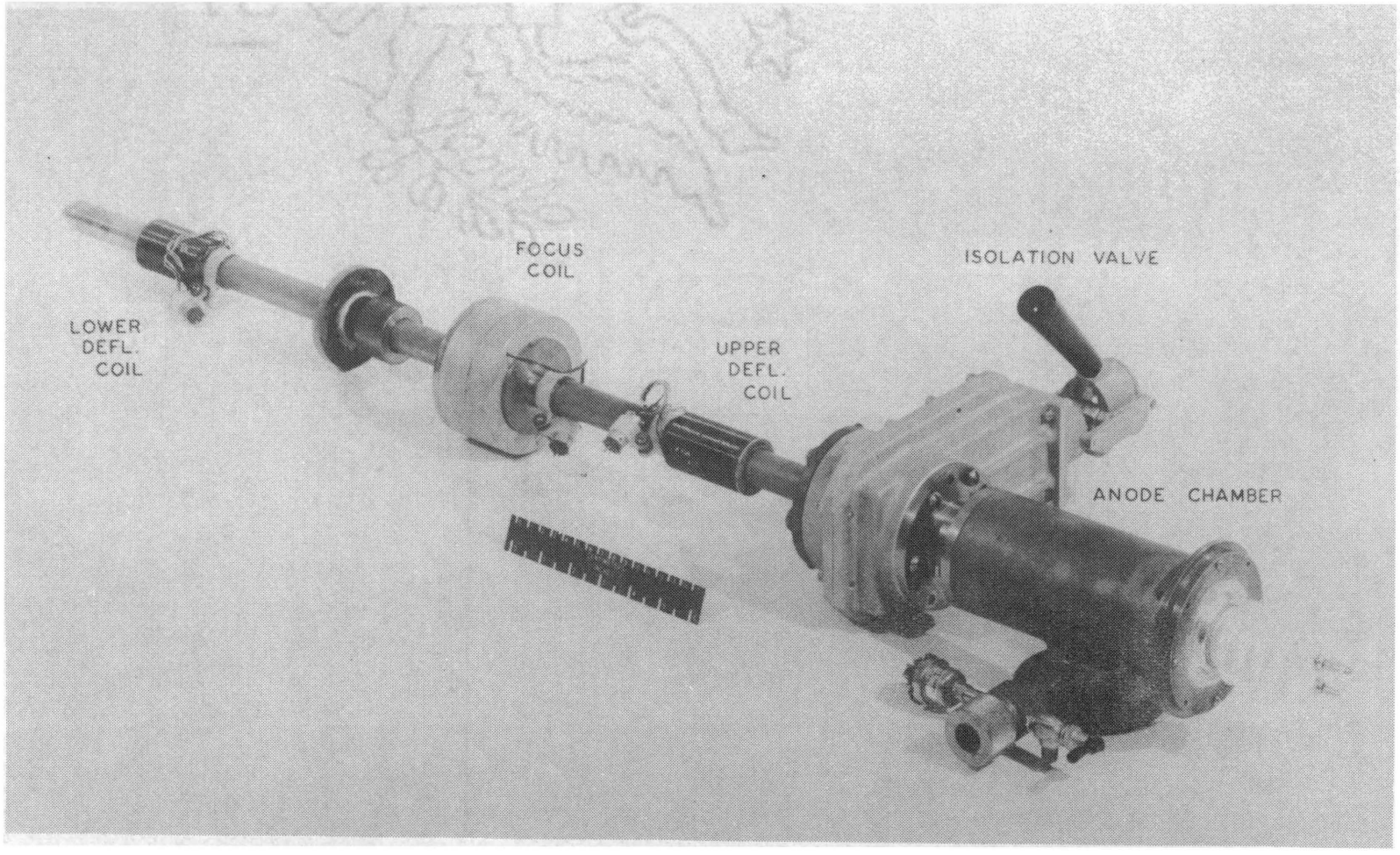

FIGURE 3.6. ELECTRON GUN ASSEMBLY, COMPLETE WITH ANODE CHAMBER, DRIFT TUBE, AND BEAM GUIDING COILS.

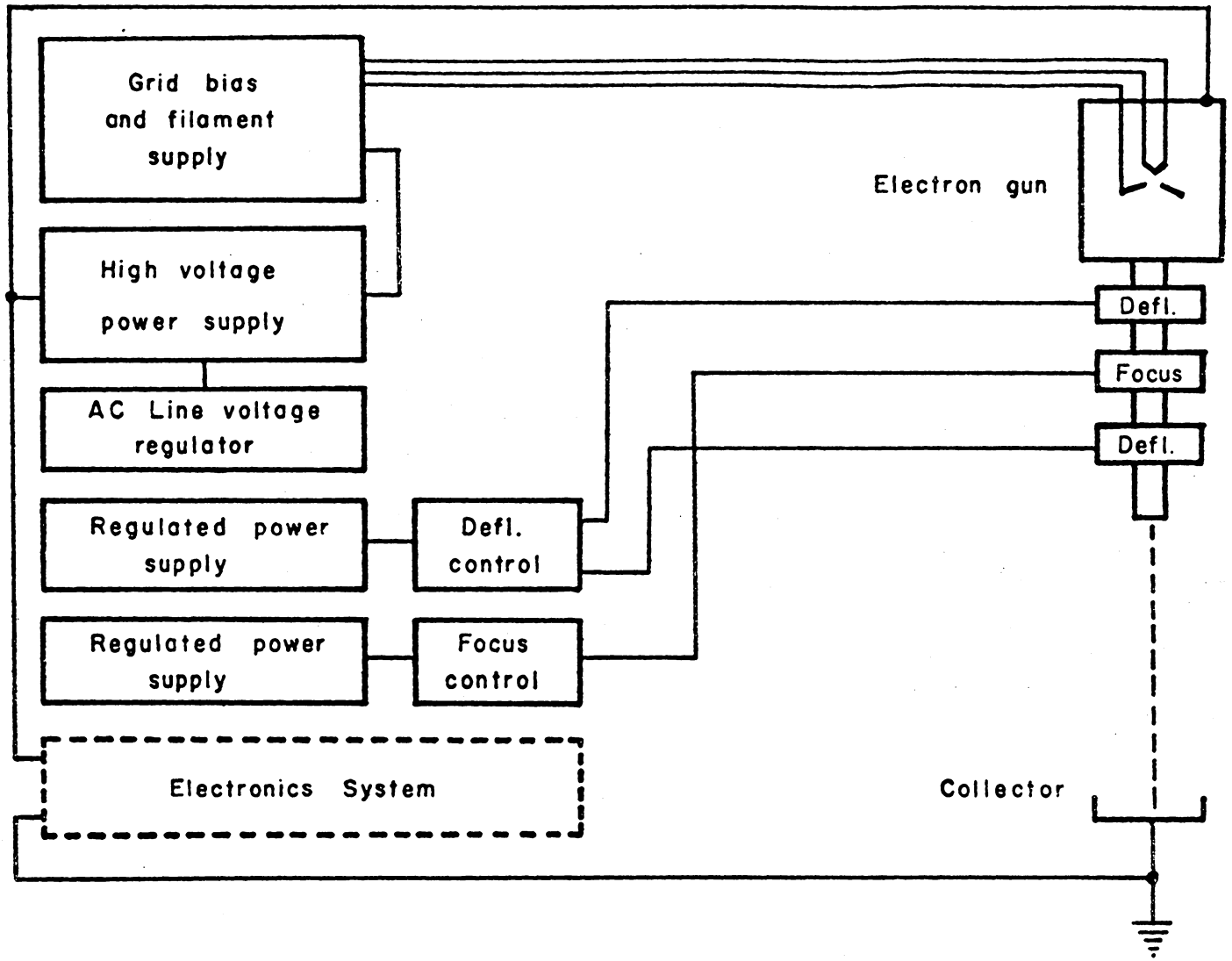

FIGURE 3.7. Block schematic diagram of the electron beam system.

diffusion pump was itself buffered by a liquid nitrogen cold trap from its respective vacuum vessel, to prevent oil backstreaming.

Mixing Chamber

Several different test arrangements were used during the course of this work. In addition to the two mentioned in the description of preliminary work, the basic laboratory program was conducted in the test chamber which will be described here. Some rotational spectra were observed at other than room temperature, in a cryostatic chamber and a wind tunnel flow described later.

Rotational intensity data were systematically observed in the chamber depicted in figure 3.8. Cylindrical in shape, the chamber was placed vertically upon a circular plate and had another fastened to the top. All parts were made of #304 stainless steel. A single viewing port is represented as the extension centered on one side. The length was 50 cm and inside diameter 15 cm. The center of the quartz window, as it was attached by an aluminum ring flange (sealed with O-rings between concentric flat aluminum rings) was located 27 cm from the geometrical center of the chamber.

The electron gun was attached through the top plate by means of an O-ring sealed vacuum fitting, such that the

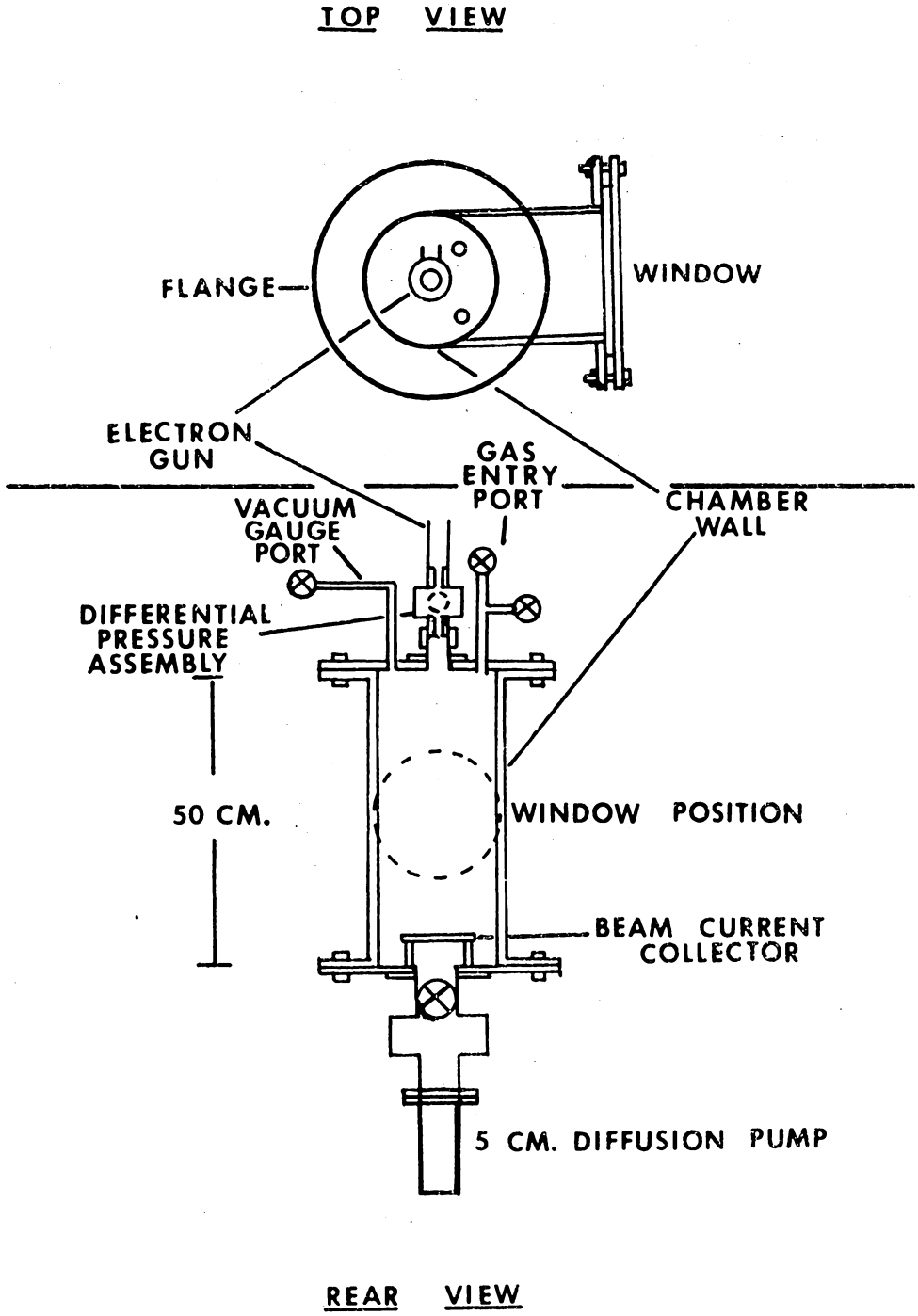

FIGURE 3.8. FINAL MIXING CHAMBER ASSEMBLY; ELECTRON GUN POSITIONED VERTICALLY.

beam traversed the chamber's vertical axis, as illustrated in figure 3.8. The cover plate attached to the bottom flange was 1.25 cm thick and had a 5.0 cm diameter hole in its center. A welded extension from that 5.0 cm hole provided for the attachment of the vacuum pumps through that plate, including a diffusion pump and mechanical pump. The mechanical pump also served to directly evacuate the test chamber, by-passing the diffusion pump, or to back the latter. The valve manifold is illustrated in figure 3.9. Using this arrangement, the ultimate pressure attained in the chamber was less than $10^{-4} N/m^2$ ($\sim 10^{-6}$ torr). As shown, the mechanical pump was connected through a filter in the direct line, to eliminate oil vapors which might otherwise enter the chamber. A pressure of 0.3 N/m^2 could be reached using the mechanical pump alone. Several other smaller openings were utilized, in the top plate, for vacuum measurement by means of mercury and capacitance manometers, and for test gas entry into the chamber. Helium and nitrogen each entered through a common 6 mm diameter port. Each gas was supplied from a high pressure bottle, through a needle valve, to the chamber.

Pressure measurements (pressure and density are considered interchangeable here for all work at room temperature) were made using several gauges. The capacitance

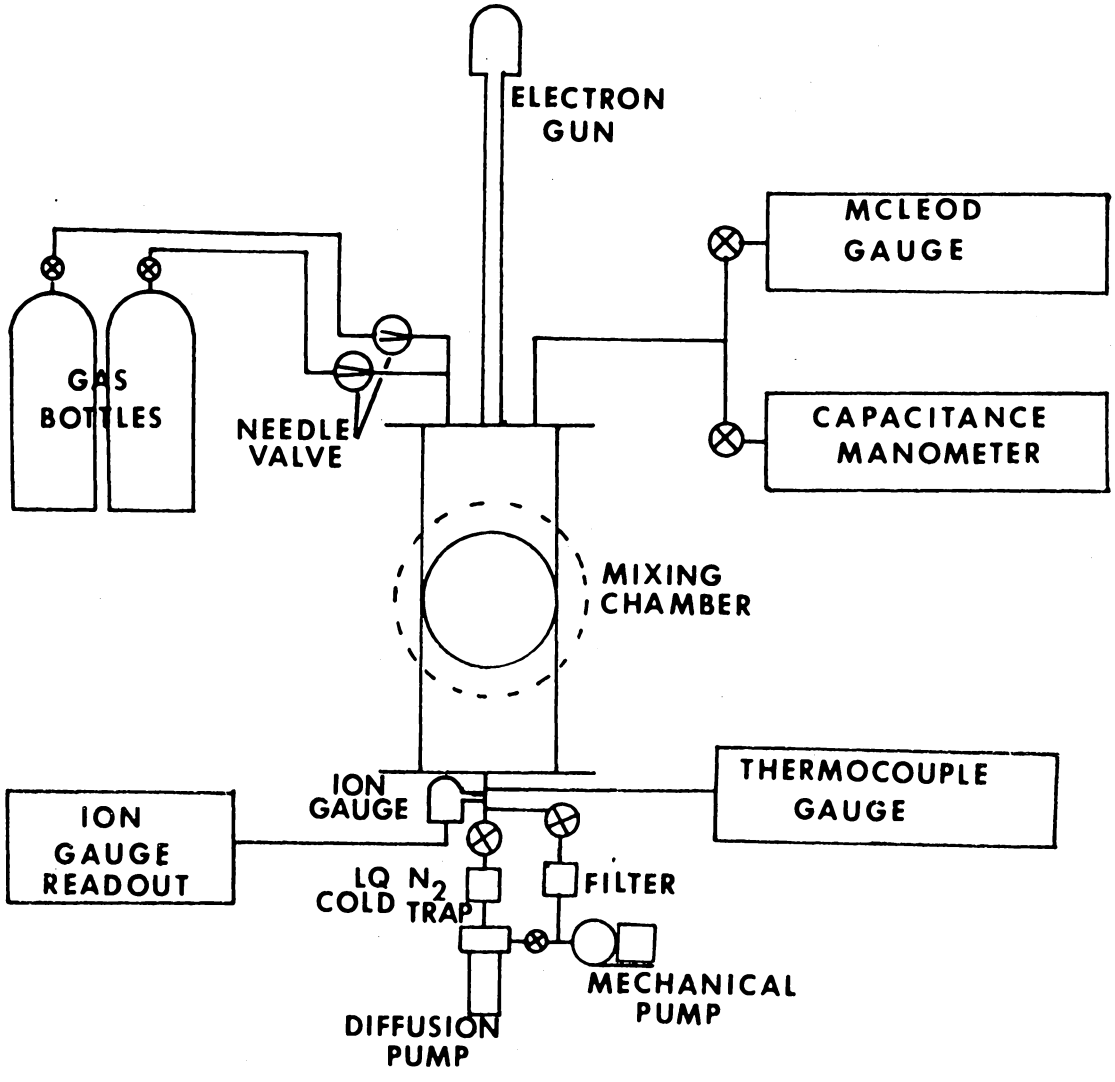

FIGURE 3.9. SCHEMATIC DIAGRAM OF THE MIXING CHAMBER. GAS ENTRY, VACUUM PUMPS, AND PRESSURE MEASUREMENTS ARE INDICATED.

manometer provided rapid response pressure readings, as low as $10^{-1}N/m^2$. A mercury manometer (McLeod gauge) provided a much slower reference measurement. Bayard-Alpert ionization gauges were used as pressure indicators to $10^{-4}N/m^2$. Figure 3.9 indicates the various gauge locations.

Optical System

Figure 3.10 indicates the elements and orientation of the optical systems used to observe the N_2^+,B-X bands. There are two distinct optical systems; the narrow-pass interference filter grouping to observe a signal proportional to the total fluorescence and the scanning spectrometer arrangement used to resolve and record the rotational spectra. Common to both are the chamber window and the beam splitter at the entrance of the filter detector system. 90% of the incident light was transmitted and directed to the spectrometer. 10% was reflected to the filter.

Figure 3.10 illustrates that a simple quartz lens collects the light from the chamber. It is then focussed on to the entrance slit of the spectrometer. Figure 3.11 is a photograph of the chamber. The one meter focal length spectrometer was utilized as the wavelength scanning device and light dispersing element. Scans were made at a rate of 2.5 nm per minute for rotational spectra and 5.0 nm per minute for rotational spectra and 5.0 nm per minute for

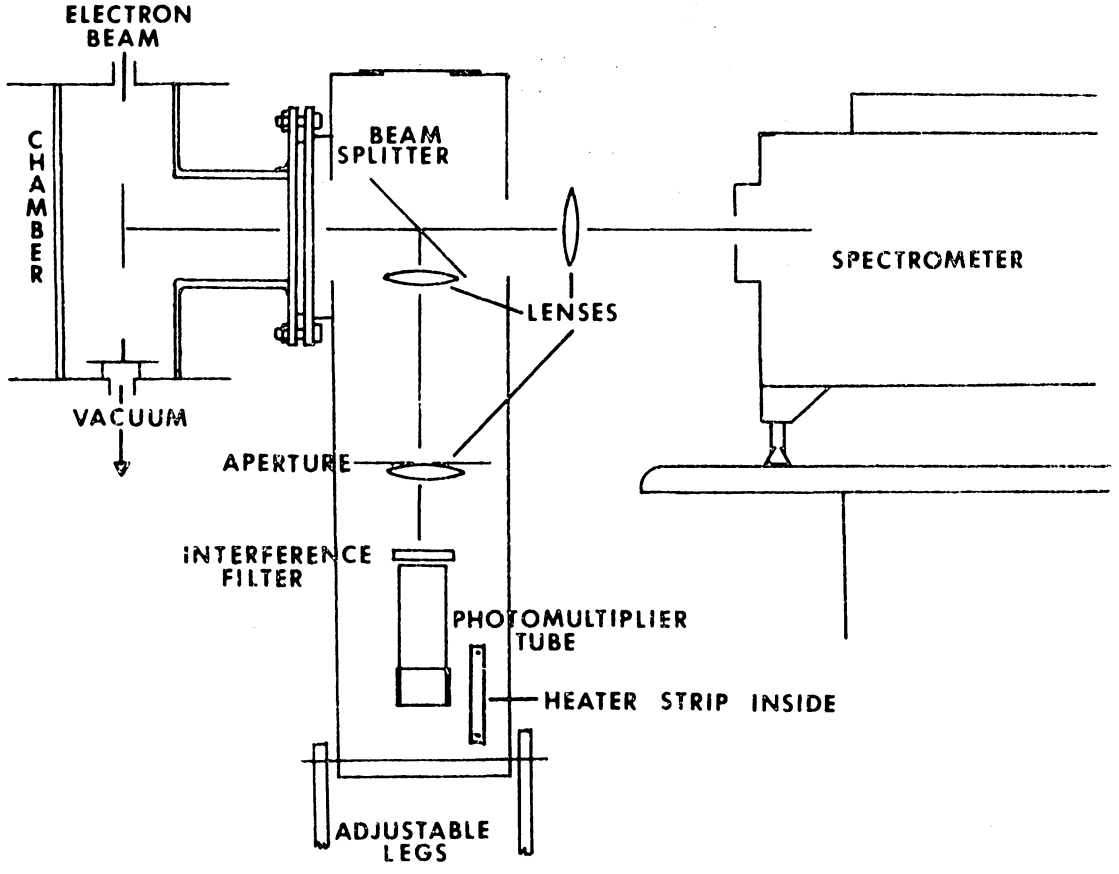

FIGURE 3.10. DIAGRAM OF THE OPTICAL INSTRUMENTS USED TO OBTAIN ROTATIONAL SPECTRA AND TO MONITOR TOTAL FLUORESCENCE.

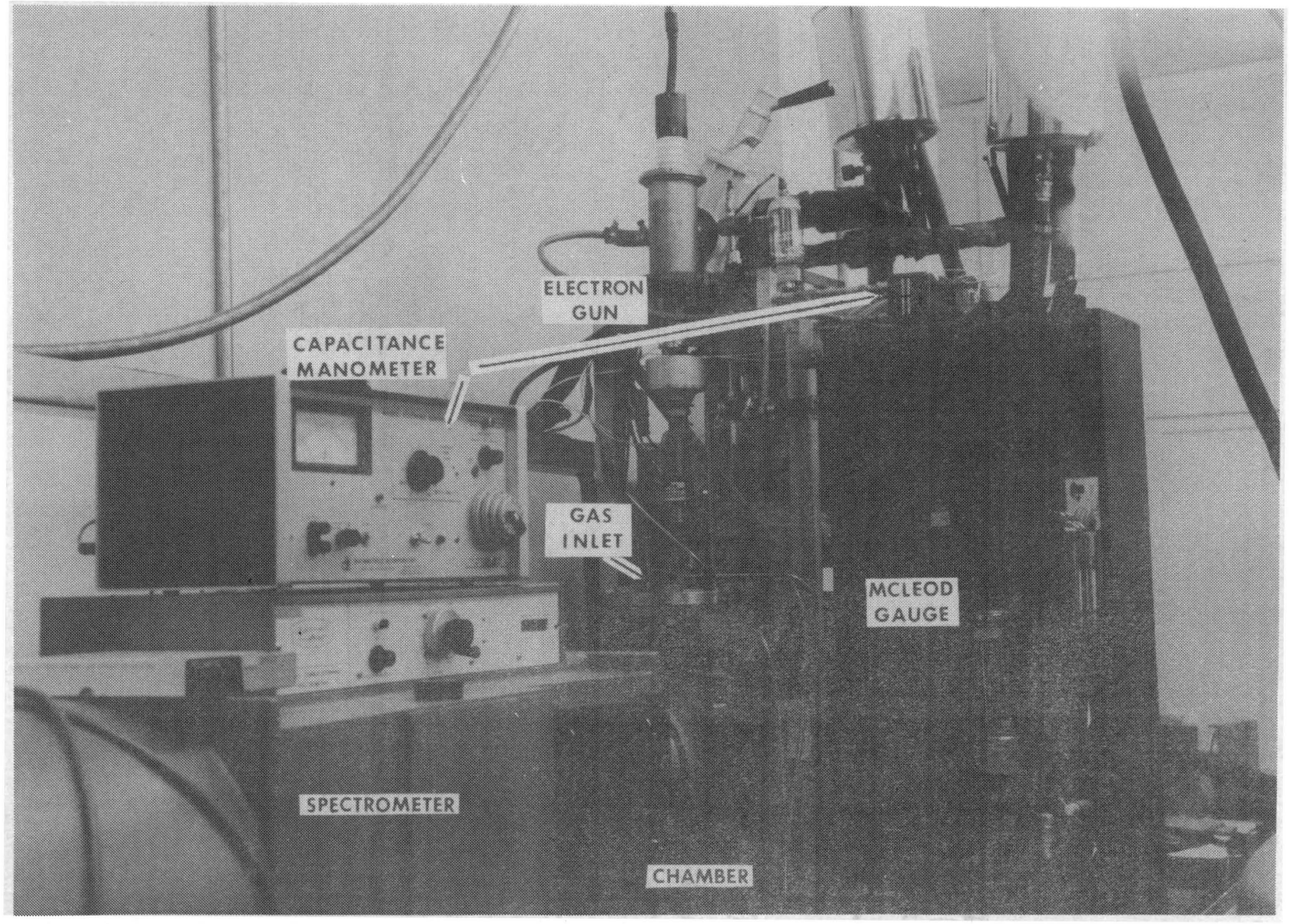

FIGURE 3.11. PHOTOGRAPH OF THE EXPERIMENTAL APPARATUS. THE 1 METER SPECTROMETER IS SHOWN.

survey scans. The resolution in wavelength was determined by the entrance and exit slit dimensions. Both were 0.05 millimeters in width by 1 centimeter in height for rotational data, and survey scans were generally obtained with those same slit dimensions. The grating dispersion provided an effective spectral width of 0.04 nm at the exit slit, for the given slit width.

The spectrometer sensitivity was examined experimentally as a function of wavelength. The results were normalized to 300 nm, the grating blaze wavelength. The purpose was to determine how spectral line intensities, far apart in wavelength, would compare. Figure 3.12 shows the observed relative sensitivity, which includes the grating, the photomultiplier tube, the other optical components, and the readout electronics.

Fluorescence diverted by the beam splitter into the interference filter system was brought to a focus at the aperture, then passed through a second lens, becoming slowly divergent. From the collimator lens, the light passed through the filter, to be collected at the photocathode for conversion to current. The filters have been described previously (peak wavelength and half-width). Since the light is not parallel, the concept of a broadened half-width applies, as it did for the preliminary tests.

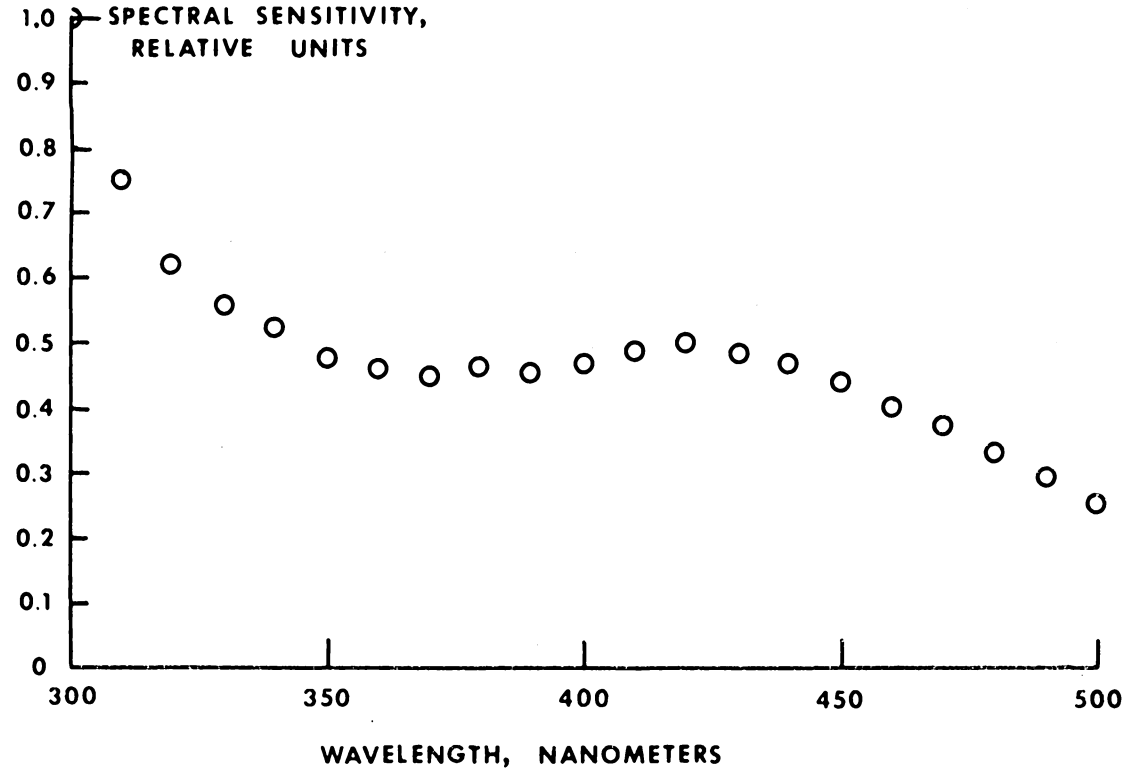

FIGURE 3.12. RELATIVE SPECTRAL SENSITIVITY FOR THE 1 METER CZERNY-TURNER SPECTROMETER. THIS CURVE INCLUDES THE OPTICS, EXTERNAL AND INTERNAL TO THE SPECTROMETER, AND THE PHOTOMULTIPLIER TUBE DETECTOR.

The aperture was designed to observe 10 cm across the beam (perpendicular to electron flow) and 1.25 mm along the beam. The intent was to monitor the entire beam cross section, which must be done to interpret the output signal directly in terms of gas density.

Electronics

In order to record the various quantities which were generated, amplified analog signals were measured. Electron beam current, photomultiplier anode current, transducer output from the vacuum gauges, the high voltage on the electron gun and photomultiplier tubes, and other quantities were either regulated precisely or measured. The block diagram of figure 3.13 illustrates the entire system for data readout and recording.

Picoammeters were used to record the electron beam from the current collector, and the photomultiplier output currents. The ammeters were connected to strip chart recorders, from which continuous traces of the signals were made. For all tests in which the shot noise was insignificant ($S/N \sim 10$), the traces were accurate to within their reading error. Repeat tests verified this. When noise became more significant, the signals varied to an extent represented by the RMS noise level.

Pressures were determined by direct reading and hand

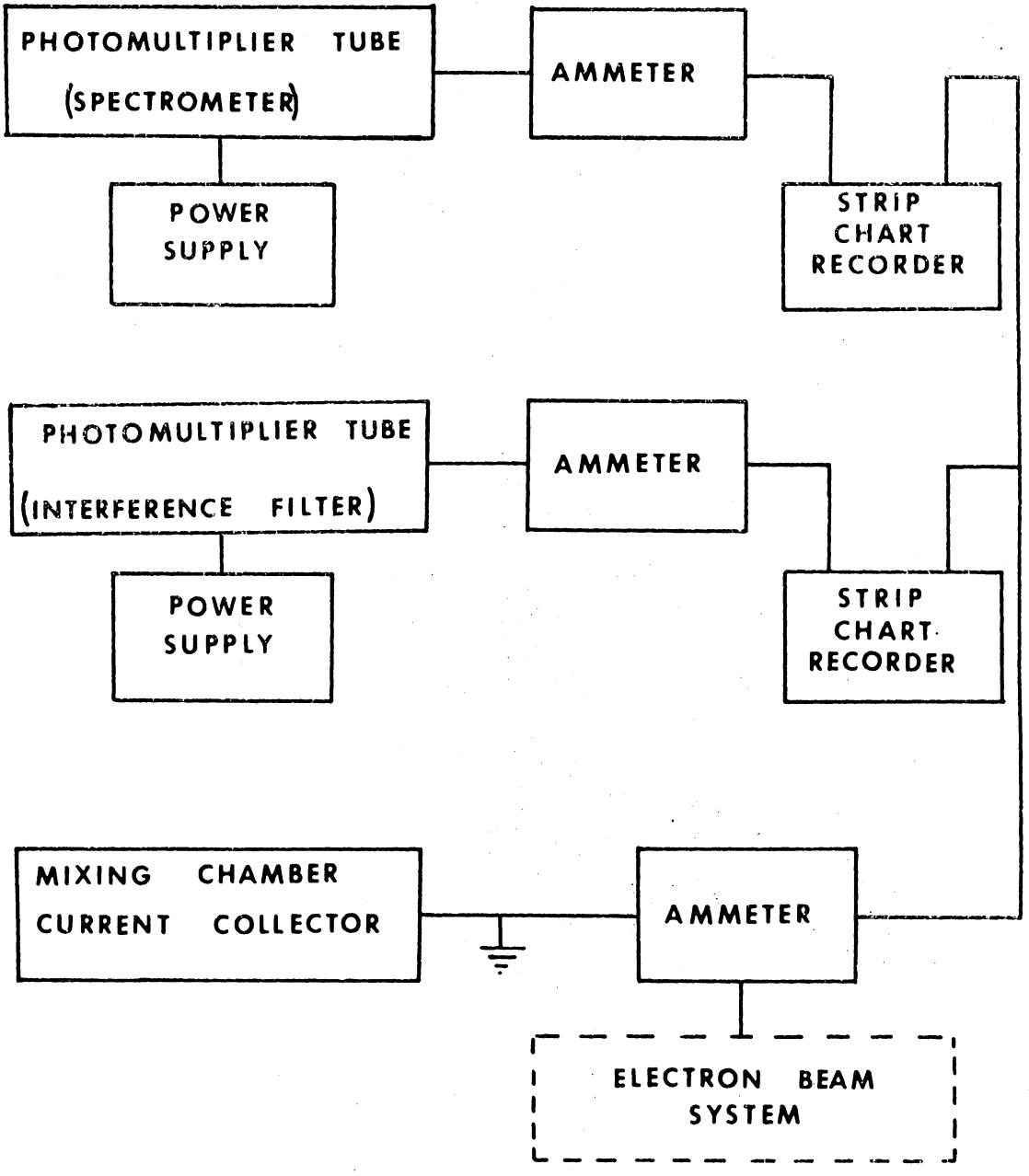

FIGURE 3.13. BLOCK DIAGRAM OF THE DATA RECORDING SYSTEM.

written record from the mercury manometer or the capacitance manometer. Figure 3.14 is a comparison of the pressure readings of the two devices, typical of periodic checks which were made. The capacitance manometer was generally operated in the null mode, permitting very precise determination of the chamber pressure (reading $\pm 10^{-2}$ N/m^2 for pressures as high as 2×10^3 N/m^2).

Procedure

Extensive trial and error testing was required to develop an appropriate procedure for observing the rotational spectra in mixtures. The method which emerged consisted of the following steps. The test chamber was evacuated sufficiently to reach a pressure below 10^{-3} N/m^2 (usually nearer to 10^{-4} N/m^2), at which point the valve to the vacuum pumps could be closed. Test gas at the lower partial pressure (0.6 to 13 N/m^2) was rapidly admitted to the chamber (1 to 2 minutes). The electron beam, previously aligned and focussed, was activated by reducing the grid bias voltage, permitting electrons to pass into the chamber. Scanning the spectrometer through the rotational lines of an appropriate band then took about 1.5 minutes. The electron beam was immediately deactivated and the test region evacuated to low pressure.

Sufficient time between runs was permitted for the

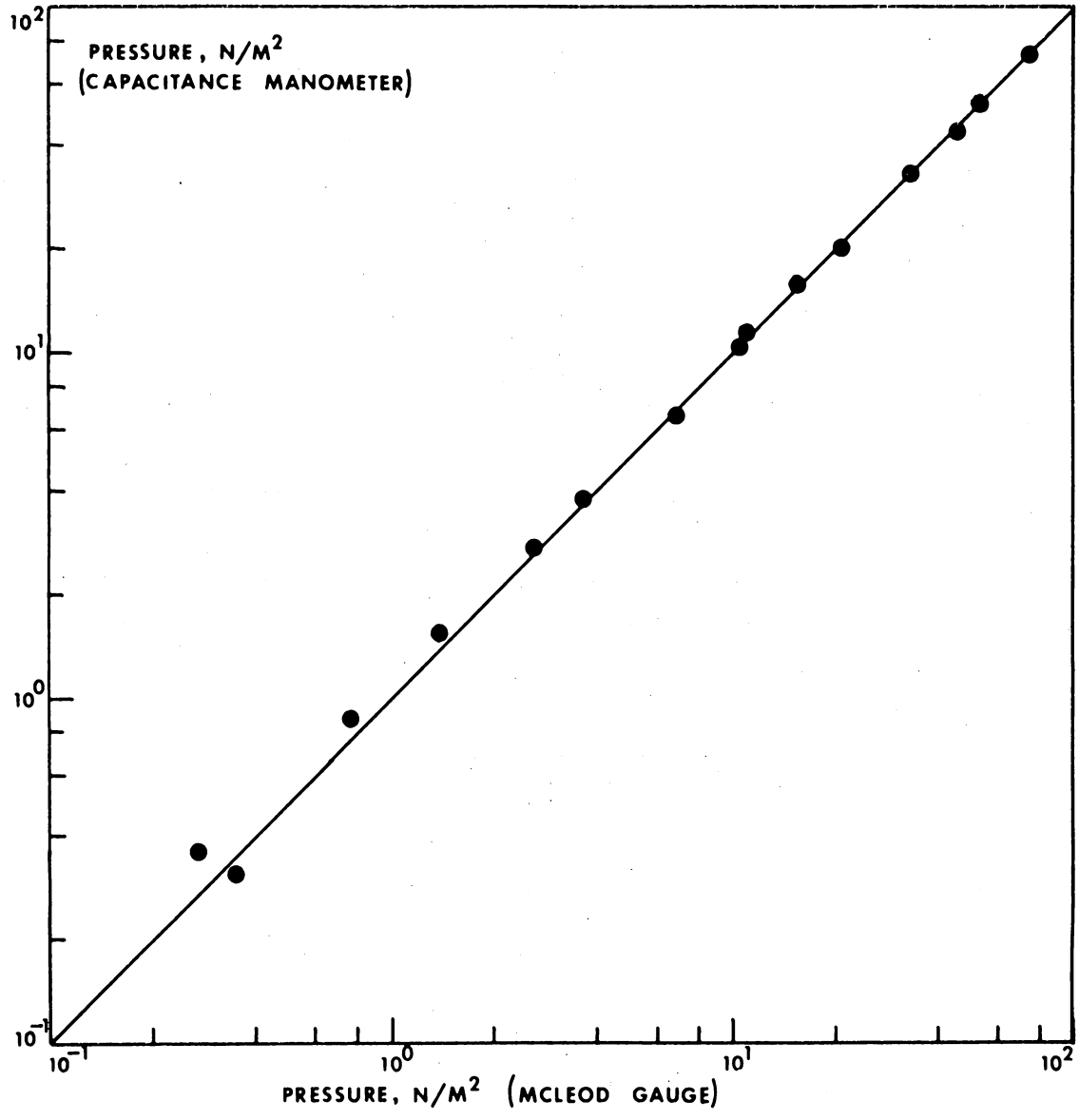

FIGURE 3.14. TYPICAL COMPARISON OF THE McLEOD GAUGE AND CAPACITANCE MANOMETER PRESSURE READINGS.

chamber pressure to reach the former low value. The electron beam "on time" was minimized in this manner, avoiding significant collector heating. (Since the collector plate was not massive and stood off the chamber bottom plate on insulators, heating occurred for extended test times.) Exposure of the photomultiplier tubes to measurable signals was brief, rendering negligible the gain changes due to photon impingement upon the photocathode. Pre-test exposures were normally conducted, however, for 15 - 30 minutes to help stablize the gain characteristic. The test chamber was also purged periodically with helium and nitrogen to pressures much in excess of those used in tests; 2×10^3 N/m^2, for instance. One additional factor, the ambient temperature, was recorded. The gain characteristics of the optical systems were found to be affected by the ambient and, for nearly all tests, it represented the comparison gas temperature.

The measurements of total fluorescence (interference filter detector) served as a control. Output from the system was monitored, in order to compare the signals from different tests with one another, to ascertain consistent mixtures and account for unexpected changes.

Two sets of data (rotational intensity scans) were obtained which differed distinctly from the rest. Three

scans were made in a premixed test gas, constituting one set. They were conducted in a low temperature chamber at two different temperatures; approximately 115°K and 50°K. The other set consisted of several scans made at a helium wind tunnel, the Langley Research Center's 22-inch tunnel. Here the test temperature was inferred, by calculation from the nozzle expansion of the test gas, to be about 3°K at 27 N/m^2(the room temperature equivalent of 20 torr). The results of these tests will be discussed later.

Observations

A brief summary of the observations which were made in accordance with the previously outlined procedure follows. The primary experimental effort was to determine the form of the rotational distribution of intensities for N_2^+,B-X bands and the dependence of that distribution upon the mixtures of nitrogen and helium. Preliminary tests are outlined in Table 3.2. Using the test chamber and procedures described in the present part of this chapter, rotational intensities were observed and recorded for the parameters shown in Table 3.3.

For that same range of pressures and mixtures, the interference filter system monitored the total band fluorescence, or the 501.6 nm helium line fluorescence. The signal was normalized to electron beam current, which rendered it

Table 3.3. Rotational Intensity Observations.
Final laboratory data; ambient temperature.

Nominal Gas Pressures Nitrogen (microns)	Helium (microns)	Resultant Gas Mixture (He/N_2)	Observed Band N_2^+, B-X ($\tilde{v}',v''$)
5	25	5	(0,0)
(0.67 N/m^2)	50	10	"
	100	20	"
	200	40	"
	500	100	"
	2500	500	"
10	20	2	(0,1)
(1.33 N/m^2)	30	3	(0,0)
	40	4	(0,1)
	50	5	(0,0)
	80	8	"
	100	10	(0,0) (0,1)
	200	20	(0,1)
	500	50	"
	1000	100	(0,0) (0,1)
	2500	250	" "
	6000	600	" "
20	140	7	(0,0)
(2.66 N/m^2)	200	10	"
	500	25	"
	1000	50	"
	3000	150	"
	6000	300	"
50	200	4	(0,0)
(6.65 N/m^2)	500	10	"
	1000	20	"
	2500	50	"
	6000	120	"
100	200	2	(0,0)
(13.30 N/m^2)	500	5	"
	1000	10	"
	2000	20	"

Table 3.3. Continued.

Nominal Gas Pressures Nitrogen (microns)	Helium (microns)	Resultant Gas Mixture (He/N_2)	Observed Band N_2^+, B-X (v',v'')
2.5(0.33 N/m^2)*	250	100(pre-mixed)	(0,0)
10	1000	100	"
10 -40 N/m^2,** Total static pressure		10^4(est.)	(0,0)

*Cryostat Chamber (low temperatures; approximately 116° K ; 50° K)

**Helium Tunnel (very low temperature; less than 4° K)

proportional to density. However, the dependence upon density was quite complex, as discussed in the section. The complicated energy transfer among helium states and from helium to nitrogen, as well as resonance fluorescence transfer, beam spreading and secondary electron effects, severely limit interpreting the filter system signals as partial densities.

Ratios of vibrational bands were spectrometrically observed for the sequence $\Delta v=-1$ of N_2^+, B-X; the (0,1),(1,2), and (2,3) bands. The mixture conditions were essentially 10 to 1 and 100 to 1 (helium to nitrogen) at several total pressures from 1.3 N/m^2 to 10^2 N/m^2. Again, these observations were made to support the rotational spectrum data by observing the ratios of band intensities as functions of the mixture. The low temperature chamber and the tunnel provided variations of the temperature, offering the opportunity to include some lower temperature data to that tabulated in Table 3.3. Indeed, these tests provide a significant additional dimension to this work.

Contributions To Experimental Error

Collective instrument errors contribute a significant part of the uncertainty in experimental work. Estimated errors may be defined by considering the experimental procedure outlined, the apparatus discussed and the

calibrations accomplished. An arbitrary grouping of these estimates is made into categories labelled gas mixtures, electron beam, optical detector systems, and physical processes which affect the fluorescence.

Gas Mixtures

Several factors influenced the determination of gas mixtures. They included the test pressure measurement, leak and outgassing rate of the chamber and the initial gas purity. Ultra-high purity grade helium was used for all tests. Any single impurity did not exceed 4 parts per million, by supplier analysis, except neon. Neon was considered to be of little consequence because it was present in very small proportion relative to helium and behaves thermodynamically like helium.

Atmospheric gases were present largely by virtue of leaks from the exterior and outgassing after exposure to atmospheric conditions. Tests were conducted to determine the conditions necessary for minimizing the leaks and outgassing. The mixing chamber, in practice, was sealed for several weeks at a time. During these periods, the rate of pressure rise, when the valves to all pumps closed after the lowest possible chamber pressure had been reached, was dependably lower than 10^{-1} N/m^2.per minute.

To determine the rate of pressure increase (leak rate),

the chamber was thoroughly evacuated, usually to $10^{-4} N/m^2$ or lower. The valve to the pumps was closed and the ion gauge and capacitance manometer readings were monitored for a substantial period (3 - 10 minutes). Figure 3.15 illustrates such tests, showing pressure plotted as a function of time. The most reliable measurements were obtained when the ion gauge was turned off, and the capacitance manometer alone used to measure Δ p.

The test pressure measurement was the most important factor in determining the gas mixture. Several aspects of the McLeod gauge and the capacitance manometer uncertainties were investigated. The working pressure range was 10^{-1} to $2x10^3$ N/m^2. For lower than 10^{-1} N/m^2, an ion gauge was used. However, accurate measurements using the ion gauge were not sought, only an indication which could be repeated. Both the McLeod gauge and the capacitance manometer were calibrated against secondary standards. They were used in comparison with each other (figure 3.14). To reduce the mercury streaming effect from the McLeod gauge[67,68,69], a liquid nitrogen cold trap was used between the test region and the mercury.

Individual pressure readings were precise (99% or better) at the higher pressures, as determined by the capacitance manometer in the null mode. The McLeod gauge,

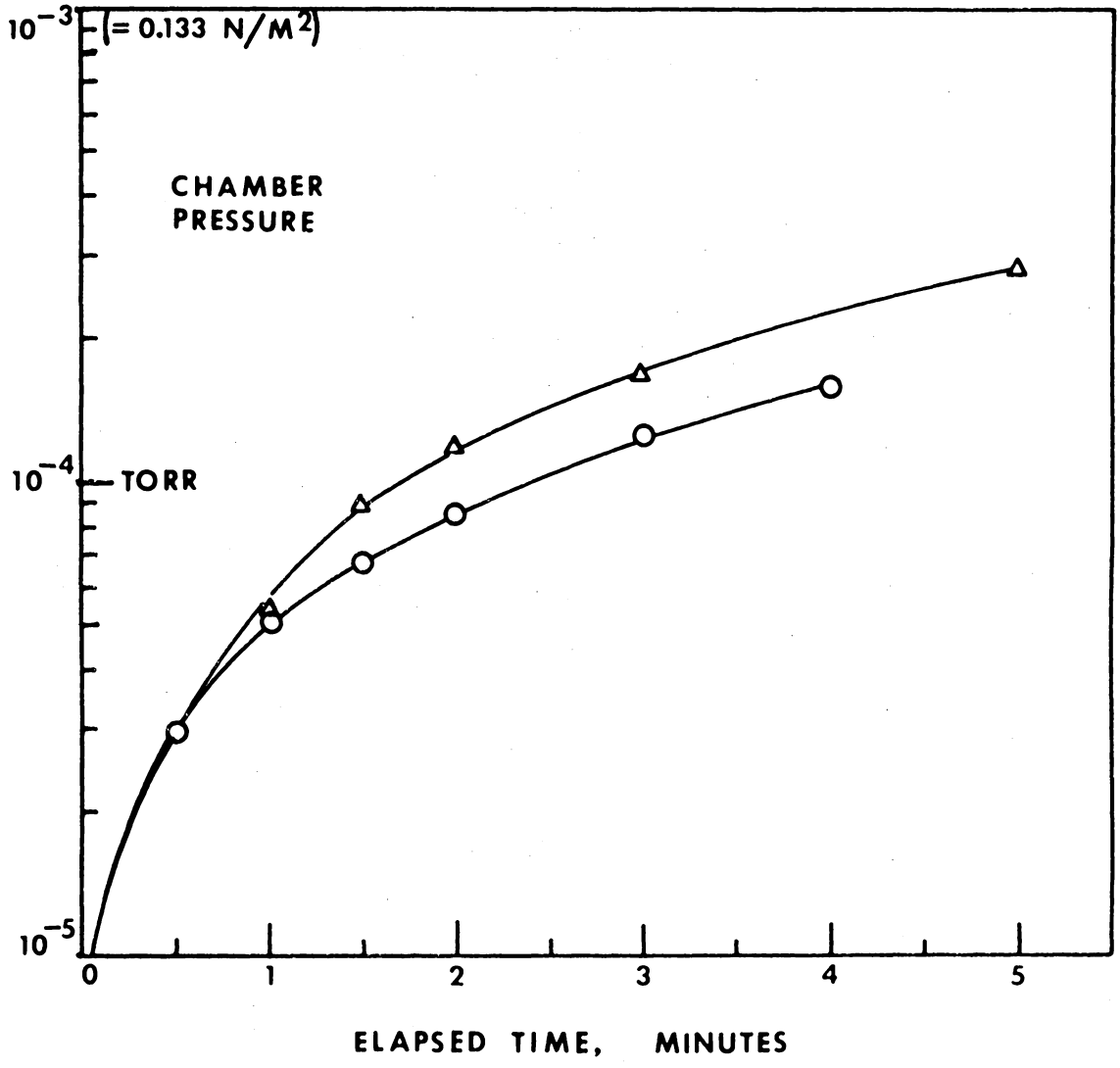

FIGURE 3.15. OBSERVED RATE OF PRESSURE RISE IN THE MIXING CHAMBER (SHOWN IN FIGURE 3.8). DATA ARE SHOWN FOR TWO TESTS TO INDICATE TYPICAL VARIATIONS.

by virtue of a change of scales at 27 N/m^2 and a larger reading error, was 97% certain at best. Low pressures, below 10^{-1} N/m^2, were uncertain by ±10% or more, based upon the lack of absolute standards[70]. In our operating range, the absolute pressure was measured to ±10% near 10^{-1} N/m^2, rapidly, improved to ±3% above ∿5 N/m^2. The precision, as tested by repetitive measurements at fixed pressures in the sealed chamber, was 90% at the low pressures and better than 99% at the highest.

The most stringent requirement for accuracy applied to the minor constituent, nitrogen. A mixture which contained nitrogen at 1.33 N/m^2 (10^{-2}torr) was uncertain by ±0.07 N/m^2 initially. The leak rate accounts for 0.01±0.005 N/m^2 per minute increase (or 0.1 N/m^2 in 10 minutes). Thus, the uncertainty was no worse than ±20% for a 10 minute test, considerably smaller for shorter periods or for larger nitrogen partial pressures.

Physical Processes

Two particular items were potential influences upon the observations of electron impact fluorescence from helium-nitrogen mixtures. The first was the spatial dependence of radiation processes, including resonance radiation transfer, transfer of helium excitation energy, and the spreading of the primary electron beam. The second was polarization of

the emitted light.

Resonance radiation transfer enlarges the region over which the desired wavelength emanates. The important transition affected is the 3^1P - 2^1S (501.6 nm) of helium. Its related resonance is 3^1P - 1^1S, roughly 50 times more likely. However, the effective distance over which 53.7 nm radiation can travel before being totally converted to 501.6 nm decreases rapidly as the helium density is increased. Not all published results agree on the pressure (equivalent density at room temperature) required to assure complete trapping. The pessimistic interpretation indicates that more than 95% is converted within 2 centimeters of the source when the pressure is 7 N/m^2, for example. Since the interference filter optical system utilized an aperture of 10 cm. in the dimension perpendicular to the electron beam, the entire 501.6 nm source was observed. The spectrometer slit dimension was much smaller and did not collect emitted helium radiation from the entire source volume.

Primary beam electrons were elastically scattered as they traversed the gas. A broadening of the fluorescence region at higher pressure resulted. This effect limited the upper pressure for which the filter system viewed the entire source of radiation. That limit was greater than 2×10^3 N/m^2 for the optical system we have described. The test

pressures did not exceed that limit (see Tables 3.1 and 3.3).-

Polarization of emitted radiation results from a "directionality", imposed by the source mechanism, for example.

$$P = \frac{I_{\parallel} - I_{\perp}}{I_{\parallel} - I_{\perp}} \qquad (3.4)$$

defines the polarization P in terms of the intensity $I_{\parallel}$, emitted parallel to a given direction (here along the beam) and $I_{\perp}$, perpendicular to that direction. Hunter[64] discussed the effects upon helium fluorescence, concluding that no effect greater than 1% was observed. No favored direction existed for nitrogen fluorescence. Nearly all of it is produced by collisions with excited helium, which acts to further reduce any directional dependence.

Electron Beam

The electron beam provided the initiating mechanism for all processes which relate to the observed fluorescence. Equations (3.1) and (3.2) illustrate that the fluorescence depends upon the electron current density, J_B, and the collision cross section, Q_{oj}^{p}. The latter depends upon the electron accelerating potential (i.e., energy). J_B depends upon the total current, I_B, and the spatial character of beam (i.e., diameter and spreading).

Divergence of the incident electrons has been dis-

cussed in the preceding section and previously[64,65]. At 1330 N/m^2(10 torr) in helium, these electrons collide once per centimeter of travel[71]. At the point of observation in the test vessel described here, the deflection gives rise to a beam diameter of approximately 3 centimeters. At the collector plate (figure 3.8) the diameter was 6-7 centimeters. Figure 3.16 illustrates the results of a typical test to assure that the total fluorescence (interference filter system signal) depended linearly upon beam current. The pressure for this test was $\sim$12.6 N/m^2 nitrogen.

The average beam current was measured as discussed earlier, for which measurements the precision was 98%. The total fluorescence system aperture was large enough to include the entire electron beam geometrical cross section up to greater than 2 x 10^3 N/m^2. Hence, J_B was determined with an error of $\pm$2% or less. The meter spectrometer output did not depend upon the absolute beam current, only variations during a given scan.

The effects of the high voltage power supply are manifested through the collision cross section, Q_{0j}^p. Only slight variations in the voltage occurred, less than 500 volts drift in 30 minutes provided warm up was sufficiently long (at least 30 minutes). Effects due to the high voltage are thus negligible, since Q_{0j}^p depends upon the accelerating

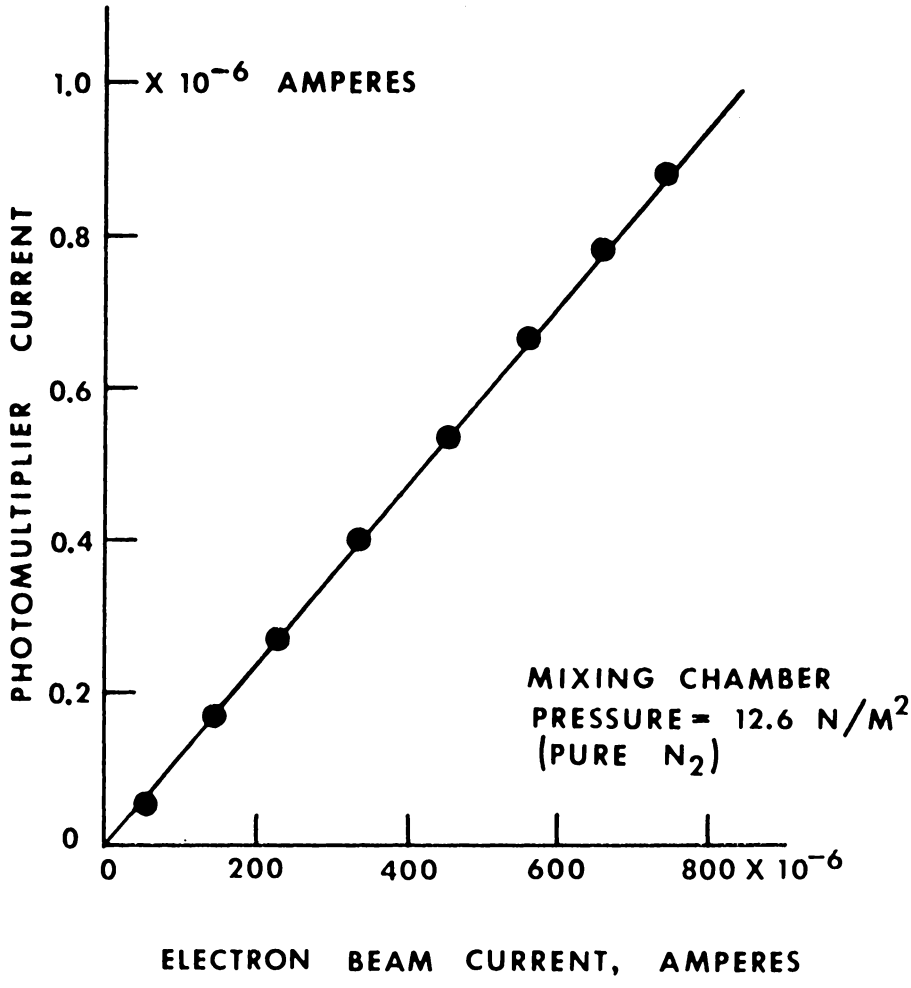

FIGURE 3.16. TOTAL FLUORESCENCE AS A FUNCTION OF BEAM CURRENT. THE PHOTOMULTIPLIER CURRENT IS THE FILTER DETETECTOR SYSTEM OUTPUT SIGNAL, FROM THE N_2^+, B–X (0,1) BAND.

voltage V as V^{-1} $\ell n V$.

Optical Detector Systems

The segment of radiation observed by the spectrometer for rotational spectra observations was 0.07 mm across the beam (some at 0.035 mm) and 14.3 mm along it. Alignment was completed by adjusting the spectrometer position to maximize output. Several factors affected the signal, including the rate of scanning, the photomultiplier tube stability, the amplifier gain (current meter) and the chart recorder response.

Scan rate was kept as rapid as possible without attenuating full scale recorder displacements (2.5 nm/minute). Thus, no error was attributable to the scanning.

Periodically, tests of the linearity of the picoammeter and recorder systems were conducted. A standard current source, which was correct to within $\pm 0.5\%$ of the current setting, fed particular currents into these systems. For readings less than approximately 30% of the full scale current, recorder reading error dominated. Above that level, the recorded currents varied from the standard by no more than $\pm 2\%$.

The statistical nature of the photon emission from atomic and molecular species, and the random emission processes which are characteristic of photomultiplier detection,

give rise to noise (random signal fluctuations). Shot noise dominates the effect and may be expressed by the signal-to-noise ratio,

$$\frac{S}{N} = \frac{i_{PMT}}{(2eG\ \Delta f\ i_{PMT})^{\frac{1}{2}}} . \qquad (3.5)$$

G is the gain of the photomultiplier tube, Δf is the system bandwidth, and i_{PMT} is the photomultiplier output current. For the current, $i_{PMT} = 5 \times 10^{-7}$ amperes, a small uncertainty is introduced by shot noise (< 1%). That is typical of the interference filter system. $i_{PMT} = 5 \times 10^{-8}$ amperes typifies the spectrometer output signals, which are subject to larger noise fluctuations ($\sim$7% r.m.s.). Individual line readings were uncertain by as much as ±20%. Several lines are present in vibrational band of N_2^+, B-X, and the entire distribution characterizes the gas temperature, T_R, as calculated by equation (2.23). Figures 1.1, 1.2 and 3.17 further illustrate this point. The behavior of the rotational distribution is much more certain than a single line intensity.

The total fluorescence observations were made to insure that the rotational intensity data could be compared for successive tests. Again, the detector element was the dominant source of uncertainty. The photomultiplier tube and interference filter were sensitive to temperature and

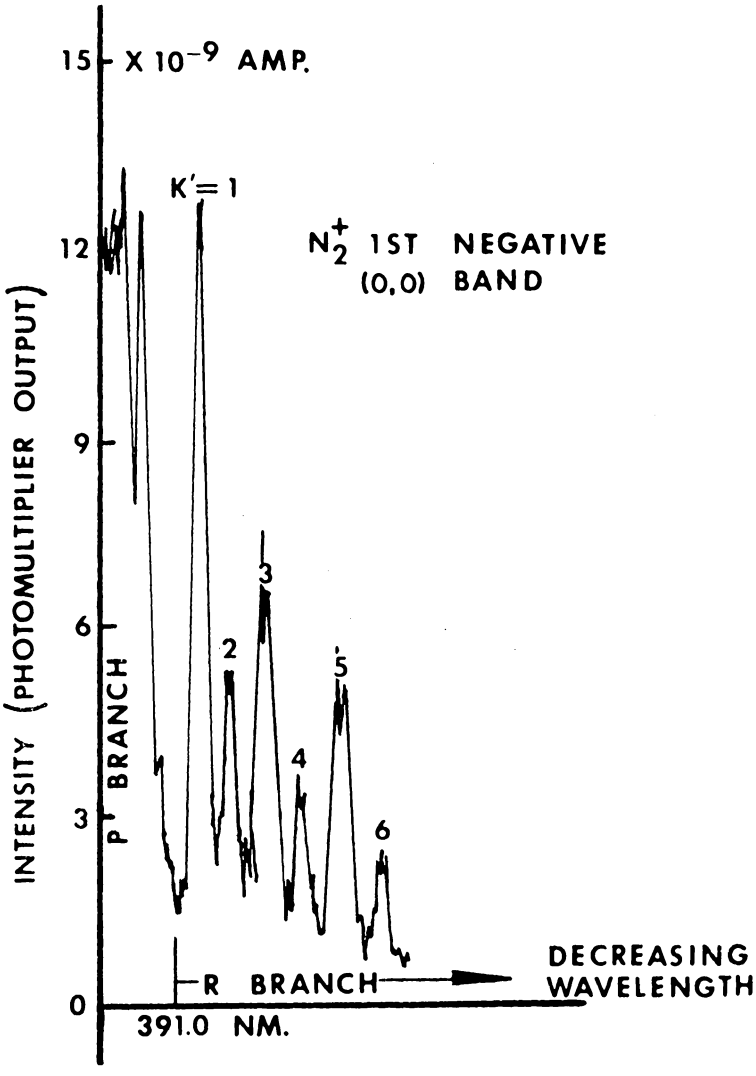

FIGURE 3.17. ROTATIONAL SPECTRUM OBSERVED IN THE LANGLEY RESEARCH CENTER 22-INCH HELIUM TUNNEL. THE GAS WAS VERY COLD, AS THE ROTATIONAL DISTRIBUTION SHOWS.

were kept at constant thermal conditions by heating the entire cavity (see figure 3.10) to 90°F. The system was calibrated in pure nitrogen, at known pressures. Sufficient signal was observed at all times to keep signal-to-noise large. Overall, the instrument errors were very small in this system, amounting to the ±2% ammeter-recorder error noted earlier.

Summary

Absolute pressure measurement (at constant temperature) was of secondary importance to repeating particular experimental conditions. Experience indicated that a particular pressure could be set precisely, above 7 N/m^2. The worst case was 95% near 10^{-1} N/m^2. Gas mixtures were repeated precisely, but changed as much as 10% in the minor constituent, nitrogen, when the partial pressure was 1 N/m^2 or less. The absolute uncertainty of a particular mixture was just the error in the nitrogen pressure, except when the ratio He/N_2 was smaller than about 10.

The detector system sensitivity was constant for a given data run. Noise produced fluctuations in the peak current readings (intensity), which became as much as 20% of the signal level for the weak rotational lines. The use of 15-20 lines (laboratory data) in a single rotational

intensity distribution reduced the uncertainty involved in interpreting the behavior of each given data set. Errors were typically ±5% or less.

Additional rotational intensity distributions were observed at temperatures other than ambient, in the cryostatic chamber and the helium wind tunnel. Figure 3.17 illustrates one such scan. Here errors are approximately the same as in the laboratory case. Test data were observed in 15-30 seconds, quickly enough to insure constant ambient conditions. The individual line intensities, i_{PMT}, were comparable to the laboratory observations.

It should be noted that the photomultiplier signal, i_{PMT}, has been and will continue to be written as I to represent the intensity. For the rotational measurements, only the relative intensity is important. The data have been corrected for beam current variations, background signal (photomultiplier dark current) and other systematic changes, then normalized for convenience.

4. RESULTS

Rotational Distribution Observations

The experiments discussed in chapter 3 focussed upon recording the resolved R-branch rotational spectrum of N_2^+, B-X bands in varied mixtures of helium and nitrogen. Observations were made mainly of the (0,0) band, although the (0,1) band was studied for comparative purposes (see Table 3.3). The R branch lines of the (0,0) band could be used for K' up to 19. For K'> 19 (shorter wavelengths), the 388.9 nm. helium line and (1,1) band of nitrogen overlapped the spectrum. The results presented here are those obtained using the mixing chamber described in figure 3.8. (The preliminary data showed complete agreement.)

In order to illustrate the results compactly but completely, an effective rotational temperature is shown for each nominal set of conditions studied. The effective temperature is determined using $- \ell n (I_{K'}')$ as described in chapter 2. (I' refers to the measured intensity.) Table 4.1 provides the complete set of results. The r.m.s. error (square root of the variance) associated with each point is given. Some are ±5% or larger. The reason is that the intensity data deviates, in a systematic fashion, from the ideal linear equation. However, this manner of presentation does not clearly indicate the deviation.

The calculated effective rotational temperature in-

Table 4.1. Effective Rotational Temperatures in Mixtures. Laboratory data; all at ambient, 295±3°K.

Nitrogen Partial Pressure (microns)	Nitrogen Partial Pressure (N/m^2)	Gas Mixture (He/N_2)	Measured Effective Rotational Temperature* °K (± std. dev.)
5.0	.67	5	309±12
5.1	.68	10	352±14
5.0	.67	42	390± 8
5.7	.76	92	427±10
5.1	.68	510	422±22
10	1.3	5	330± 4
10.5	1.4	10	361± 8
10.2	1.4	96	395±20
10.3	1.4	234	419±23
10.1	1.3	599	433±16
10.	1.3	1000	446±12
21.6	2.9	9	369± 7
20.0	2.7	45	433±19
20.3	2.7	141	451±17
20.2	2.7	298	427±15
51.6	6.9	10	394± 8
49.7	6.6	20	419± 9
50.0	6.7	54	446±14
50.1	6.7	123	429±13
94.2	12.6	6	383± 7
96.0	12.8	12	406± 9
94.8	12.6	25	419±10
95.8	12.8	44	429±11
2.7	.36 (Cryostat)	99 (55,52°K)	92±19, 82±10
10.5	1.4 (Cryostat)	99 (116°K)	212±27

*A linear least squares analysis was used to determine these "best fit" temperatures.

creases as the ratio of helium to nitrogen increases. That tendency is clear. Figures 4.1 illustrate the effect of helium upon the rotational spectrum by showing experimental values for the l.h.s. of equation (2.23) plotted as a function of K' (K' + 1). For pure nitrogen, figure 4.1a, the result is reasonably linear but when several times as much helium is added to the nitrogen, systematic departures from linearity occur (figures 4.1b-4.1d). There are several possible explanations for such behavior. The nitrogen ground state rotational distribution may become altered by collisions. Variations from the dipole approximation which describes the ionization-excitation process are possible. Collisional effects may alter the excited N_2^+B rotational states. (An explanation is given in the next chapter.)

The rotational intensities are also displayed by plotting $I'_{K'}$ as a function of K' . $I'_{K'}$ is multiplied by 2 for each line with K' even. (This accounts for the nuclear spin factor of ½.) Figure 4.2 illustrates the distribution of intensities for electron impact fluorescence in pure nitrogen, according to the dipole excitation model. Figures 4.3a-4.3d compare N_2^+, B-X spectra observed in mixtures at room temperature, for the mixtures indicated. These are normalized as indicated.

The choice of a line for normalization is somewhat

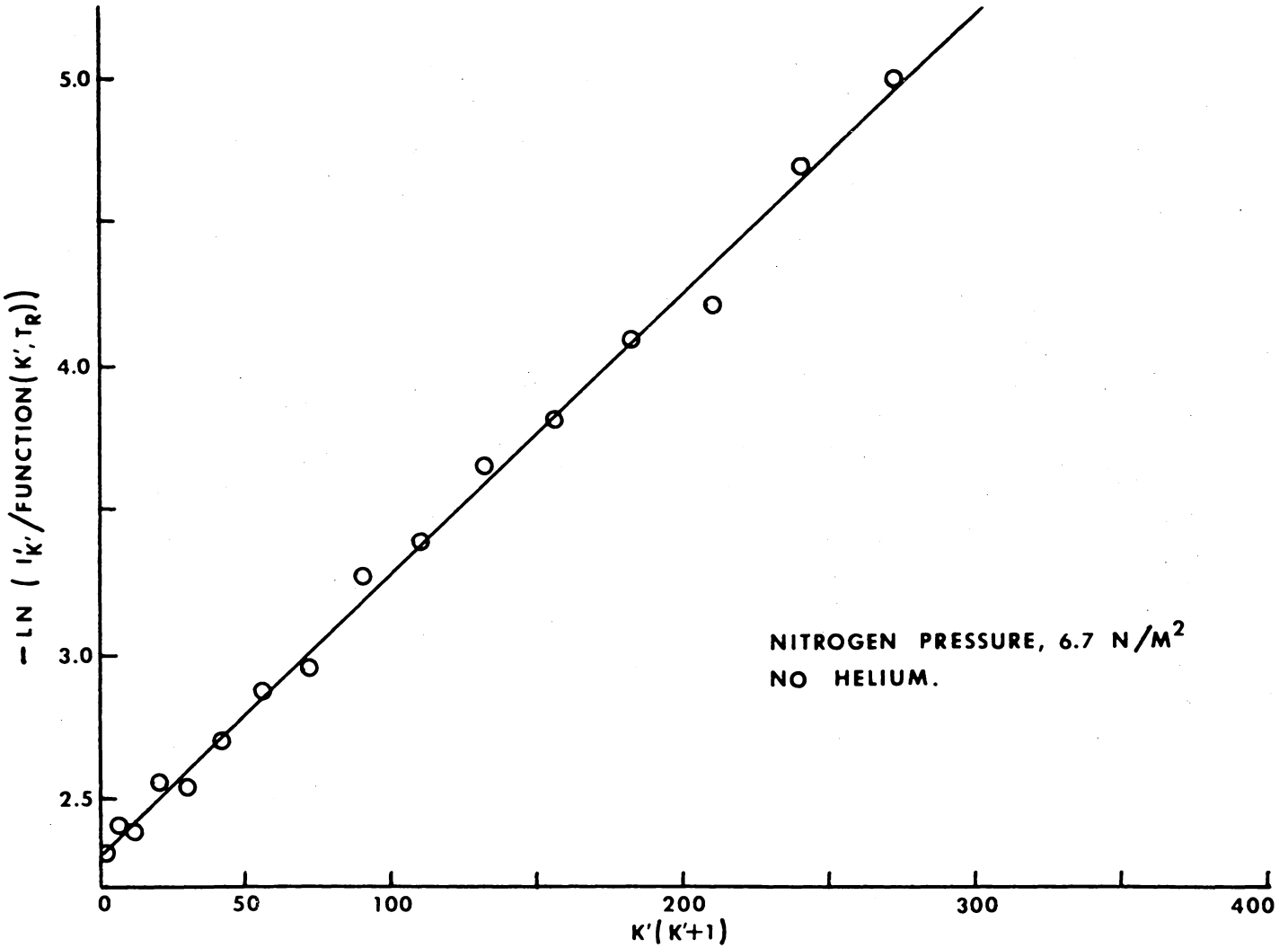

FIGURE 4.1a. LOGARITHMIC FUNCTION FROM EQUATION (2.23), PLOTTED FOR THE OBSERVED ROTATIONAL INTENSITIES, $I'_{K'}$, OF THE N_2^+, B–X (0,0) BAND. THE MEASURED ROTATIONAL TEMPERATURE IS 291° K.

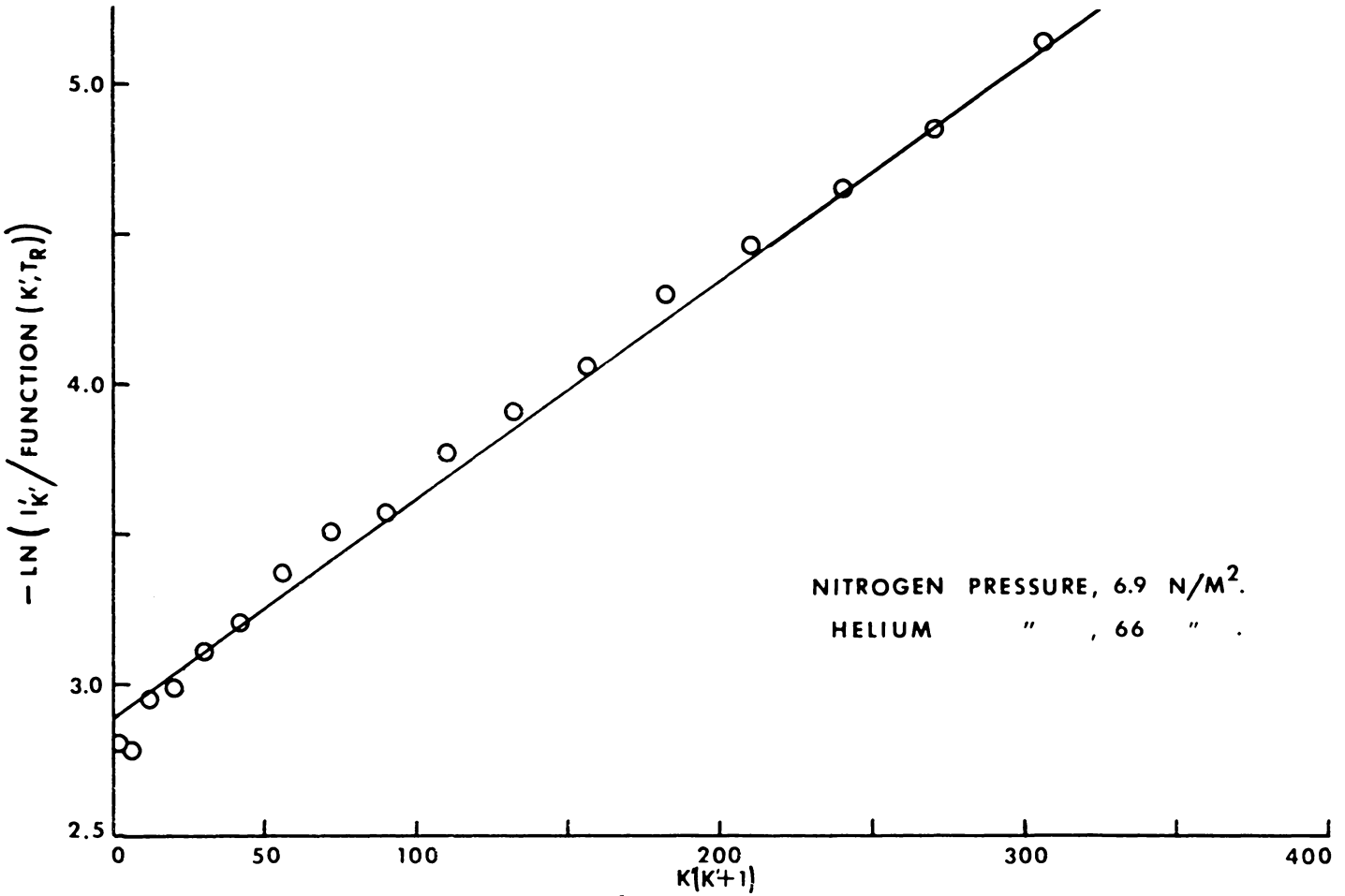

FIGURE 4.1b. LOGARITHMIC FUNCTION FROM EQUATION (2.23), PLOTTED FOR THE OBSERVED ROTATIONAL INTENSITIES, $I'_{K'}$, OF THE N_2^+, B–X (0,0) BAND. THE MEASURED ROTATIONAL TEMPERATURE IS 394° K.

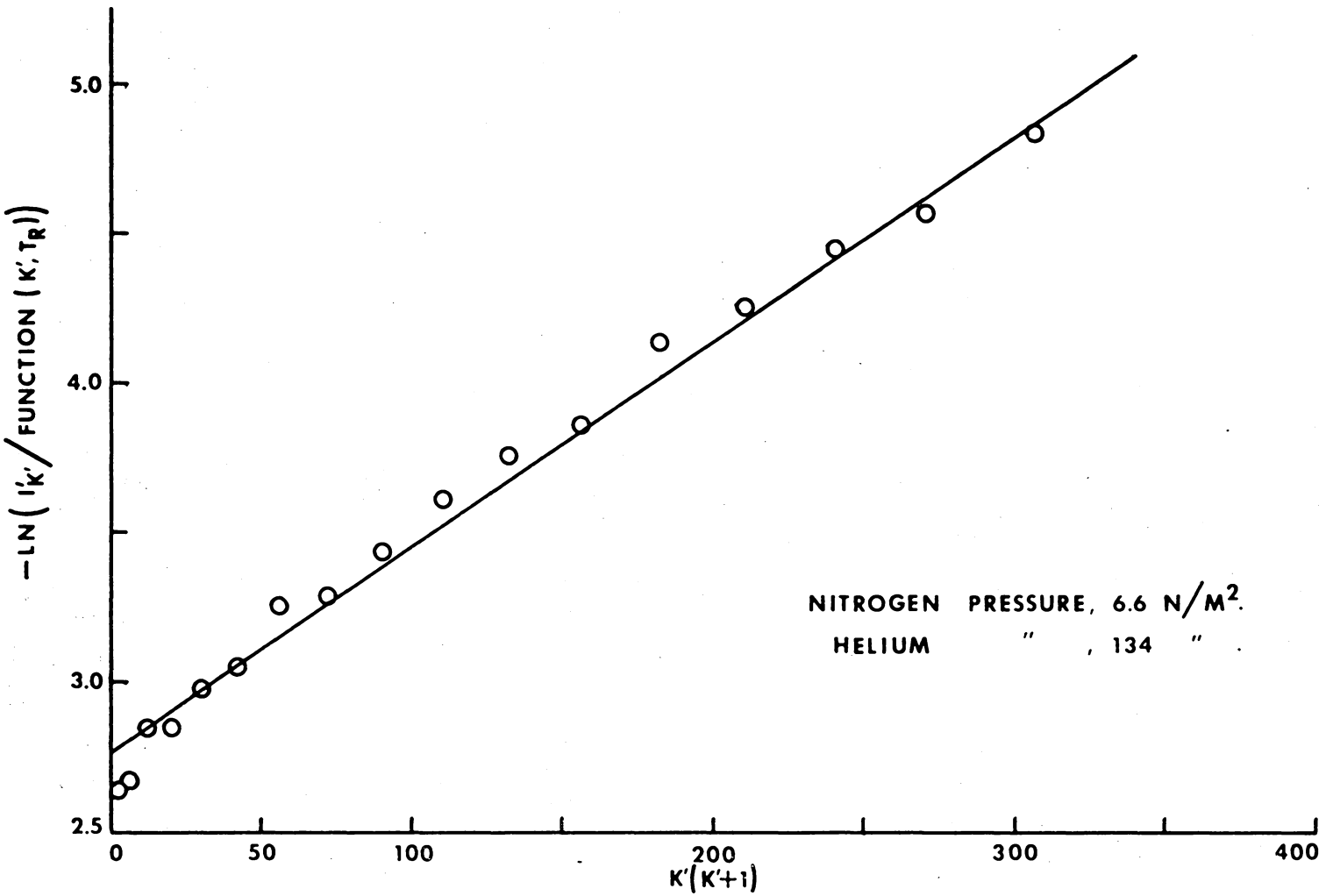

FIGURE 4.1c. LOGARITHMIC FUNCTION FROM EQUATION (2.23), PLOTTED FOR THE OBSERVED ROTATIONAL INTENSITIES, $I'_{K'}$, OF THE N_2^+, B–X (0,0) BAND. THE MEASURED ROTATIONAL TEMPERATURE IS 419°K.

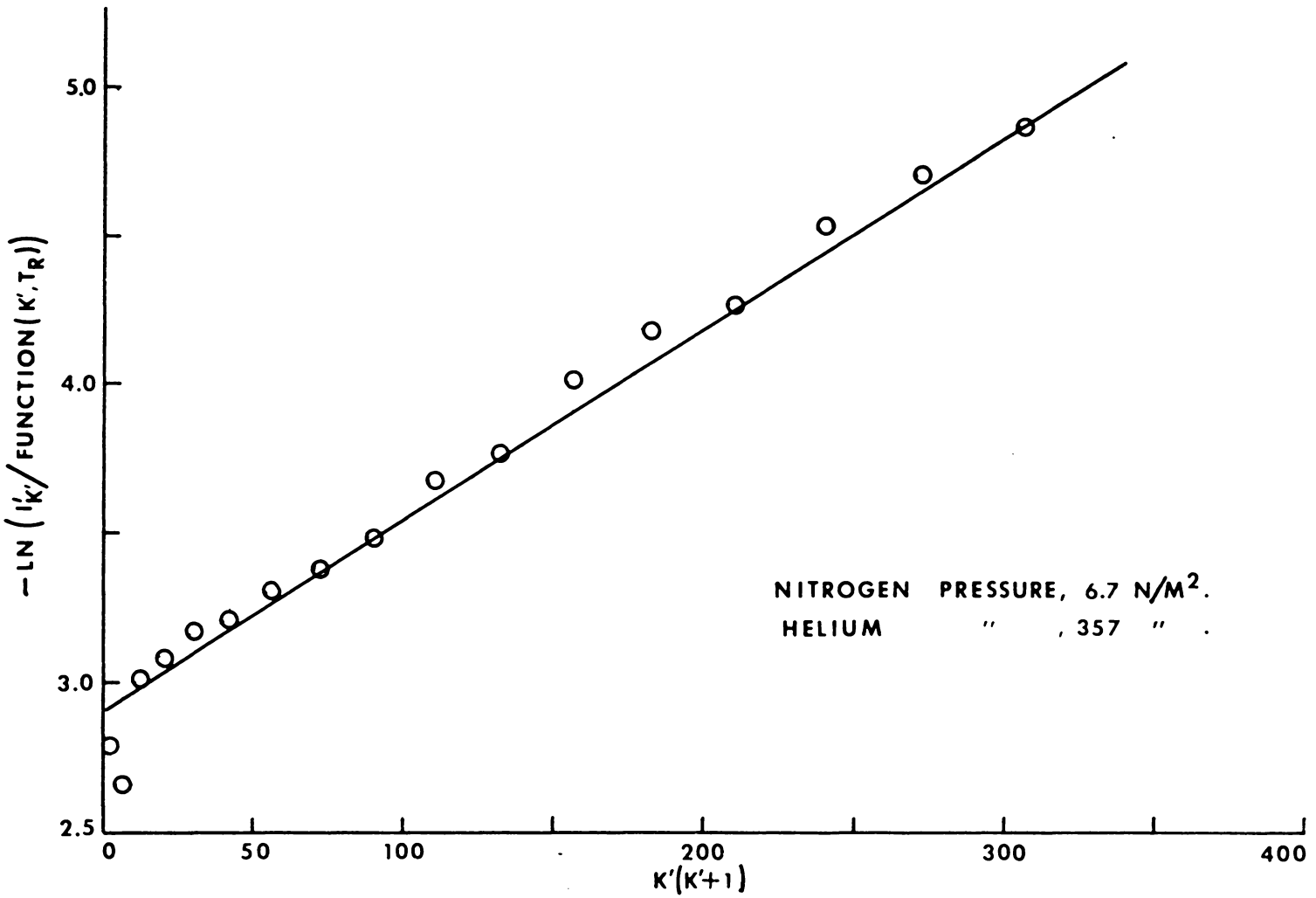

FIGURE 4.1d. LOGARITHMIC FUNCTION FROM EQUATION (2.23), PLOTTED FOR THE OBSERVED ROTATIONAL INTENSITIES, $I'_{K'}$, OF THE N_2^+, B–X (0,0) BAND. THE MEASURED ROTATIONAL TEMPERATURE IS 446° K.

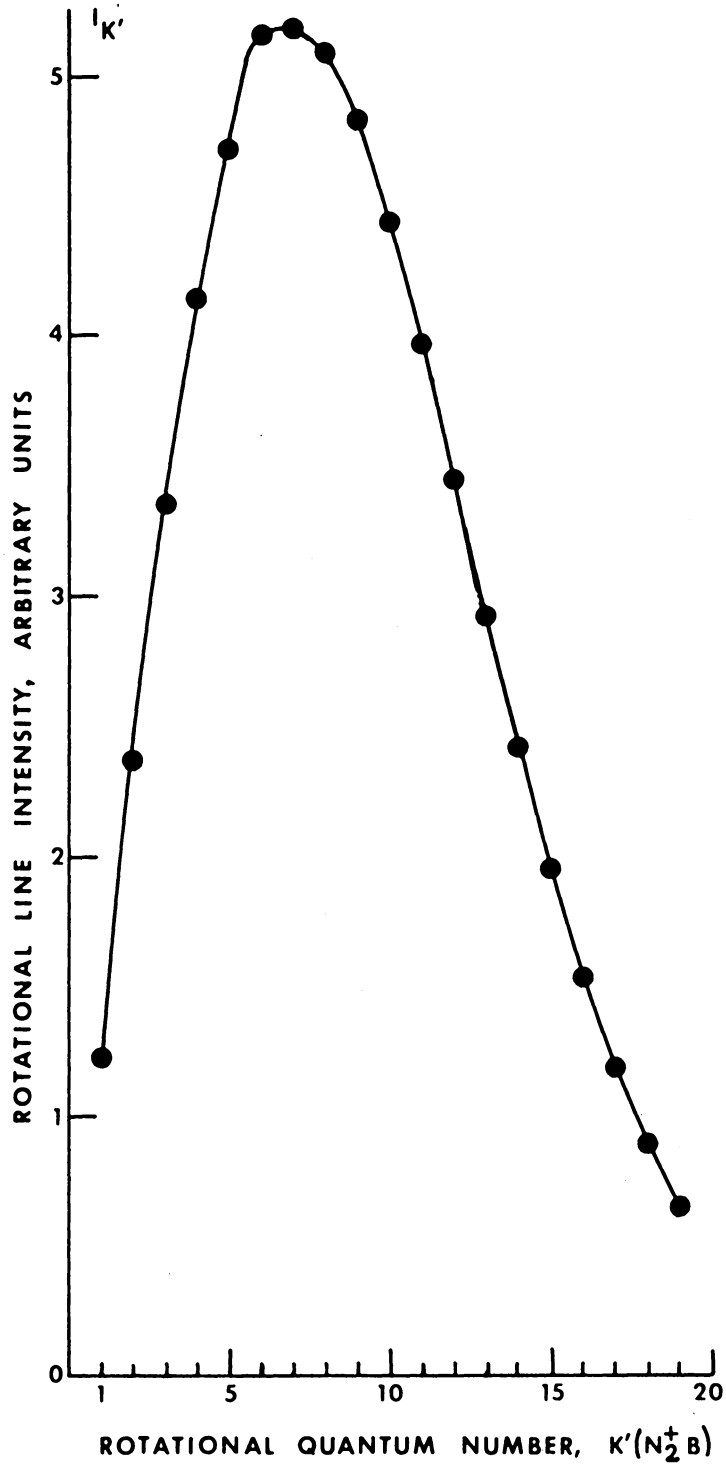

FIGURE 4.2. CALCULATED ROTATIONAL INTENSITIES FOR 300° K, BASED UPON THE DIPOLE MODEL OF N_2^+B EXCITATION AND SUBSEQUENT FIRST NEGATIVE EMISSION. THE SOLID CIRCLES ARE THE CALCULATED RELATIVE INTENSITIES. THE CURVE IS DRAWN FOR COMPARATIVE PURPOSES.

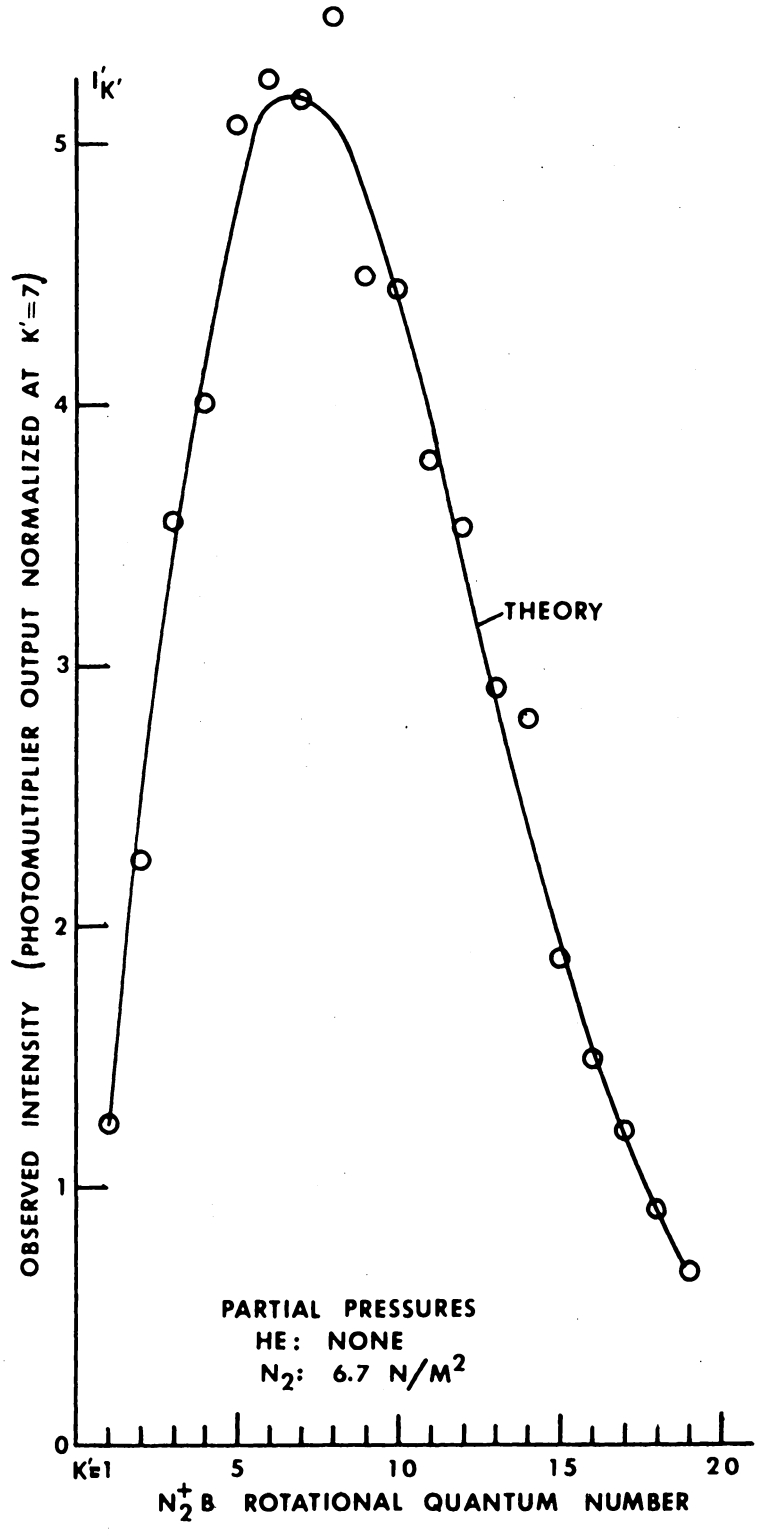

FIGURE 4.3a. OBSERVED ROTATIONAL INTENSITIES. THE DATA (OPEN CIRCLES) OF FIGURE 4.1a ARE COMPARED WITH THE DIPOLE EXCITATION THEORY FOR 300° K.

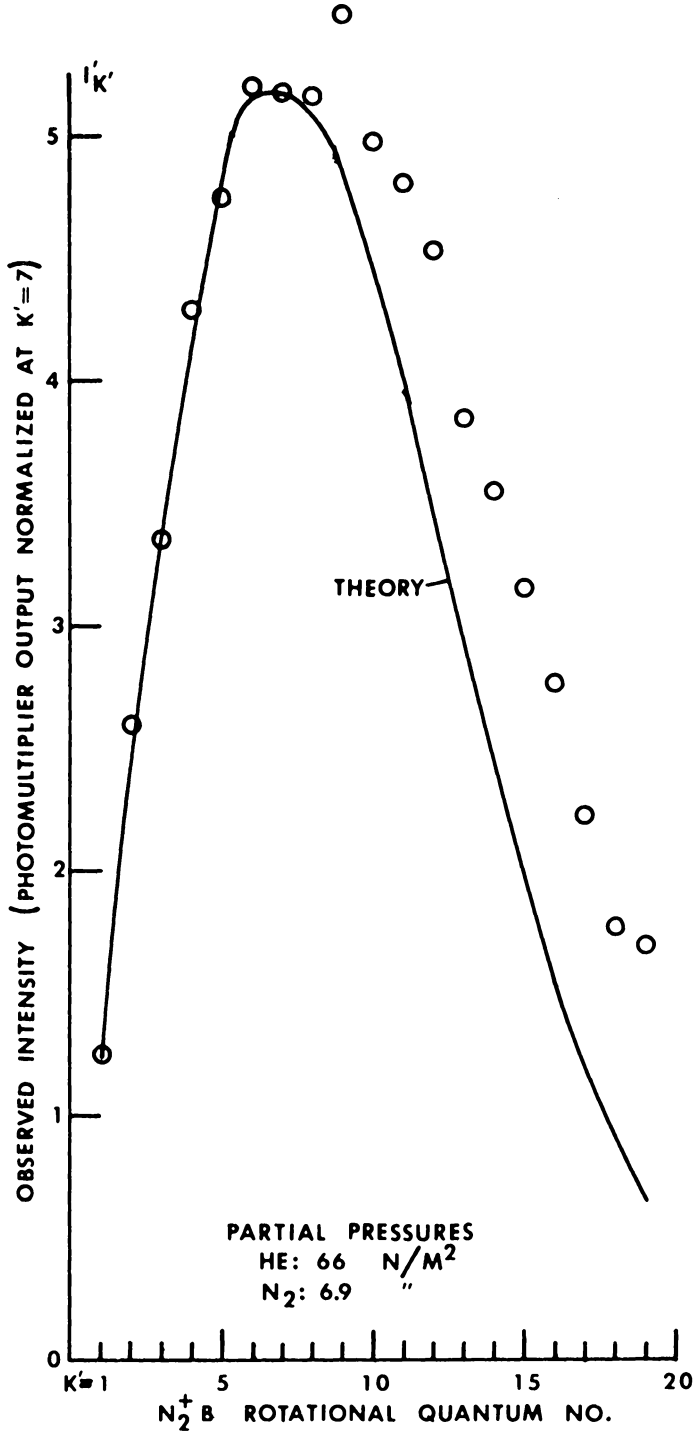

FIGURE 4.3b. OBSERVED ROTATIONAL INTENSITIES. THE DATA (OPEN CIRCLES) OF FIGURE 4.1b ARE COMPARED WITH THE DIPOLE EXCITATION THEORY FOR 300° K.

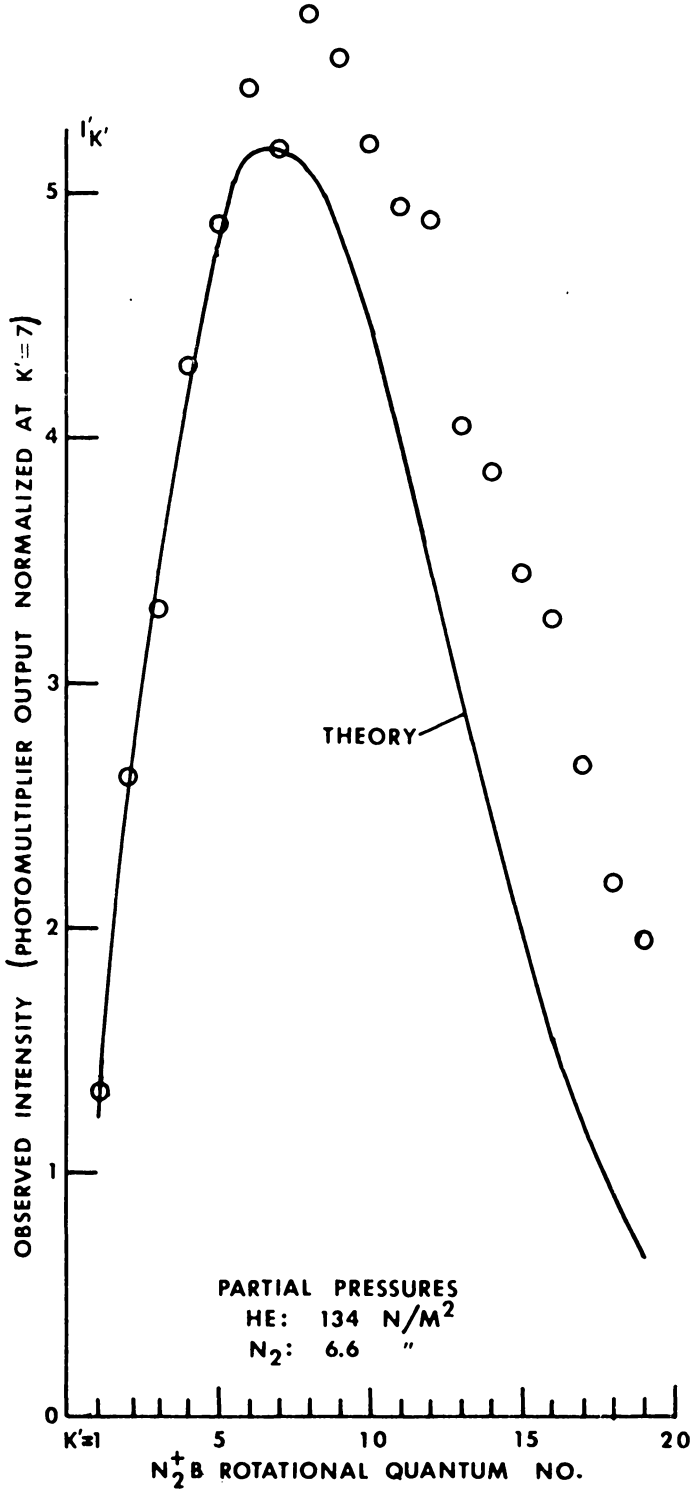

FIGURE 4.3c. OBSERVED ROTATIONAL INTENSITIES. THE DATA (OPEN CIRCLES) OF FIGURE 4.1c ARE COMPARED WITH THE DIPOLE EXCITATION THEORY FOR 300° K.

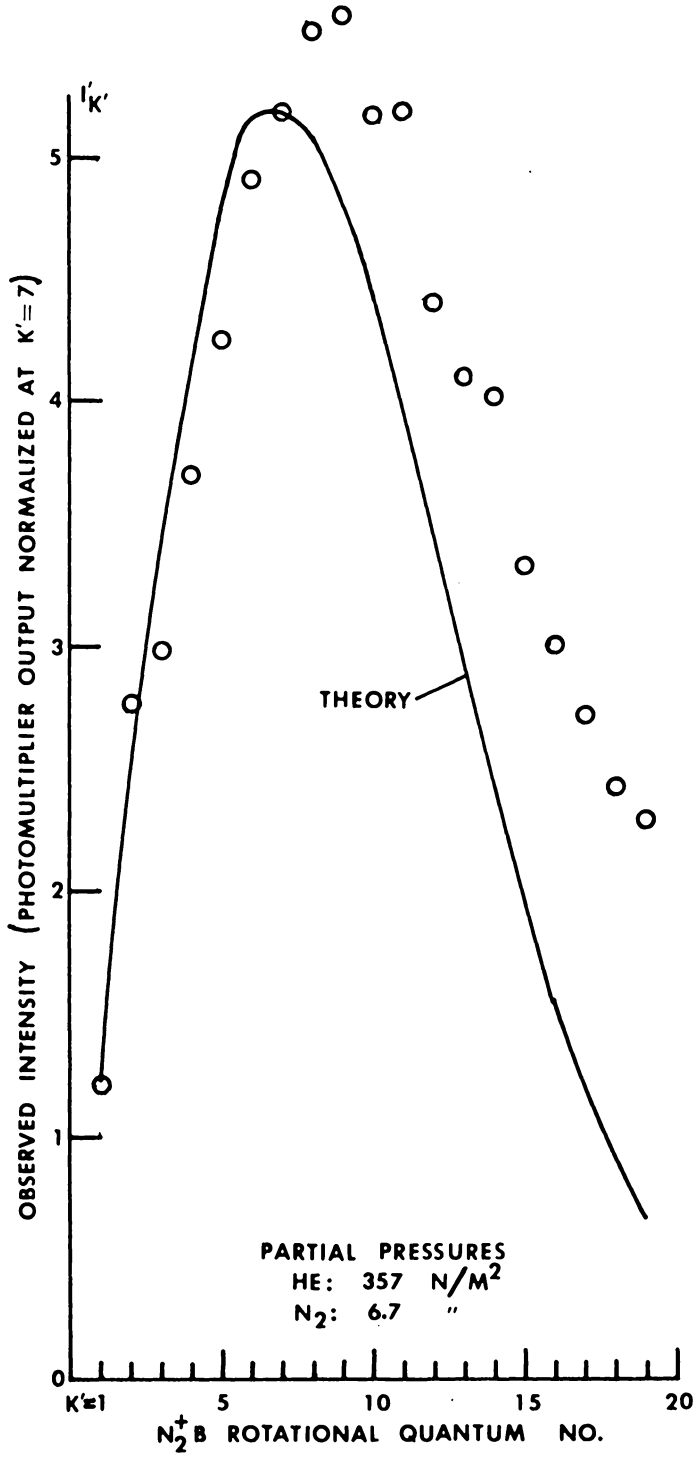

FIGURE 4.3d. OBSERVED ROTATIONAL INTENSITIES. THE DATA (OPEN CIRCLES) OF FIGURE 4.1d ARE COMPARED WITH THE DIPOLE EXCITATION THEORY FOR 300° K.

arbitrary. For the plots in figures 4.3, the most intense line of the theoretical distribution (Figure 4.2), K'=7, is used. The spectrum is systematically shifted, however, if normalization is performed at $K' \geq 8$. Then, the lines for $K' \lesssim 8$ are forced below the case for pure N_2. Such a selective reduction of intensities would be very difficult to explain and has not been previously observed. Increased $I_{K'}$ for the rotational lines above $K' \simeq 7$ is a more plausible explanation, as will be discussed further.

P branch lines overlapping into the R must also be considered when normalization is accomplished. In nitrogen, P branch lines fold back upon themselves. Hence, the P branch line for which K' =26 lies very near the R branch line for which K' =1 in the (0,0) band. Their separation was not resolved in these experiments. Previous work[72,73,74] shows that the overlapping is small (a 2% contribution to the K'=1 and K'=2 lines) at room temperature, and negligible at lower temperatures.

At elevated rotational temperatures, the overlap can significantly affect several R branch lines; 400° K requires corrections out to K'=6. All of the work reported here was accomplished at room temperature, or below. However, as the tabulated results illustrate, the effective calculated temperature becomes significantly higher at particular

mixture conditions. Trial normalizations for a given spectrum, based upon different lines for which $K' \leq 7$, showed slight differences in some instances.

An important parameter variation was achieved when several tests were conducted in mixtures for which the gas temperature was substantially below 300° K. Figures 4.4a and 4.4b show $I'_{K'}$, for N_2^+, B-X, (0,0) at two gas temperatures, where the gas was introduced pre-mixed and cooled in a cryostatic chamber, the same chamber as in reference 64. Figure 4.5 illustrates the (0,0) band rotational spectrum observed in the hypersonic, very cold helium flow of Langley Research Center's 22-inch Helium Tunnel. The calculated static temperature of that flow was less than 4° K. The nitrogen content was not precisely known in the latter case, but did not exceed 400 parts per million. The results indicate that the intensity values observed are significantly enhanced for the higher rotational energy states.

The clearest manner of display, to show the enhancement effect due to helium mixtures, as exhibited by the rotational spectra, is to plot $\Delta I_{K'}$ as a function of K'. $\Delta I_{K'}$ is the difference between the calculated intensity, $I_{K'}$, according to the dipole excitation theory and the observed intensity, $I'_{K'}$, normalized appropriately. Figures 4.6a-4.6d illustrate

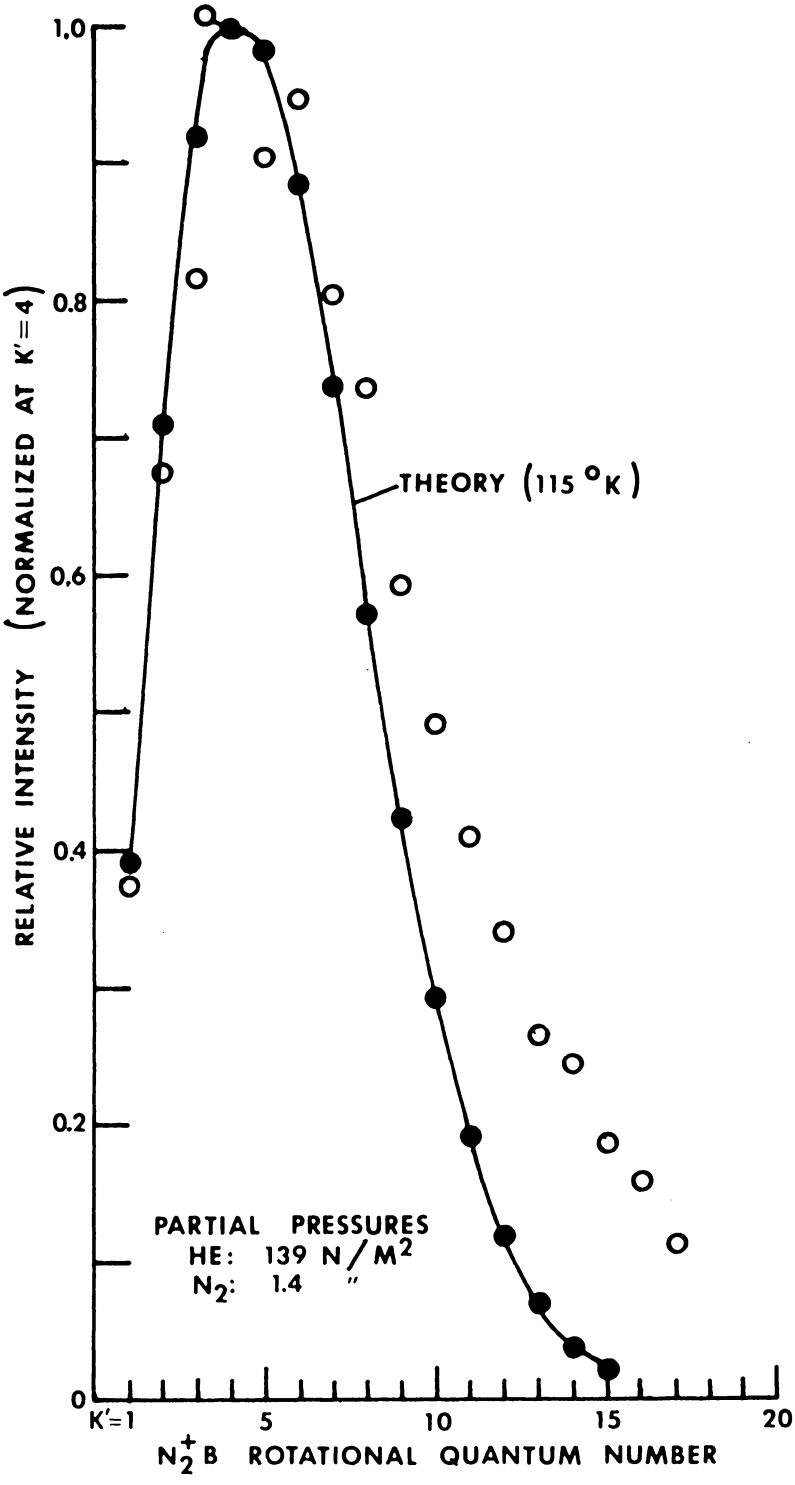

FIGURE 4.4a. N_2^+ B–X (0,0) BAND ROTATIONAL SPECTRUM; CHAMBER TEMPERATURE ≈116°K. DATA (OPEN CIRCLES) ARE COMPARED WITH THE DIPOLE EXCITATION THEORY.

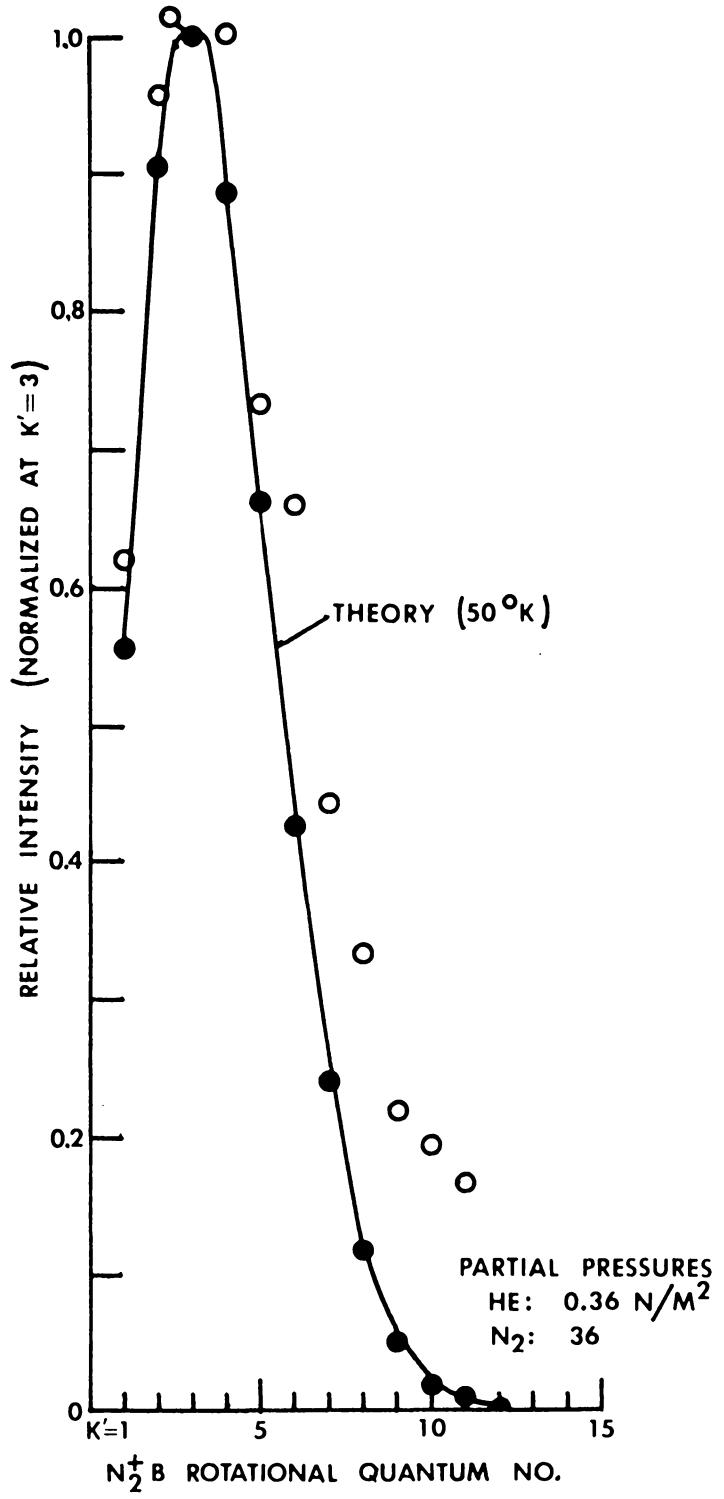

FIGURE 4.4b. N_2^+ B–X (0,0) BAND ROTATIONAL SPECTRUM; CHAMBER TEMPERATURE ≈50° K. DATA (OPEN CIRCLES) ARE COMPARED WITH THE DIPOLE EXCITATION THEORY.

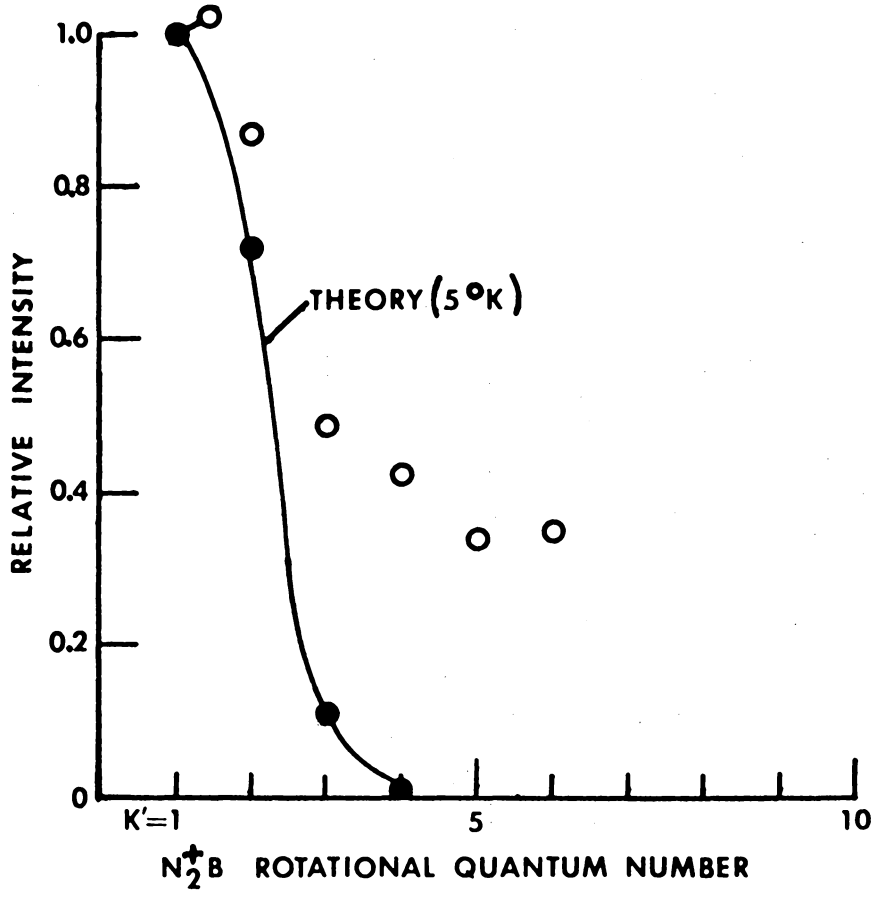

FIGURE 4.5. N_2^+, B–X (0,0) BAND ROTATIONAL SPECTRUM AT VERY LOW TEMPERATURE. OPEN CIRCLES ARE DATA FROM FIGURE 3.17.

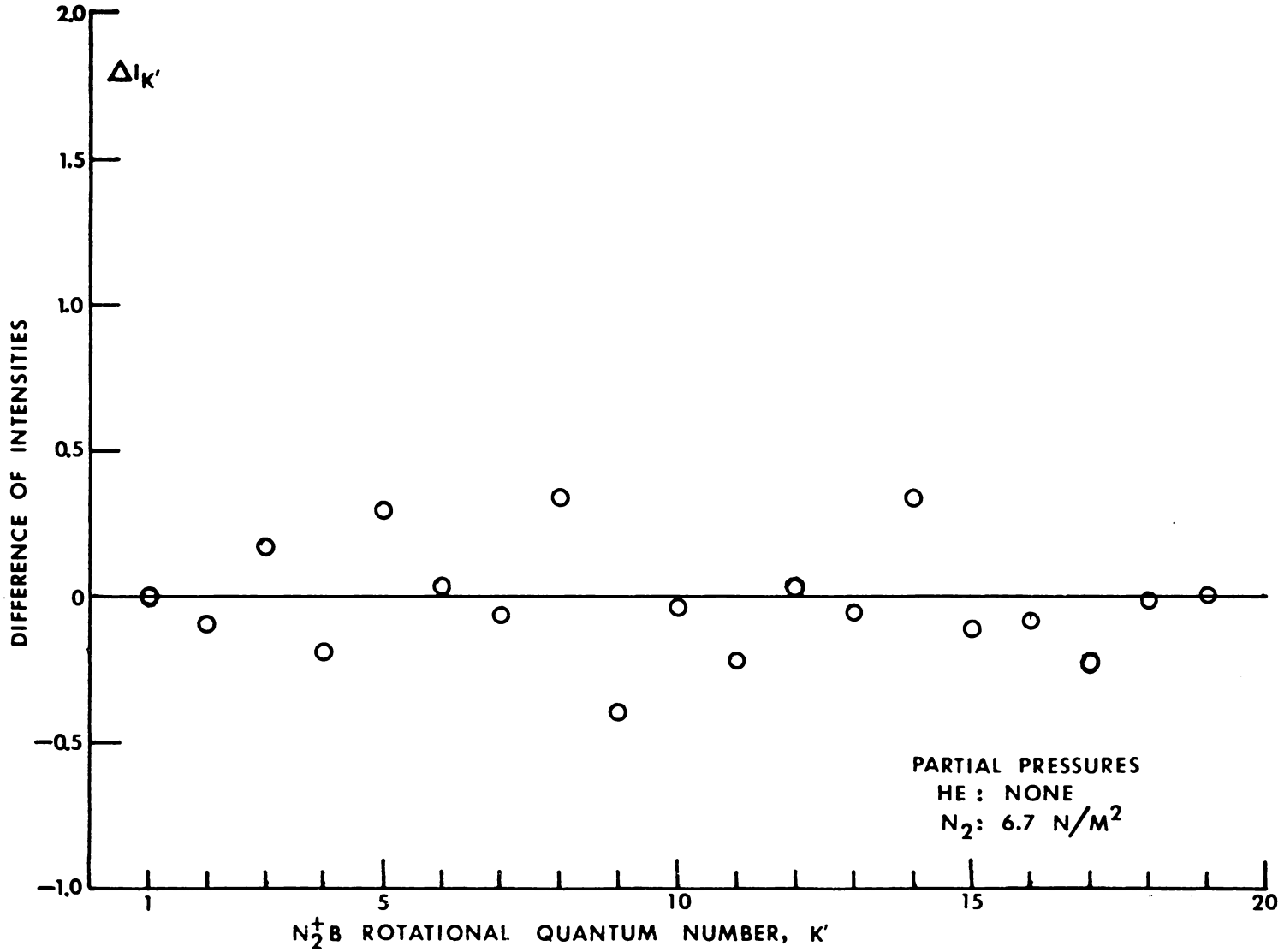

FIGURE 4.6a. INTENSITY DIFFERENCE BETWEEN THE I'_K, OF FIGURE 4.3a AND THE DIPOLE EXCITATION THEORY. (NORMALIZED AT K'=1.)

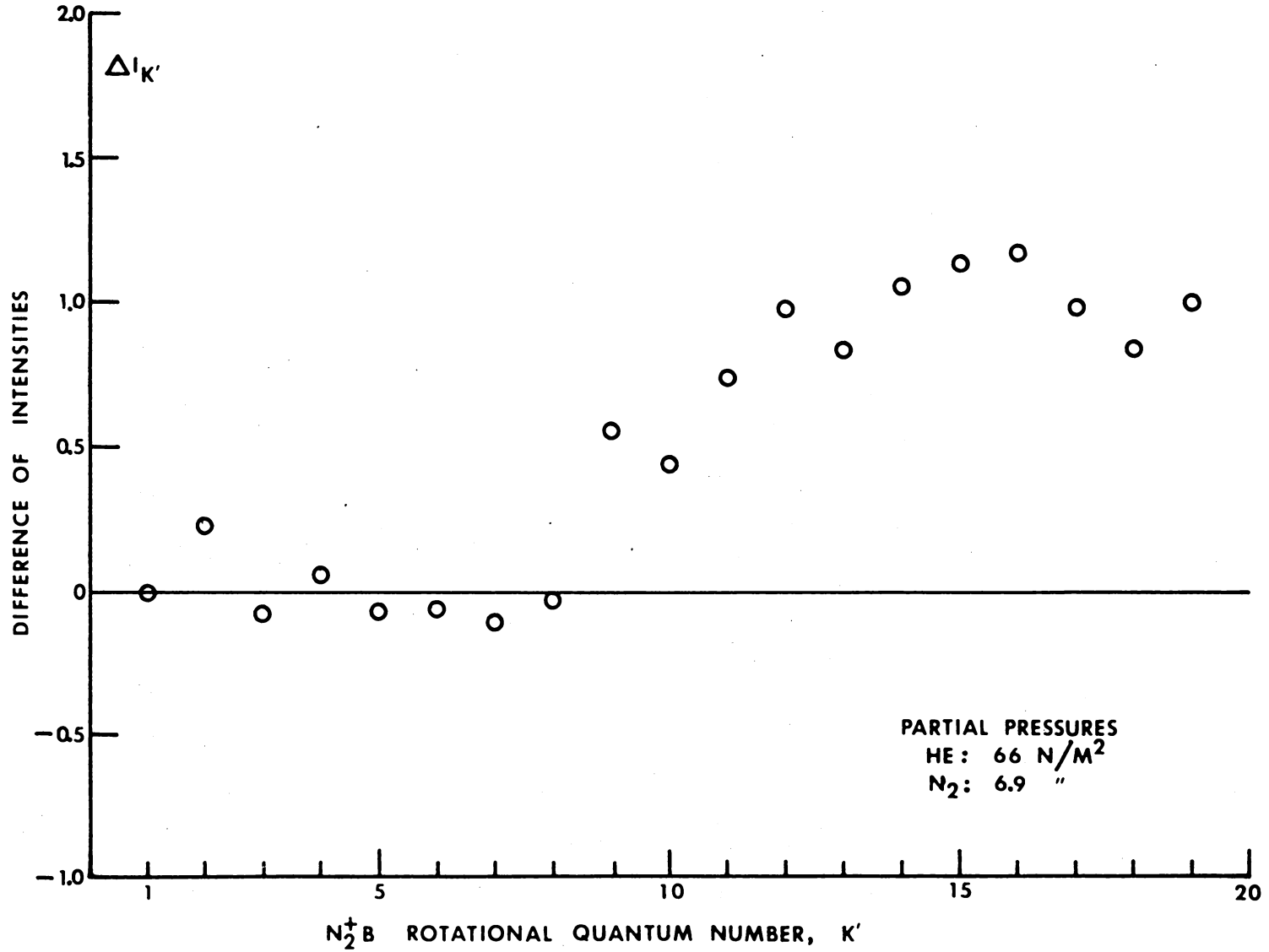

FIGURE 4.6b. INTENSITY DIFFERENCE BETWEEN THE $I'_{K'}$ OF FIGURE 4.3b AND THE DIPOLE EXCITATION THEORY. (NORMALIZED AT K'=1.)

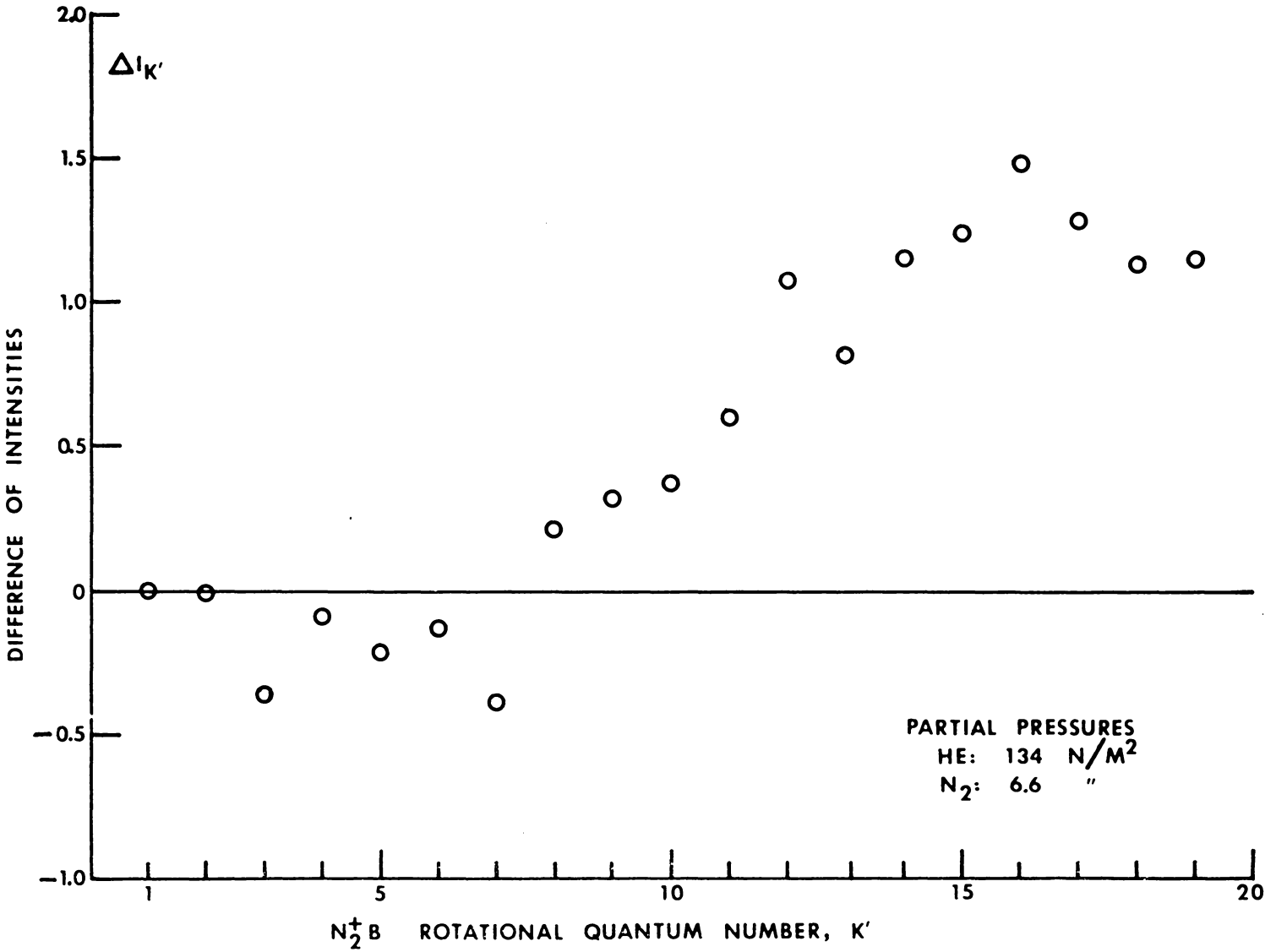

FIGURE 4.6c. INTENSITY DIFFERENCE BETWEEN THE $I'_{K'}$ OF FIGURE 4.3c AND THE DIPOLE EXCITATION THEORY. (NORMALIZED AT K'=1.)

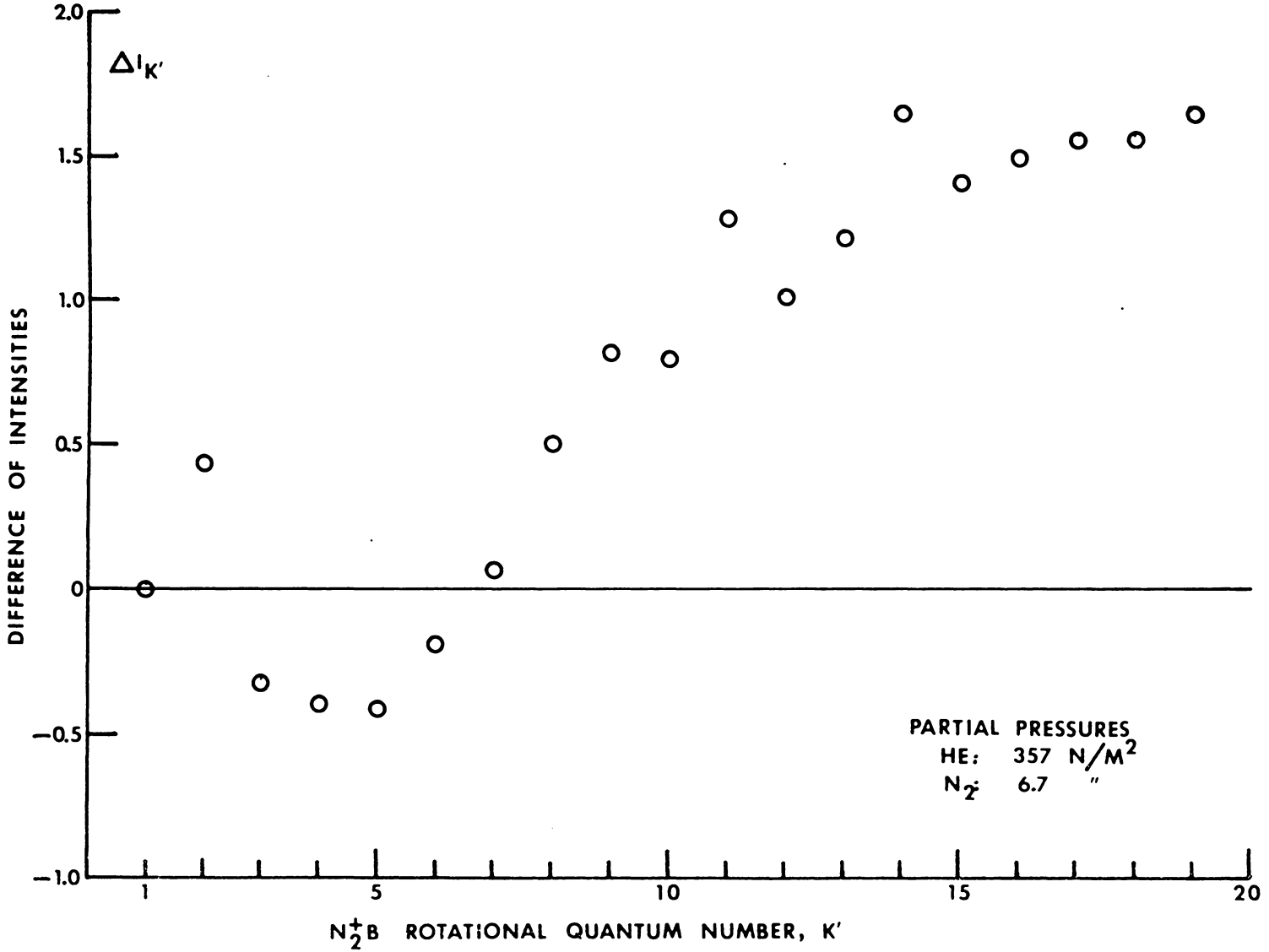

FIGURE 4.6d. INTENSITY DIFFERENCE BETWEEN THE I'_K, OF FIGURE 4.3d AND THE DIPOLE EXCITATION THEORY. (NORMALIZED AT K'=1.)

$\Delta I_{K'}$ for the data series shown in the figures 4.1 and 4.3. The enhancement for $K' \geq 7$ shows up very clearly.

Survey Spectra

Qualitative spectral scans were recorded at several mixture conditions, as previously described. Table 3.2 indicates the most prominent features which occurred for a moderate mixing condition. Table 4.2 adds spectral lines which were observed at higher helium density and a larger mixing ratio. These surveys do not include intensities because such quantitative observations were not practical with the apparatus which was utilized.

The first negative band system of N_2^+ and the excited neutral helium atoms account for nearly all the prominent features. Some high vibrational quantum number N_2^+, B-X bands ($v \geq 12$, red-shaded) were found at the highest pressure conditions. A single line, which is apparently He^+, consistently appeared. The presence of hydrogen was noted, particularly by the Balmer series lines at 486.13, 434.05, and 410.17 nm. (Pump oil backstreaming was found to be the source of this impurity.) Other major spectral sources were absent; notably He_2, which bands have been observed using an electron beam at high helium pressures ($\sim 2 \times 10^3$ N/m^2), and N_2 second positive bands. N^+ lines, probably due to the predissociation of $N_2^+ C\,^2\Sigma_u^+$, were observed when

Table 4.2. Spectral Survey Results.*

Spectral Feature	Assigned Wavelength	Special Notes
He I, 10^3D-2^3P	355.44 nm.	**
" , 9^3D-2^3P	358.73	**
N_2^+,B-X, (20,16)	376.3	Red shaded. **
" , " , (18,15)	378.3	Red shaded. **
He I, 6^1S-2^1P	416.90	**
N_2^+,B-X, (4,6)	451.59	**
" , " , (3,5)	455.41	**
" , " , (2,4)	459.97	**
He II, 4-3	468.6	**
N_2^+, B-X, (13,15)	474.4	Red shaded. **
" , " , (14,16)	485.0	Red shaded. **
H I, 4-2	486.1	Weak, but present in most tests.
N_2^+,B-X, (4,7)	495.8	**
N II, 3^3P-3^3S	500.1,500.5	Observed only for low He/N_2.
N_2^+,B-X, (2,5)	507.7	**
" , " , (19,20)	513.7	Red shaded. **
" , " , (1,4)	514.9	**
" , " , (0,3)	522.8	**

*Included here are additional spectral lines and bands observed during various survey tests. See Table 3.2 for the remainder which were identified.

**All of these features were found at high helium pressure and for large helium to nitrogen ratios (100).

the helium pressure was not high ($\lesssim 20$ N/m^2), but they were greatly diminished as the helium pressure increased (not found for $p_{He} \sim 133$ N/m^2).

Other Results

Spectrometric observations of the N_2^+, B-X $\Delta v = -1$ sequence were attempted. The results are very difficult to interpret. The major reason stems from the total band fluorescence spatial dependence. To insure that the observed signal for a band ($\sum_{K'} I'_{K'}$) is representative of its intensity, the entire source (here the electron beam effective geometrical cross section) must be included by the optics. The spectrometer did not observe the entire cross section as the beam spread at higher densities. Hence, the signal was not necessarily correlated with the emitted intensity.

The filter systems were designed to overcome that handicap. However, in the mixing chamber of figure 3.8, the primary electrons were scattered back from the collector. There was also light reflected from the walls of the chamber into the field of view. Both of these effects varied with the gas pressure and mixture conditions. While signals resulting from the electron beam passage through the gas could be repeated for a given set of conditions, the correlation with number density of the excited species was lost.

Hence, the interference filter system served only a monitoring function during the final mixing chamber test series. The trends of the N_2^+, B-X fluorescence and the He (3^1P - 2^1S) from the preliminary tests were shown in figure 1.3 and 3.2. These were supported by the later results to the extent possible.

5. INTERPRETATION

The tabulated spectral features indicate that numerous excited helium singlet and triplet atoms were observed in S, P, and D levels. To a good approximation, the primary electron beam excites only the n^1P states directly. Several energy transfer mechanisms, including cascade from higher excited states, the mixing of the F states, and violation of the strict dipole excitation model produced the proliferation of excited species. These processes, which are known in discharges and afterglow sources, occurred due to the higher energy electron beam source.

Three species of excited helium are particularly important because they are energetic enough to excite and ionize nitrogen to N_2^+B. They persist for periods longer than typical dipole radiation lifetimes, since collisional processes account for their excitation and decay. These are He^+, He_2^+, and $He(2^3S)$.

The abundance of atomic excited states indicated that He_2^+ was formed by the associative ionization process, equation (2.15b). He_2^+ radiation has not been observed to date. The presence of the ion may sometimes be inferred from He_2 bands, formed by recombination[26,75]. However, no diatomic helium bands were definitely identified from the spectral surveys. Their presence as very weak spectral emission may have gone undetected at high helium pressures ($> 10^2$ N/m^2).

Rapid collisional processes with impurities are known to deplete He_2^+[76].

The atomic ion was directly observed at 468.6 nm, as shown in Table 4.2. All of the survey traces for moderate and higher pressures ($p_{He} \geq 10^2$ N/m^2) exhibited that line. Both the He_2^+ and He^+ ions have been observed previously to occur at the same test conditions, and to transfer charge[77,78,79]. He^+ conversion to He_2^+, according to equation (2.15a), becomes significant at high pressures. That conversion and the associative ionization thus presumably produced significant He_2^+.

Both ions excite and ionize nitrogen, as indicated in the first chapter. The molecular ion energy overlaps the vibrational energy levels of N_2^+B, while He^+ occurs close to N_2^+C levels. The reaction, $He^+ + N_2 \rightarrow He + N_2^+C$, with subsequent N_2^+, C-X fluorescence, and the occurrence of N^+ produced by N_2^+C predissociation[60-63], both indicate the existence of the atomic helium ion. However, N^+ lines were observed in nitrogen fluorescence only when little or no helium was present. N_2^+, C-X bands occur at wavelengths shorter than 350 nm and were not recorded. Excitation to other nitrogen ion excited states was not observed, consistent with other work[77]. The total N_2^+, B-X fluorescence increased notably with an increase in helium partial pressure (figure 1.3).

That change is more rapid than linear. It is explained by the excitation of helium, followed by the excitation transfer to nitrogen, in general.

A major contributor to the nitrogen fluorescence was the helium 2^3S metastable state. That particular state was populated through several mechanisms, including radiative decay from higher triplet states, collisional energy transfer and conversion of the 2^1S state. Since the triplet metastable state provides a nearly resonant source of N_2^+B excitation and is lost only through collisional mechanisms, it has long been identified as the dominating excitation source for excited impurity species[80-84]. This Penning ionization process dominated the excitation of N_2^+B. Although some disagreement exists, the process has generally been interpreted to follow the Franck-Condon principle. That is, the excitation process described by

$$He(2^3S) + N_2\,{}^1\Sigma_g^+(v_i'',K_i'') \rightarrow He(1^1S) + N_2^+B^2\Sigma_u^+(v',K') \quad (5.1)$$

occurs in such a manner that the v' states follow a population distribution governed by the vertical overlapping of wavefunctions, $\int\psi_{v'}^*,\psi_{v_i''}d^3r$. That is equivalent to saying that the internuclear distance is constant during the excitation-ionization. Therefore, it is assumed that

$$q_{v_i''v'} = |\int\psi_{v'}^*,\psi_{v_i''}d^3r|^2 \quad (5.2)$$

represents the Franck-Condon factor of the earlier equation (2.18).

The rotational states are also excited according to the principles described in the first chapter. Basically, the intensity of a rotational line is governed by the physics embodied in equation (2.22), with dipole selection rules applying to the excitation process. The primary mechanism is an $He(2^3S)$ atom collision with $N_2 X\,^1\Sigma_g^+$, as distinct from the electron impact for which the theory was originally developed. If these principles apply without deviation, $\ell n\{I^{v'v''_2}_{K',K''_2}/K'(G)\sigma^4_{K',K''_2}\}$ relates linearly to $K'(K'+1)$ for measurements of $I^{v'v''_2}_{K',K''_2}$. Furthermore, $\Delta I_{K'} = I'_{K'} - I_{K'}$ would be zero for all K provided $I'_{K'}$ and $I_{K'}$ are normalized in the same manner. Observations do not conform to these expectations; $\Delta I_{K'}$ deviates systematically from zero, and the $\ell n\{I'_{K'}\}$ function, equation (2.23), is not linear with respect to K'.

Recently, further studies of vibrational band populations of the nitrogen first negative system have been reported in helium-nitrogen mixtures[77,85]. The results of these studies were interpreted to indicate that N_2^+, B-X fluorescence departs from the Franck-Condon principle. In those cases, the nitrogen fluorescence was excited in a discharge, which contained predominantly helium. Only inconclusive trends

of the vibrational intensities could be derived from observations made during the present experiments. Band intensities for N_2^+,B-X, (0,1), (1,2) and (2,3) were observed and the populations of the v'=1 and v'=2 levels increased relative to v'=0 as helium was added to nitrogen at a constant partial pressure.

The detailed rotational spectra obtained in our work can be interpreted as stemming from N_2^+B, excited by $He(2^3S)$, He^+ and He_2^+. Detailed balance equations are very difficult to develop due to the complexity of the physical processes. A consistent interpretation of the experiments is possible, however. The results of several past research programs, in which only one or two excitation processes were dominate, support the following interpretation.

Let us briefly summarize the situation again. The three helium species $He(2^3S)$, He^+, and He_2^+ are identified as the principle source of nitrogen excitation. (The atomic and molecular helium ions will not be distinguished for the moment, but are considered together.) The observed rotational intensities, identified as $I'_{K'}$, were produced by passing an electron beam through helium which contained a small amount of nitrogen. These spectra consistently showed departure from the model presented in chapter 2. This departure may apply more widely than for just the helium mixtures.

However, the interpretation here applies strictly to helium. The results presented in the previous chapter illustrate the effect in several ways.

The hypothesis which explains the departure of $I'_{K'}$ from the dipole excitation model provides that two independent excitation-ionization processes occur at the same time in these mixtures. $He(2^3S)$ strongly excites N_2^+B and accounts for a major portion of the observed $I'_{K'}$. This Penning ionization process does follow the original model devised for energetic electrons. Equations (2.18)-(2.23) apply, except that the parameters associated with the electron beam have to be replaced with the triplet metastable density, $He(2^3S)+N_2(X)$ cross section, and so forth.

Helium ions also excite and ionize the impurity nitrogen. However, the ion-molecule excitation process does <u>not</u> follow the dipole excitation model. This conclusion is supported by the numerous previous experimental results cited. It is further borne out by some theoretical work done by J.C. Light and several co-workers[86-88]. They developed a so-called "phase space theory" to describe reactive collison processes in gases.

Their approach circumvents detailed calculations of cross sections (or reaction rates). Instead, the concept that production cross sections are averages over numerous

initial phase space coordinates is applied. The portion of phase space available to products in specific states is calculated. Its ratio to the total available phase space, considering energy and momentum conservation, provides the conditional probability for those product states. That probability, integrated over energy and momentum variables, yields the particular cross section sought.

A fundamental aspect of this theory, which applies to helium ion excitation of nitrogen at thermal energies, is the concept called strong coupling. This term is used in the context of reaction kinetics, and relates to how the reacting species behave. The reaction partners must interact by means of a potential which is substantially greater than zero over long ranges. That is, a reaction "complex" must form, or the particles must influence one another for a period long compared with characteristic internal motions of the molecule in the case of heavy particle-molecule interactions.

Gioumousis and Stevenson[90] present an approach, based upon classical mechanics, to estimate cross sections and reactions rates. Their calculations are based upon the interaction potential for an ion acting upon a spherical neutral molecule, given by

$$V_I(r) = \frac{-\alpha e^2}{2r^4} \quad . \tag{5.3}$$

α represents the molecular polarizability. The interaction is based upon the ion-induced dipole effect, and it oversimplifies matters. The reaction rate, for instance, depends upon the ion only through μ, the system's reduced mass. The cross section is a function of μg^2, where g is the relative velocity. Hence, this model does not distinguish between the He_2^+ and He^+ interactions with nitrogen in any fundamental manner. The results presented here, in Table 4.1 as values of T_R, and in the figures of chapter 4 as $\Delta I_{K'}$, are probably too coarse to reveal any fine distinction between He_2^+ and He^+. Thus, the two ions may be distinguished only on the basis of energetics. He_2^+ is, however, strongly favored over He^+ to produce N_2^+B from this consideration. Indeed, it is possible to infer that, at high helium pressures when He^+ is largely converted to He_2^+, $He(2^3S)$ and He_2^+ are the dominant sources of nitrogen first negative excitation. He_2^+ is then responsible for the enhancement of rotational lines at $K \geq 7$ in N_2^+, B-X bands.

An application of the phase space model was made by Moran and Fullerton[91]. They calculated the rotational excitation-ionization cross sections for $He^+ + N_2 \rightarrow He + N_2^+(C)$, among others. The results of these calculations included the dependence upon the vibrational state, upon the reaction energy, and particularly upon the rotational quantum number.

Figure 5.1 illustrates the cross section for excitation of the lowest vibrational state of N_2^+C, at thermal energy. $\Delta I_{K'}$, as plotted in the figures of chapter 4, resembles the behavior of these calculated cross sections. $\Delta I_{K'}$ compares with the ion excitation cross section since the $He(2^3S)$ excitation of nitrogen is independent of the ion excitation. The rate of excitation describing $N_2^+B^2\Sigma_u^+(v',K')$ production can be expressed by

$$R'_{ex} = \frac{dN}{dt}(He(2^3S)+N_2) + \frac{dN}{dt}(He^+,He_2^++N_2) \qquad (5.4)$$

The first term represents metastable production of N_2^+B (by $He(2^3S)$), the second, ion excitation. Overall, the rate of change in the population of K' state, assuming only radiative decay, is written

$$\frac{dN}{dt}K' = R'_{ex} - \sum_{v_2'',K_2''} N_{K'} A_{K'K_2''}^{v'v_2''} \qquad (5.5)$$

The terms of R'_{ex} are further described as

$$\frac{dN}{dt}(He(2^3S)+N_2) = \sum_{v_1''K_1''} g_1 N^M Q_{XB}^M(v_1'',K_1'';v',K')N_{v_1''K_1''}^{v'K'}(N_2) \qquad (5.6)$$

and

$$\frac{dN}{dt}(He^+,He_2^++N_2) = \sum_{v_1''K_1''} g_2 N^{ion} Q_{XB}^{ion}(v_1'',K_1'';v',K')N_{v_1''K_1''}^{v'K'}(N_2). \qquad (5.7)$$

g represents the average relative velocity between the colliding species, M refers to $He(2^3S)$, and Q is cross section (also averaged over velocity). This representation is anal-

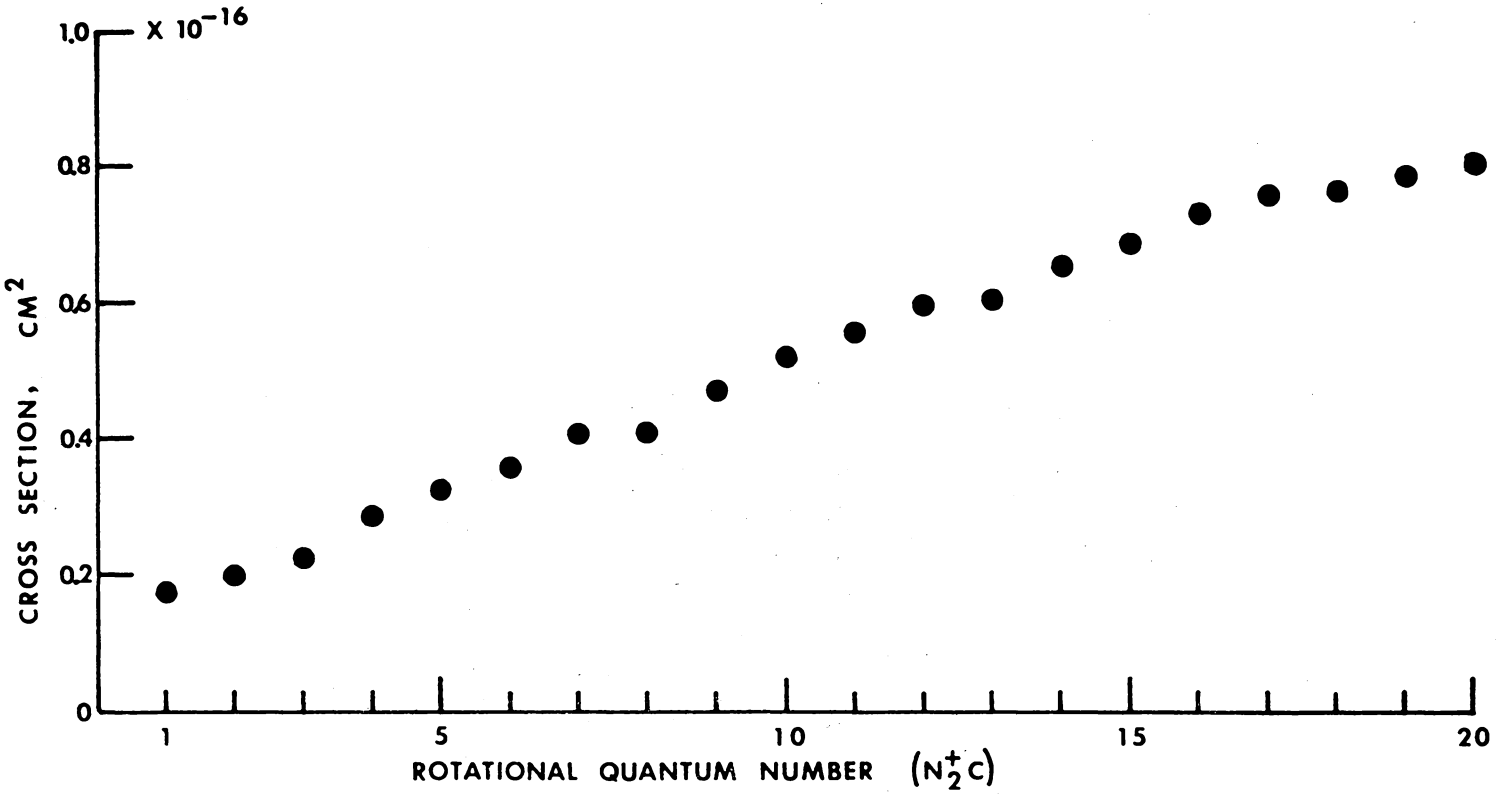

FIGURE 5.1. PHASE SPACE THEORY CROSS SECTIONS FOR $N_2^+(C^2\Sigma_u^+, v'=0, K')$ FORMED BY $HE^+ + N_2(X^2\Sigma_g^+, v'', K'') \rightarrow N_2^+C$. (THIS CURVE APPROXIMATES FIGURE 3, REFERENCE 91. RELATIVE REACTION ENERGY WAS 0.04 EV (THERMAL).)

ogous to that used in equations (2.18) - (2.23). The v_1'', K_1'' subscripts act as dummy variables, since we have not defined the v_1'', K_1'' and v', K' relationship to be the same for both equations (5.6) and (5.7).

It is important to recognize the complexity inherent in these two equations. N^M and N^{ion} are determined by complicated processes involving several rate expressions. The mechanism inherent in Q_{XB}^{ion} is difficult to express. Hence, the phase space theory presents a means to estimate the cross sections. If equilibrium is assumed, $\frac{dN_{K'}}{dt} = 0$. Writing the resulting expression for $N_{K'}$ into the intensity equation, we derive

$$I_{K'K_2''}' = \frac{(\sum_{vK} g_1 N^M Q^M N(N_2) + \sum_{vK} g_2 N^{ion} Q^{ion} N(N_2))}{A(K')} h\nu_{K'K_2''} A_{K'K_2''}. \tag{5.8}$$

Here, $A(K') = (A_{K'K'-1}^{v'v_2''} + A_{K'K'+1}^{v'v_2''})$, the symbols have been supressed, and the Q_{XB}^M, Q_{XB}^{ion} notation shortened. $Q_{XB}^M N_{v_1''K_1''}^{v'K'}$ follows the original dipole excitation theory, by hypothesis. Hence, $K_1''=K'\pm1$ and two terms result. $v_1'' = 0$ since only the lowest vibrational level of N_2 is significantly populated at room temperature or below.

The result is that

$$\frac{g_1 N^M Q^M_{XB} N_{v'_1 K'_1} h\nu_{K'K''_2} A_{K'K''_2}}{A(K')} = (\text{constant}) \cdot I_{K'K''_2}, \quad (5.9)$$

where $I_{K'K''_2}$ is the intensity of equation (2.22).
Thus,

$$\Delta I_{K'} = I'_{K'K'-1} - (\text{constant}) \cdot I_{K'K'-1}$$

$$= \left(\sum_{v''K''} g_2 N^{ion} Q^{ion}_{XB} N_{v''K''}(N_2) \right) \frac{h\nu_{K'K-1} A_{K'K'-1}}{A(K')} \quad (5.10)$$

for R branch lines of N_2^+,B-X. I' represents the measured intensity, as before. In practice, both the intensities are normalized at the same K'. Since experimental and phase space results indicate a larger effect at higher K', the K' = 1 line has been used for normalization of the results presented in figures 4.6a-4.6d. P branch overlapping causes some difficulty. However, adjustments made to compensate this overlapping by changing the choice of normalization do not alter the conclusions. Our comparison is made to the calculated cross sections for N_2^+C since N_2^+B calculations were not published for helium. N_2^+B comparisons have been made by Moran and Fullerton[91] for heavy inert atomic ions. Their behavior is generally similar to that illustrated in figure 5.1.

Results at low temperature support this interpretation of $\Delta I_{K'}$. The effect was observed at the lower temperatures,

as figures 4.4 and 4.5 show, and the K' values involved are smaller as the temperature decreases. Moran and Fullerton's calculations indicate such a trend, the peak cross section occurring at lower K' values as the relative energy is reduced.

Excitation of N_2^+B which occurs by transfer from excited neutral atomic states, other than the metastable, should further enhance the term proportional to $I_{K'K'-1}$ in equation (5.10). The constant for normalization can be adjusted to include any processes which are like $He(2^3S)+N_2$, including primary electron beam excitation.

6. CONCLUSIONS

Rotational spectra of N_2^+, B-X bands, produced from impurity nitrogen in helium, have been investigated spectrometrically. A beam of 26 kilovolt electrons, up to 1 milliampere in current, provided the primary source of excitation. Fluorescence from a number of directly and indirectly excited helium atomic states was resolved during spectral surveys of the wave length region 350.0 to 550.0 nm. One He^+ line appeared, at 468.6 nm. Several N_2^+, B-X bands were found in the surveys. The presence of He_2^+ ions and of the helium triplet metastable $He(2^3S)$ was inferred.

The major contribution to the N_2^+, B-X spectrum was due to the helium species colliding with N_2 , exciting and ionizing the molecules. $He(2^3S)$, He^+, and He_2^+ account for substantially all of the excitation. A model of the process has been derived, which attributes a large fraction of the observed rotational line intensity to $He(2^3S)$. $He(2^3S) + N_2 \rightarrow He(1^1S) + N_2^+ B + e$, the Penning ionization, follows the Franck-Condon principle and behaves as a rapid energy transfer, permitting dipole selection rules to govern. He^+ and He_2^+ charge transfer processes do not follow this principle. Since the two types of interaction are independent, the observed rotational line intensity represents their sum. The measured intensities were normalized to the intensity distribution calculated from a dipole excitation theory,

devised for high energy collisions (electrons). $I'_{K'}-I_{K'}$ was then evaluated, line by line. The resulting $\Delta I_{K'}$ follows qualitatively a "phase space theory" model. That fact, together with extensive past research related to the $He(2^3S)$, He^+, and He_2^+ reactions with nitrogen, established this interpretation of N_2^+, B-X fluorescence for mixtures of helium and nitrogen. Specific phase space calculations of the $He_2^+ + N_2 \rightarrow 2He + N_2^+B$ and $He^+ + N_2 \rightarrow He + N_2^+B$ should be accomplished in the future to further support the concepts derived here.

Energy considerations favor the molecular ion charge transfer reaction. The electron beam induced first negative system fluorescence for high helium pressures was inferred to be due to the helium triplet metastables and the diatomic helium ion. The latter is responsible for the observed enhancement in the populations of the higher rotational N_2^+B states, exhibited by larger intensities than predicted by the dipole excitation model.

LITERATURE CITED

1. D. J. McCaa and D. E. Rothe, A.I.A.A. Journal, 7, 1648 (1969).

2. E. P. Muntz, NATO AGARDograph 132, printed by Technical Editing and Reproduction, Ltd., London (December, 1968).

3. E. P. Muntz, Phys. Fluids, 5, 80 (1962).

4. S. L. Petrie, ARL-65-222, Ohio State University, Columbus, Ohio (1965).

5. D. I. Sebacher and R. J. Duckett, NASA TR R-114, Washington, D.C. (1964).

6. F. Robben and L. Talbot, Phys. Fluids, 9, 644 (1966).

7. W. W. Hunter, NASA TN D-4500, Washington, D.C. (May,1968).

8. H. Ashkenas, Phys. Fluids, 10, 2509 (1967).

9. R. O'Neil and G. Davidson, AFCRL-67-0277, Final Report-contract No. AF 19 (628) - 4080 (January, 1968).

10. A. von Engel, Ionized Gases, Oxford University Press, London (1965). Chapter 1.

11. F. M. Penning, Electrical Discharges in Gases, Phillips Technical Library, Einhaven, The Netherlands (1957). Distributed by Gordon and Breach, Science Publishers.

12. A. C. G. Mitchell and M. W. Zemansky, Resonance Radiation and Excited Atoms, Cambridge University Press, London (1971). (First Edition 1934).

13. R. W. B. Pearse and A. G. Gaydon, The Identification of Molecular Spectra, Third Edition, John Wiley and Sons, New York (1963). pp. 209-220.

14. A. Vallance-Jones and D. M. Hunten, Canadian J. Phys., 38, 458 (1960).

15. E. P. Muntz, UTIA Report No. 71, AFOSA TN 60-499, University of Toronto, (April, 1961).

16. G. O. Langstroth, Proc. Roy. Soc. (London), A146, 166 (1934).

17. L. V. Wallace and R. W. Nicholls, J. Atmos. Terr. Phys., 7, 101 (1955).

18. B. W. Schumacher and E. O. Gadamer, Canadian J. Phys., 36, 654 (1958).

19. R. G. Bennett and F. W. Dalby, J. Chem. Phys., 31, 434 (1959).

20. G. N. Polyakova, V. I. Tatus', Ya. M. Fogel', Soviet Physics - JETP, 25, 430 (1967).

21. G. N. Polyakova, V. F. Erko, V. A. Gusev, A. V. Zats and Ya. M. Fogel', Soviet Physics - JETP, 29, 91 (1969).

22. J. L. Dunn, Ph.D. thesis entitled "Spectral Analysis of Mechanism and Kinematics of Thermal Energy Reactions of Long-lived Energetic Helium Species with Simple Molecules", University of California at Santa Barbara, California (November, 1966).

23. H. S. W. Massey, E. H. S. Burhop and H. B. Gilbody, Electronic and Ionic Impact Phenomena, Volume III, Oxford University Press, London (1971). Chapter 18, 5 and Chapter 19, 3.2.

24. D. I. Sebacher, J. Chem. Phys., 42, 1368 (1965).

25. R. G. Whetsel and F. M. Shofner, IEEE Trans. Aero. Elect. Sys., AES-5, 91 (1969).

26. M. E. Hillard,Jr., S. L. Ocheltree, and R. W. Storey, NASA TN-D6005 (October, 1970).

27. J. H. Lees, Proc. Roy. Soc. (London), A137, 173 (1932).

28. J. H. Lees and H. W. B. Skinner, Proc. Roy. Soc. (London), A137, 186 (1932).

29. R. M. St.John, F. L. Miller, and C. C. Lin, Phys. Rev., 134, A888 (1964).

30. V. Cermak, J. Chem. Phys., 44, 3774 (1966).

31. H. K. Holt and R. Krotkov, Phys. Rev., 144,82 (1966).

32. J. van Eck and J. R. deJongh, Physica, 47, 141 (1970).

33. J. D. Jobe and R. M. St.John, J. Opt. Soc. America, 57, 1449 (1967).

34. S. E. Frisch and Yu. E. Ionikh, Opt. Spectry., 25 91 (1968).

35. G. W. F. Drake, Phys. Rev., 181, 23 (1969).

36. See the extensive review on pages 56-57 of reference 2.

37. A. H. Gabriel and D. W. O. Heddle, Proc. Roy. Soc. (London), A258, 124 (1960).

38. J. L. G. Dugan, H. L. Richards, and E. E. Muschlitz, Jr., J. Chem. Phys., 46, 346 (1967).

39. P. H. Wine, Ph.D. thesis entitled " Studies of Collisional Excitation Transfer Processes in Helium", Florida State University, Tallahassee, Florida (1974).

40. B. L. Moiseiwitsch and S. J. Smith, Rev. Mod. Phys., 40, 238 (1968).

41. H. S. W. Massey, E. H. S. Burhop, and H. B. Gilbody, Electronic and Ionic Impact Phenomena, Second Edition, Oxford University Press, London (1969). Volume I.

42. N. F. Mott and H. S. W. Massey, The Theory of Atomic Collisions, Third Edition, Oxford University Press, London (1965).

43. C. B. Collins and W. W. Robertson, J. Chem. Phys., 40, 2202 (1964).

44. F. E. Niles and W. W. Robertson, J. Chem. Phys., 40, 2909 (1964).

45. D. Villarejo, R. R. Herm, and M. G. Inghram, J. Opt. Soc. America, 56, 1574 (1966).

46. R. W. Huggins and J. H. Cahn, J. Appl. Phys., 38, 180 (1967).

47. R. M. St.John and R. G. Fowler, Phys., Rev., 122. 1813 (1961).

48. R. B. Kay and R. H. Hughes, Phys. Rev., 154, 61 (1967).

49. Reference 23; chapter 18, sections 4 and 5.

50. C. C. Lin and R. G. Fowler, Annals Phys., 15, 461 (1961).

51. R. L. Abrams and G. J. Wolga, Phys. Rev. Letters, 19, 1411 (1963).

52. J. Bakos and J. Szigeti, J. Phys. B, 1, 1115 (1968).

53. A. V. Phelps, Phys. Rev., 171, 81 (1968).

54. L. D. Schearer, Phys. Rev., 171, 81 (1968).

55. F. K. Elder,Jr. and W. J. Wintzer, Report No. NADC-AW-6428, U. S. Naval Air Development Center (December, 1964), Johnsville, PA.

56. L. J. Kieffer and G. H. Dunn, Rev. Mod. Phys., 38, 1 (1966).

57. B. L. Maguire, Rarified Gas Dynamics, Vol. II, C. L. Brundin, editor, Academic Press, New York (1967), p. 1497.

58. J. A. Hornbeck and J. P. Molnar, Phys. Rev., 84, 621 (1951).

59. H. F. Wellenstein and W. W. Robertson, J. Chem. Phys., 56, 1077 (1972).

60. E. C. Y. Inn, Planet. Space Sci., 15, 19 (1967).

61. M. B. McElroy, Planet. Space Sci., 13, 403 (1965).

62. W. B. Maier, II, Planet. Space Sci., 16. 477 (1968).

63. J. Heimerl, R. Johnsen, and M. A. Biondi, J. Chem. Phys., 51, 5041 (1969).

64. W. W. Hunter,Jr., Ph.D. thesis entitled "Temperature Dependence of $He3^1P$ Excitation Transfer Cross Section", Virginia Polytechnic Institute and State University, Blacksburg, VA (1972).

65. S. L. Ocheltree and R. W. Storey, Rev. Sci. Instrum., 44, 367 (1973).

66. C. E. Moore and P. W. Merrill, Partial Grotiran Diagrams of Astrophysical Interest, NSRDS-NBS 23, National Bureau of Standards, U. S. Department of Commerce, GPO, Washington, D. C. (1968).

67. S. Dushman, Scientific Foundations of Vacuum Technique, Second Edition, edited by J. M. Lafferty, John Wiley and Sons, Inc., New York (1962). Chapter 5.

68. A. E. deVries and P. K. Rol, Vacuum, 15, 135 (1965).

69. R. J. Tunnicliffe and J. A. Rees, Vacuum, 17, 457 (1967).

70. C. F. Morrison,Jr., Research/Development (September, 1969), 54-64.

71. A von Engel, Ionized Gases, Second Edition, Oxford University Press, London (1965) p. 63.

72. E. W. Thomas, Excitation in Heavy Particle Collisions, John Wiley and Sons, Inc., New York (1972). Section 8-3.F.1, pp. 264-266.

73. F. Cramarossa and G. Ferraro, J. Quant. Spectry. Radiat. Trans., 14, 159 (1974).

74. J. C. Hoppe, J. Quant. Spectry. Radiat. Trans., 10, 823 (1970).

75. W. W. Hunter,Jr. and T. E. Leinhardt, J. Chem. Phys., 58, 941 (1973).

76. A. R. DeMonchy and H. J. Oskam, Z. Physik, 224, 324 (1969).

77. L. G. Piper, L. Grundel, J. E. Velazco, and D. W. Setser, J. Chem. Phys., 62, 3883 (1975).

78. G. E. Bearman, J. E. Earl, R. J. Pieper, H. H. Harris, and J. L. Leventhal, Phys. Rev. A, 13, 1734 (1976).

79. T. D. Mark and H. J. Oskam, Phys. Rev. A, 4, 1445, (1971).

80. W. W. Robertson, J. Chem. Phys., 44, 2456 (1966).

81. E. S. Fishburne, J. Chem. Phys., 47, 58 (1967).

82. A. L. Scheltekopf, E. E. Ferguson, and F. C. Fehsenfeld J. Phys. B, 48, 2966 (1968).

83. R. C. Bolden, R. S. Hemsworth, M. J. Shaw, and N. J. Twiddy, J. Phys. B, 3, 61 (1970).

84. T. T. Kassal and E. S. Fishburne, J. Chem. Phys., 54, 1363 (1971).

85. S. J. Young and K. P. Horn, J. Chem. Phys., 57, 4835 (1972).

86. J. C. Light, J. Chem. Phys., 40, 3221 (1964).

87. P. Pechukas and J. C. Light, J. Chem. Phys., 42, 3281 (1965).

88. J. C. Light and J. Lin, J. Chem. Phys., 43, 3209 (1965).

89. J. Lin and J. C. Light, J. Chem. Phys., 45, 2545 (1966).

90. G. Giomousis and D. P. Stevenson, J. Chem. Phys., 29, 294 (1958).

91. T. F. Moran and D. C. Fullerton, J. Chem. Phys., 56, 21 (1972).

The vita has been removed from the scanned document

AN EXPERIMENTAL STUDY OF THE ROTATIONAL DISTRIBUTION OF N_2^+B (v) STATES EXCITED BY ELECTRON BEAM IMPINGEMENT UPON HELIUM AND NITROGEN GAS MIXTURES

by

John Cameron Hoppe

(ABSTRACT)

A large number of atomic helium states are excited by inelastic collisions. That excitation may be induced by various methods, including gas discharges, flowing afterglows and electron beams. The first negative nitrogen bands, $N_2^+(B^2\Sigma_u^+ - X^2\Sigma_g^+)$, have been observed with relatively high intensity from small quantities of nitrogen in helium, also induced by such methods. These bands have been studied by passing 26 kev electrons through mixtures. The resolved rotational spectra of the (0,0) and (0,1) bands have been analyzed as functions of pressure and mixture. An observed enhancement of the intensities has been interpreted in terms of selectively enhanced N_2^+B rotational state populations. The particular helium species responsible for the enhancement are discussed. Experimental results are compared with a general "phase space" approach for calculating the reaction cross sections.